

Thesis 1
1874

**THE DEVELOPMENT OF LOW TEMPERATURE
HEAT CAPACITY RESULTS**

**A Heat Capacity Study of some
Chloroammine Cobalt(III) Compounds**

by

M. Hegarty, B.Sc.



**A thesis submitted for the Degree of Doctor of Philosophy
in the University of Stirling**

8/92

ABSTRACT

TITLE: The Development of Low Temperature Heat Capacity Results: A Heat Capacity Study of some Chloramine Cobalt(III) Compounds.

CANDIDATE: Mark Hegarty

DEGREE: Doctor of Philosophy

DATE: October 1991

A laboratory for heat capacity measurements by adiabatic calorimetry in the range from 2 to 100 kelvin was developed. A complete vacuum and gas-handling system was designed and constructed to serve a refurbished pumped-helium cryostat. Automatic data-collection, real-time display of temperature and semi-automation of heating and adiabatic control were achieved with a low-cost interface and microcomputer.

The apparatus was calibrated with a benzoic acid thermometric standard. The heat capacity of chloropentaammine cobalt(III) dichloride was measured from 3.8 to 100 kelvin; thermodynamic functions are quoted from 6 to 100 kelvin. The heat capacity of trans-dichloro-tetrammine cobalt(III) chloride was measured from 4.7 to 100 kelvin; thermodynamic functions are quoted from 10 to 100 kelvin. No thermal anomalies were observed in these temperature ranges.

ACKNOWLEDGEMENTS

I wish to express my gratitude to my Supervisor, Dr R. M. Clay for his advice and encouragement throughout the course of this work.

I am also indebted to Mr D. F. Dance for many valuable discussions of vacuum systems and methods of leak detection.

The assistance of the technical staff is also greatly appreciated: in particular Mr C. Chesterman and Mr J. Dyer for engineering work, along with Mr W. Stirling and Mr A. Michaels for electronics and microprocessor services.

I must also thank my mother for word processing the text, and my wife and son for their patience and understanding; all of which was essential to the completion of this thesis.

Mark Hegarty
M. Hegarty

CONTENTS	PAGE
CHAPTER 1 PHYSICS AND CHEMISTRY AT LOW TEMPERATURES	5
CHAPTER 2 LOW TEMPERATURE CALORIMETRY	14
CHAPTER 3 INSTRUMENTATION	44
CHAPTER 4 OPERATION AND CALIBRATION	84
CHAPTER 5 HEAT CAPACITY STUDIES	130
APPENDIX TO CHAPTER 2	162
APPENDIX TO CHAPTER 3	163
APPENDIX TO CHAPTER 4	173
REFERENCES	175

CHAPTER 1**PHYSICS AND CHEMISTRY AT LOW TEMPERATURES**

1 PHYSICS AND CHEMISTRY AT LOW TEMPERATURES

The overall aim of this work was to establish a new laboratory for heat capacity measurements by adiabatic calorimetry in the range from 2 to 100 kelvin.

This temperature range is particularly useful as it extends low enough for the heat capacity to be matched to Einstein and Debye models. It also allows overlap with higher temperature calorimeters, in particular the commercially available differential scanning calorimeters, which can operate from 70 kelvin up to several hundreds of kelvin. The provision of measurements at low temperatures allows a more complete thermal-history of a substance to be obtained. Such measurements are not widely available since there are very few laboratories outside of America and Japan which operate in the 2 to 100 kelvin range.

There are numerous and obvious reasons for carrying out calorimetry at high temperatures. For example, the heat capacity of synthetic sapphire (α - Al_2O_3) has been measured up to 700 kelvin⁹ because it is an important industrial abrasive. Also for example, WS_2 has been studied up to 1500 kelvin⁹ because it is a widely used catalyst and high temperature lubricant.

The abundance of such practical applications at and above room temperature causes a somewhat biased viewpoint, and by comparison the study of matter at cryogenic temperatures can appear rather esoteric. However, in terms of solid state behaviour, room temperature (or 300 kelvin) is a relatively high temperature. When heated in the range from 300 to 3000 kelvin, most solids first show a rapid deterioration in mechanical properties and then become liquids or vapours. The increase in temperature by one order of magnitude has

thus produced a different phase and the solid state can no longer be studied.

With the exception of helium (which also requires applied pressure) all matter becomes solid at suitably low temperatures, and the properties of the low temperature solid can be very different from those at room temperature. On cooling from 300 kelvin to 30 kelvin, solids generally become stronger but more brittle. The lattice specific heat decreases by a factor of ten or more, and is accompanied by a tenfold increase in the electrical and thermal conductivities.

In the 30 kelvin to 0.3 kelvin range, the heat capacity usually reduces by a factor of 1000 below the room temperature value. Thermal conductivity can be 1000 times greater, while the electrical conductivity can be as much as 10^5 times greater as is the case for pure single crystals of tin, cadmium and zinc. Spontaneous order-disorder phenomena are also prevalent, as are superconducting transitions in noble metals such as Aluminium (1.2 kelvin), alloys of the type $\text{Nb}^{50}\text{Tl}^{40}$ (9.5 kelvin) and intermetallic compounds such as Nb_3Sn (18.4 kelvin).

Currently, the lowest temperature to which matter has been cooled is 5×10^{-8} kelvin.³ This was reached by precooling copper to 2 millikelvin in a $\text{He}^3\text{-He}^4$ dilution refrigerator,⁴ followed by adiabatic demagnetisation of the copper nuclei. The achievement of this temperature clearly indicates that at cryogenic temperatures there are several orders of magnitude which may be exploited in studying the properties of the solid state.

The progression to such low temperatures has been the result of significant technical advances in cryophysics, several of which have now found diverse applications. Superconductivity has been extensively exploited, particularly in the form of the Josephson junction.⁵ This electronic device is formed from two pieces of superconductor weakly coupled together by a thin oxide layer. Quantum mechanical tunnelling of this layer gives rise to a supercurrent which is highly sensitive to applied magnetic fields and can be totally suppressed by a few millitesla. The formation of a

superconducting loop containing two Josephson junctions results in a highly sensitive magnetic interferometer through which the flow and suppression of supercurrent is regulated at a frequency equivalent to the oscillation frequency of the magnetic flux. This loop is referred to as a SQUID⁴ (superconducting quantum interfering device) and its use represents the state of art in monitoring heart and brain activity by magnetocardiography and encephalography. The performance is at least one order of magnitude better than the most sensitive NMR scanners which employ supercooled magnets.

A further medical application is that of the "microminiature" refrigerator⁷. This compact device avoids immersion in liquid cryogens by employing Joule-Kelvin expansion to produce cooling, and has achieved temperatures low enough for cryosurgery.

In space and upper atmosphere experiments, helium cooled semiconductor devices⁸ are now regularly used as detectors and amplifiers. This is because the level of Johnson noise is so significantly reduced that the background level of cosmic radiation can be resolved and quantified. Finally, superconducting devices such as the QUITERON⁹ have recently been reported. These operate similarly to a power transistor and have potential in the quest for low energy consumption superconducting computers.

Whilst many of the tangible applications of low temperature technology are associated with Applied Cryophysics, the significance of cryogenic temperatures to Chemistry is no less important. For example, the chemical thermodynamicist is interested in measurements of the specific heat capacity of a substance since this provides information on three fundamental thermodynamic properties; namely, the enthalpy (H), entropy (S) and Gibbs energy (G). Normally, the heat capacity measurements start at some conveniently high temperature and are extrapolated to absolute zero to allow evaluation of the standard thermodynamic functions $H^{\circ}(T)$, $S^{\circ}(T)$ and $G^{\circ}(T)$ from the equations:

$$H^{\circ}(T) = \int_0^T C_p dT ; S^{\circ}(T) = \int_0^T \frac{C_p dT}{T} ; G^{\circ}(T) = H^{\circ}(T) - TS^{\circ}(T).$$

These values may then contribute to other thermodynamic calculations. For example, the molar calorimetric entropy and the standard enthalpy of formation may be used to determine a standard Gibbs energy change, and from this the equilibrium constant for a particular reaction.

These calculations may be in error, however, since the above extrapolation method cannot take account of additional contributions to the entropy which may occur at low temperatures.

When a crystalline solid is cooled from a temperature at which an equilibrium state is disordered, some of the disorder may be frozen-in and persist in the lattice down to absolute zero. In this case, the crystal is in a non-equilibrium state and retains 'residual entropy' as has been predicted for ordinary ice.¹⁰ More commonly, the crystal may achieve an ordered state by undergoing one or more transitions. Provided that heat capacity measurements start at a sufficiently low temperature, an anomalous contribution may be observed which is associated with the order-disorder transition. Statistically, the entropy of transition is $\Delta S_t = R \ln \left(\frac{N_1}{N_2} \right)$ where N_1 and N_2 are respectively the number of independent configurations below and above the transition temperature. These contributions can be significant. For example, $R \ln 6$ entropy units are associated with the order-disorder transition of $\text{MnCl}_2 \cdot 4\text{H}_2\text{O}^{11}$ which occurs at 1.62 kelvin. Thus, since the thermodynamic functions are cumulative, it can be very important to account for such transitions over as wide a temperature range as possible.

However, the chemical interest does not end with the achievement of more accurate thermodynamic functions. The occurrence of an order-disorder transition at a particular temperature may also be viewed as the balance point between the crystalline forces which favour the ordered structure (or hinder rearrangement) and the thermal agitation which causes the disorder. Here, the chemist has particular interest in characterising the disorder in terms of specific molecular motions or ionic interactions within the crystal. Full characterisation is usually dependent on crystallographic data being available to elucidate structure, plus NMR or neutron scattering studies to

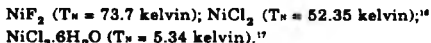
classify the dynamics of the lattice motion. Such studies, along with the quantitative data from heat capacity measurements, can result in the macroscopic properties of the crystal being accurately modelled by statistical mechanics, and thus may lead to a microscopic description of the disorder present in the crystal.

Three general types of disorder can be encountered in stoichiometric crystals: positional, magnetic and orientational. Positional disorder can arise in two different ways. In the first case, the number of lattice sites is equal to the total number of particles in the crystal, and the random occupation of the sites by different types of particle results in the disorder. This is typical of metal alloys such as β - brass (CuZn).¹³ The second form of positional disorder occurs when the number of particles is less than the number of lattice sites, and the sites are associated with positions of different energy within the crystal. Again, random distribution of the particles results in disorder. Examples of this are provided by super-ionic conductors such as α -AgI¹⁴ for which exceptional mobility arises due to the availability of 21 sites for each Ag⁺ ion. A further example is RbAg₄I₃ which exhibits a higher electrical conductivity ($0.27\Omega^{-1}\text{cm}^{-1}$) than any other solid ionic conductor at room temperature. The origin of the increase in conductivity has been associated with a structural phase transition at 121.8 kelvin,¹⁴ as observed by low temperature heat capacity measurements. The transition has been classified as first-order as it shows isothermal changes in the enthalpy and density functions and a change in volume for the crystal.

Magnetic disorder commonly occurs in rare-earth metal and transition metal compounds which contain ions with unpaired electrons. In the higher temperature paramagnetic state thermal agitation causes the spins of the magnetic ions to be randomly oriented throughout the crystal lattice. At sufficiently low temperatures, the magnetic moments can couple to form ordered arrangements which may be ferromagnetic or antiferromagnetic. Ferromagnetism occurs when the spins of the magnetic ions align parallel to each other, thus imposing a nett magnetic moment on the lattice. Antiferromagnetism occurs when the spins align antiparallel, resulting in zero magnetic moment in the case of a

perfectly ordered crystal. The resultant entropy change for the transition is $R\ln(2S+1)$ where S is the total spin quantum number of the magnetic ion.

Here the main chemical interest lies in the fact that many occurrences of magnetic ordering are not determined by the direct interaction of the two metal cations, but by an indirect interaction involving electron transfer from an anion adjacent to the two cations. This is referred to as superexchange, and it normally involves overlap of a filled p-orbital of the anion with an empty or half-filled d-orbital of the cation. The strength of the interaction is determined by the degree to which anions or ligands can delocalise the cation electrons, and is reflected in the magnitude of the transition temperature. For example, whilst elemental Ni remains ferromagnetic up to 627 kelvin, superexchange causes its halide salts to be antiferromagnetically ordered at low temperatures as follows:



The series may also be extended to include the extremely weak exchange interaction which occurs in $\text{Ni}(\text{NH}_3)_6\text{Cl}_2$ ($T_N = 0.3$ kelvin), a salt which is further discussed in Chapter 5. In each case, the entropy change is $R\ln 3$, the effect of which is clearly manifest as a lambda point discontinuity in the heat capacity curve. No latent heat is involved and the Gibbs, enthalpy and entropy functions are continuous, making this a second-order phase transition. The transition is cooperative in nature because the interactions result in relatively long range forces which extend beyond nearest-neighbours.

Orientalional disorder can occur when diatomic or polyatomic molecules or ions randomly occupy two or more distinguishable orientations in a crystal lattice. When the crystal is cooled, orientational disorder may be *frozen* into the lattice if the reorientational motion is hindered. This occurs at the temperature where the molecules or ions no longer possess the activation energy required to surmount the local potential barrier between each

orientation. A classic example is carbon monoxide which has residual entropy at absolute zero.¹² This has been associated with the random distribution of the molecules between the two orientations CO and OC in the crystal lattice.¹³ Although the molecular dipole moment is very small, "head to tail" interchange requires an activation energy of 18.9 Jmol^{-1} , which cannot be achieved below 2 kelvin.

The heat capacity studies reported in this thesis are concerned with a particular type of orientational disorder which has been observed in metal-ammine complexes.¹⁴ The disorder is associated with the restricted rotation of the NH_3 ligands about the axis of the metal-nitrogen bond. As temperature decreases, the torsional oscillation of the NH_3 groups reduces in amplitude and frequency, and classical reorientation is prohibited.

However, at very low temperatures an anomalous contribution to the heat capacity may be detected. This demands a quantum mechanical explanation, and has been ascribed to splitting of the ground state torsional energy level due to coupling of the rotational and nuclear spin wavefunctions. Transitions between the independent sets of internal energy levels are equivalent to NH_3 reorientations and must occur by proton tunnelling of the potential barrier, the height of which determines the splitting energy. When cooperative effects are negligible, the population of the energy levels is purely temperature dependent and may lead to an asymmetric bell-shaped contribution, referred to as a Schottky anomaly, in the specific heat curve. The detection of such anomalies is particularly interesting since it can result in the magnitude of the hindering potential being quantified, and thus promote greater understanding of the molecular interactions within the crystal.

The author wishes to make it clear that, at the start of this project, he was introduced to an empty room and the challenge of transforming it into a very specialised laboratory. Consequently, the bulk of this thesis deals with the design and construction of apparatus and the development of practical working methods. Chapters 2, 3 and 4 fully describe the development programme, the main topics of which are

summarised below:

- 1 Refurbishment of the cryostat and calorimeter;
- 2 Design and construction of vacuum systems;
- 3 Design and construction of instrumentation;
- 4 Incorporation of semi-automated process control;
- 5 Calibration of apparatus and validation of methods.

The completion of the above tasks was very prolonged due to the significant amount of problem solving involved. As a result, only two heat capacity studies could be undertaken in the time which remained. Chloropentaammine Co(III) dichloride and trans-dichlorotetraammine Co(III) chloride were investigated with a view to detecting Schottky anomalies and relating any changes in the barrier heights to the variation of the ligand environment. The studies are detailed in Chapter 5.

CHAPTER 2**LOW TEMPERATURE CALORIMETRY**

CONTENTS	PAGE
2. 1 GENERAL PRINCIPLES	16
2. 1. 1 Calorimetric Techniques	
2. 2. 2 Cryostat Designs	
2. 1. 3 Principles of Cryostat Construction	
2. 2 THE CALORIMETRIC CRYOSTAT	20
2. 2. 1 History of this Cryostat	
2. 2. 2 Outline of the Cryostat Design	
2. 3 REFURBISHMENT OF THE CRYOSTAT	26
2. 3. 1 Reconstruction Details	
2. 3. 2 The Cryostat	
2. 3. 3 The Calorimeter Vessel	
2. 3. 4 The Adiabatic Shield	
2. 3. 5 The Differential Thermopile	
2. 3. 6 Further Wiring	
2. 4 THE CRYOSTAT VACUUM SYSTEMS	34
2. 4. 1 The Experimental Rig	
2. 4. 2 The Main Vacuum Lines	
2. 4. 3 The Gas Handling Line	
2. 4. 4 The New Leak Detector/Analyser	

2. 1 GENERAL PRINCIPLES

2. 1. 1 Calorimetric Techniques

The basic calorimetric method of evaluating the heat capacity of condensed phases by measuring the temperature rise dT for a given electrical input is attributed to W. Gaede in 1902²¹. The concept was utilised in an isothermal technique developed by Nernst and Euker²² in 1909, and in 1910 refinements by Nernst led to the precursor of modern adiabatic calorimetry.²³

Although techniques have been developed and refined by advances in instrumentation, the general principles remain the same with most methods using high vacuum to maintain thermal insulation, and differences arising in the preferred methods of controlling heat leaks due to mechanical contact and thermal radiation.

In the completely isothermal technique, there is no nett temperature change during the experiment, and the calorimeter temperature remains constant with time. An example of this is the Bunsen ice-calorimeter²⁴ in which the solid-liquid phase change ensures constant temperature while the volume change is a measure of the enthalpy increment.

The heat-flow isothermal technique relies on the removal of evolved heat by either fluid flow or conduction, convection or radiation.²⁵

Iso-peribolic methods²⁶ use an isothermal radiation shield surrounding the calorimeter vessel, and rely on calculations of the heat leak with respect to the constant reference temperature of the shield. As these corrections can only be made with limited accuracy, the operational temperature range is severely restricted in order that the corrections will be small.

In adiabatic calorimetry, the heat leak is reduced to an insignificant level by use of an adiabatic radiation shield¹⁷ which closely matches the temperature of the calorimeter vessel throughout a heating period and also over the whole range of operating temperatures. Temperature differences between the shield and calorimeter should not exceed a millidegree, and the surfaces of the shield and calorimeter should also be isothermal to within a millidegree. Temperature control is monitored by a differential thermocouple with junctions at the shield and calorimeter surfaces.

Development of the adiabatic method at cryogenic temperature has been attributed to Southard and Andrews (1930).¹⁸ Like all of the methods quoted, this requires the combination of precision thermometry and accurate energy measurement, both of which are dependent upon the achievement of good thermal isolation.

The techniques and instrumentation for thermometry and energy measurement are dealt with in Chapters 3 and 4. The remainder of this chapter deals with the design and construction of low temperature apparatus to minimise heat exchange, and thus provide adequate thermal isolation.

2. 1. 2 Principles of Cryostat Design and Construction

A low temperature cryostat is designed to set up a ladder of uniform and progressively lower temperatures (see Figure 2A). Copper flanges and vacuum chambers form the uniform heat-sinks at each temperature level. The heat-leak, by conduction between levels, is made small by use of thin-walled stainless steel tubing to connect each level and provide evacuation lines; the thermal conductivity of stainless steel being less than that of copper by a factor of 1400 at 4.2 kelvin.¹⁹ The number of connections is kept to the minimum which will produce a rigid apparatus with completely independent vacuum chambers.

In general the heat-leak contribution from gas conduction and convection is eliminated by evacuation to 10^{-6} mbar. Hill, Martin and Osborne²⁰

have shown, however, that calorimeter vessels operating at liquid-helium temperatures require insulation of at least 10^{-9} mbar if heat exchange is to be negligible. Normally this is achieved by the combined effect of evacuation to 10^{-6} mbar and cryopumping (adsorption of residual gas molecules by surfaces at cryogenic temperatures) by the lowest cryostat heat-sinks. All cryostat joints and components must, therefore, be leak-tight to at least 10^{-9} mbar, and pumping tubes capable of withstanding a differential pressure of 1 atmosphere. Because of the large difference in thermal conductivity, copper/stainless steel joints require soft soldering with non-superconducting solder. Permanent copper/copper or copper/brass joints may be silver brazed provided that the joint is not held under tension at cryogenic temperatures.

Radiative heat transfer is reduced by polishing surfaces to maximise reflectivity. Calorimeter vessels and radiation shields are made from materials of high thermal diffusivity to ensure that isothermal conditions are achieved. The materials must also be of comparable thermal emissivity so that radiated frequencies will also be absorbed and a state of radiative equilibrium will be established.

Conduction along the electrical leads cable is minimised by use of very fine gauge wire. Where needed, the cable is looped to maximise the conduction path length, and all wires are thermally anchored at each temperature level before passage to electrical lead-throughs. Vertical conduction is also reduced by use of monofilament nylon for all suspensions such as floating ring baffles and the calorimeter vessel.

2. 1. 3 Types of Cryostat

A considerable variety of cryostat designs can be found in the literature.^{21, 22, 23, 24} However, since the basic design is usually determined by the method of cooling and the temperature range of operation, the diversity can be reduced to variations on one or two themes.

With the aneroid cryostat²⁵ the supply of cryogen is sealed inside the main vacuum chamber as a completely self-contained unit, thus

resulting in very low refrigerant consumption. The main disadvantage of the design is that the thermal transfer is solely dependent on mechanical conduction which produces very slow cooling rates.

The immersion type cryostat²⁴ has less stringent design requirements, being simply immersed in a dewar containing the primary refrigerant. Refrigerant consumption is high, but fast cooling can be obtained by use of a thermal exchange gas.

Combination cryostats such as the immersion/aneroid²⁵ provide a successful compromise between refrigerant economy and fast cooling. The aneroid helium tank is held inside the vacuum chambers of a normal immersion cryostat. This provides long periods of high stability at low temperatures which has proved useful for work in the vitreous state²⁶ where long relaxation times predominate.

Pumped-immersion type cryostats combine features of a normal immersion cryostat with an internal vessel into which cryogen can be throttled and then sublimed by increased pumping. The main design feature of such cryostats is the use of a mechanical heat-switch²⁷ which enables cooling of the calorimeter vessel without the use of exchange gas. This avoids the problem of surface adsorption of the exchange gas which would give rise to desorption errors during calorimetry, particularly at pumped liquid helium temperatures.

The construction of this type of cryostat is dealt with in detail in section 2. 2.

2.2 THE CALORIMETRIC CRYOSTAT

2.2.1 History of this Cryostat

The cryostat used in this laboratory has been the subject of several reconstructions and modifications^{16,17} throughout the years. It is, however, essentially based on an immersion cryostat built by Dr. R. M. Clay in 1965.¹⁸

As liquid helium was not widely available and also relatively expensive at that time, the cryostat was immersed in liquid hydrogen boiling at normal pressure for initial cooling to 20K. The liquid hydrogen was then replaced with liquid helium boiling at atmospheric pressure to cool the cryostat to 4.2K. Temperatures close to 2K could then be achieved by sealing the vent to atmosphere, and pumping on the whole refrigerant bath to reduce the vapour pressure and solidify the helium refrigerant. Above 20K heat capacity measurements were made under adiabatic conditions by manual control of a radiation shield. Below 20K the conditions were isoperibolic, with the radiation shield being maintained at 4.2K by use of helium as a thermal exchange gas between the shield and the refrigerant.

By 1978, liquid helium had become more economical, and a major reconstruction was made by Dr. M. Jewess,¹⁹ through which the highly volatile liquid hydrogen could be dispensed with. This was achieved by constructing a small tank as part of the cryostat assembly. This internal vessel could then be filled with liquid nitrogen which solidified under reduced pressure to cool the calorimeter and adiabatic shield to approximately 50K. Once all of the solid nitrogen had sublimed, liquid helium could then be drawn into the internal vessel, and increased pumping cooled the interior to approximately 1.6K.

Low temperature cryostats, and particularly those using demountable solder seals, require constant maintenance. This is due to corrosion caused by the acid fluxes used during soldering, and also due to the stress caused by differential contractions and expansions in thermal cycling between the extremes of room temperature and cryogenic temperatures. Inevitably a point is reached where repairs are no longer feasible, and full refurbishment is required. Such a point had been reached when the cryostat arrived at this laboratory, and a complete reconstruction with modifications was undertaken by the author.

The original calorimeter vessel and thermal switch designed by Dr. Clay were found to be in good condition and were retained, as was the internal pumping method of Dr. Jewess. A complete vacuum and gas handling system was designed and constructed by the author.

2. 2. 2 Outline of the Cryostat Design

Figure 2A shows a schematic diagram of the calorimetric cryostat. It is of the classic immersion-type, with the calorimeter vessel A surrounded by concentric vacuum chambers F, L, M. These chambers provide the three independent levels of vacuum insulation which are necessary for accurate adiabatic calorimetry in a pumped liquid helium cryostat.

The inner vacuum chamber F serves a dual purpose:

- (a) providing a high vacuum to nullify thermal convection;
- (b) acting as the adiabatic shield which counteracts radiative heat transfer and cryopumps the inner vacuum space at low temperatures.

As required, the calorimetric leads cable C is made from very fine gauge wire and is thermally anchored at the base of the shield. Direct

mechanical contact is further reduced by suspending the calorimeter vessel on small loops of nylon monofilament arranged pseudo-tetrahedrally and attached to tensioning screws on the wall of the shield. Experience has shown that 0.3 mm diameter monofilament provides a good compromise between high tensile strength and low thermal conductivity.⁴

The suspension can be finely adjusted so that the copper tube extending from the top of the calorimeter vessel can be gripped tightly between the jaws of the thermal switch E when cooling is required. The jaws are spring-loaded copper blocks faced with indium metal, and they are operated from the cryostat top-plate V by means of a knurled screw and stainless steel wire. The phosphor/bronze bellows O provide a flexible vacuum seal to the mechanism.

The helium³ vessel I is a small copper chamber (5 cc capacity) which sits directly on top of the adiabatic shield. This can be used to condense liquid helium³ when the internal assembly is below 2K. Evaporation under reduced pressure can then cool the calorimeter to 1K or below.

The middle vacuum chamber L contains the internal pumping vessel K which is a copper tank of 75 cc capacity. This can be filled with either liquid nitrogen or liquid helium contained in the glass dewar S. The flow of refrigerant is controlled by the needle valve N which moves a stainless steel rod vertically and without rotation onto a phosphor/bronze seat. The vessel is evacuated through a stainless steel tube of internal diameter 2 mm to inhibit the passage of superfluid helium at 4.2K. At the top of the outer can M, the tube diameter is 10 mm, and it is further increased at the cryostat top-plate to maximise the pumping rate. The pumping can be throttle controlled with a rotary pump and diaphragm valve to cool the internal assembly to 48K with nitrogen or 1.5K with helium.

The outer vacuum chamber M insulates the middle chamber and the internal pumping system from the higher temperature of the external refrigerant bath.

The economiser vessel T is filled with liquid nitrogen to prevent vertical heat conduction down the pumping tubes and the electrical leads cable P which emerges to room temperature at the top-plate. It thus reduces the consumption of liquid helium.

Cryogenic grade thin-walled stainless steel is used for all of the pumping tubes and the larger diameter tubes are fitted with radiation baffles at each level of the cryostat temperature ladder. The vacuum cans and horizontal flanges are all made from copper to ensure good equilibration at each level. Electrical connections between the cryogenic lead-throughs H are of fine gauge manganin wire, and cables are thermally anchored at each temperature level.

The cryostat is immersed in the glass dewar S which acts as the primary refrigerant bath, and can be isolated from the atmosphere by means of the rubber Leiden seal U. The stainless steel dewar W gives protection to the cryostat and glass dewar, and it can be filled with liquid nitrogen to provide a further insulating layer. Liquid helium is transferred into the glass dewar by the syphon R which enters through a tube in the economiser vessel. The syphon can be replaced with a funnel when liquid nitrogen is being used. The mountings 1-5 are provided, at convenient levels on the cryostat, to hold liquid helium depth-sensors (see Chapter 3) for the control of helium transfer into the glass dewar.

Figure 2A

THE CALORIMETRIC CRYOSTAT

A	Calorimeter vessel
B	Thermometer housing
C	Calorimetric cable
D	Filling port: copper cap, silver tube
E	Thermal switch assembly
F	Adiabatic shield / Inner vacuum chamber
G	Differential thermopile junctions
H	Cryogenic electrical lead-throughs
I	Demountable indium solder seals
J	Helium ³ evaporation vessel
K	Internal liquid helium / nitrogen pumping vessel
L	Middle vacuum chamber
M	Outer vacuum chamber
N	Needle valve
O	Metal bellows
P	Electrical leads cable
1-5	Liquid helium depth sensors
R	Liquid helium transfer syphon
S	Glass inner dewar
T	Liquid nitrogen economiser vessel
U	Rubber Leiden seal
V	Cryostat top-plate
W	Stainless steel protective dewar

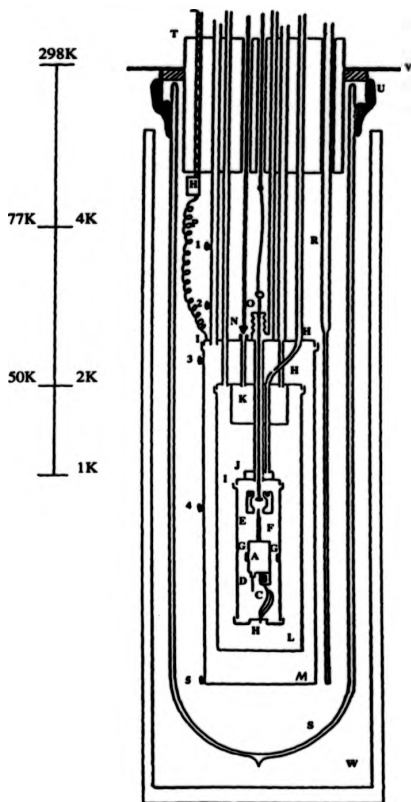


Figure 2A - The Calorimetric Cryostat

2.3 REFURBISHMENT OF THE CRYOSTAT

2.3.1 Reconstruction Details

The work outlined below was the first of its kind to be undertaken by the workshops of this University. Lack of experience in the rather specialised area of Cryogenic Engineering severely hindered the production of a working instrument. Overall, the reconstruction took two-and-a-half years of continuous assembly, testing and reassembly before real progress was made. This included two full-scale reconstructions in the Engineering Workshops, followed by several partial assemblies by the author in this laboratory.

Ideally a refurbished cryostat should come back from the workshop completely free of vacuum leaks at room temperature. This minimises the number of repairs required when low temperature testing begins. Because cryostats are solder assembled, one repair tends to lead to another, and too many repairs shorten the useful working life of the apparatus.

Unfortunately the first cryostat was rather poorly assembled and, after eighteen months of constant fault finding and repair, it was clear that it would not be suitable for low temperature work. Although this seemed a retrograde step at the time, the author scrapped the first cryostat and initiated a new construction putting to good use the experience and hard-learned lessons of the first assembly. What follows is a detailed description of the more successful second reconstruction.

2.3.2 The Cryostat

All of the cryostat pumping tubes were replaced with cold-drawn stainless steel tubing (grade 321) supplied by Oxford Instruments Ltd. These thin-walled tubes ranged in outer diameter from 2.03 mm for the internal vessel lines, to 12.7 mm o.d. for the vacuum can lines. The range of wall thickness was 0.15 mm to 0.25 mm respectively.

New copper flanges were machined to match the tubing, and also to accommodate a new arrangement of vacuum lead-throughs. All permanent joints were made with a binary eutectic solder (40% Pb, 60% Sn) which melts at 183°C. The use of commercial solder was avoided due to the presence of antimony which lowers the melting point and also inhibits the free flowing of the solder on copper and brass. Dilute ortho-phosphoric acid is the required flux for joints between stainless steel and copper, and surfaces must be scrupulously clean and pre-tinned.

The first assembly had revealed that bubbling of the hot flux during soldering could cause very small diffusive leaks which only became apparent at low temperatures; a problem also reported by A. J. Croft. Great care was taken, therefore, to ensure that all bubbling had subsided and the solder ran freely to form a smooth, shiny surface to the joint which was then examined under a magnifying glass. This process was repeated until each joint appeared perfect; a state usually achieved at the rate of one joint per hour.

The original top-plate and economiser vessel were found to be in good order and were reused. The needle valve was also used after regrinding of the phosphor/bronze seat. The thermal switch assembly was refurbished with new indium blocks and copper braid to ensure good thermal contact. The phosphor/bronze bellows were replaced with a new set of seamless construction: wall thickness 0.15 mm; o.d. 20 mm; i.d. 12.5 mm. The copper vacuum cans were all highly polished with abrasives and their base plates resaeled.

The reconstruction was interrupted at various stages for helium leak testing of the partially assembled levels of the cryostat with an Edwards LT104 mass spectrometer leak detector. Testing was carried out initially with the components at room temperature, and then with them immersed in liquid nitrogen. During testing of the internal vessel K, it was discovered that the walls had become porous. This is a common problem in copper vacuum vessels subject to thermal cycling, and is attributed to defects caused by the high temperatures required during silver brazing.⁴ The vessel was flame annealed, and a light coating of solder over the whole surface made it vacuum tight.

Once it had been established that the main body of the cryostat was free of leaks, the vacuum lead-throughs H were sealed into place. The use of new cryogenic lead-throughs tested to 4.2K by Oxford Instruments required the redesign of the middle and outer flanges of the cryostat to accommodate six 4-pin lead-throughs on the edges of each flange.

Lead-through failures had been encountered in the work of Clay, Jewess *et al.*, and this new batch proved to be no different. From the experience of the first assembly, it was deduced that the epoxy insulation on some of the lead-throughs was adversely affected if it became too hot during soldering.

The problem was overcome by individually testing the lead-throughs by sealing them onto a small test-flange connected to the helium leak-detector. The flange was then immersed in liquid nitrogen and the lead-through completely surrounded with helium gas. Only those lead-throughs, which showed no sign of helium leakage after several thermal cycles, were then used on the cryostat.

The assembly was finally completed by sealing on the demountable vacuum cans F, L, M with a quaternary eutectic solder (Bi 49%, Pb 18%, In 18%, Sn 15%) which melts at 80°C. After further vacuum testing at liquid nitrogen temperatures, copper flexitube and Klein flanges were attached to the pumping tubes at the cryostat top-plate for ease of connection to the new vacuum system.

2. 3. 3 The Calorimeter Vessel

The original calorimeter vessel A was tested and found to be in good condition, and the refurbishment consisted mainly of cleaning and rewiring.

The vessel is made from a platinum-iridium cylinder: 5 cm long; 2.5 cm diameter; 0.2 mm wall thickness. It is capped with platinum-iridium discs soldered into place with gold to ensure that the whole vessel is chemically inert to most experimental samples. The copper tube used for mechanical heat conduction is soldered onto the top of the vessel. The filling pot D is a short length of platinum tube (5 mm diameter) which is closed with a copper cap and a soft solder seal. The cap is previously fitted with a silver tube (1.1 mm diameter) for evacuation of the vessel and admittance of helium³ exchange gas.

The thermometer housing B is a protective compartment made from thin copper foil. It contains a small copper block soldered onto the base of the vessel, and drilled to accommodate two germanium resistance thermometers. The thermometers are coated with Apiezon T grease to make good thermal contact with the block. Soldered beside the block is a short copper tube for thermal anchoring of the calorimetric leads cable C. This 25 cm long cable consists of the current and potential leads of the thermometer and of the calorimeter thermopile junction.

The calorimeter heater was made with 10 m of 43 swg fibre-glass insulated Karma wire obtained from The Scientific Wire Company. The wire was wound non-inductively onto the cylindrical surface of the vessel and fixed into position with two coats of GE7031 low temperature varnish (Oxford Instruments). Karma alloy (76% Ni, 20% Cr, 4% Al/Fe) provides a high resistance heater with a very low temperature coefficient of resistance. This results in high stability for the current and voltage measurements required during calibration (see Chapter 4). The current leads to the heater are 34 swg double rayon insulated manganin wire. Each contributes a lead resistance of approximately 2 ohms to the circuit and would result in

an energy dissipation between the shield and the calorimeter amounting to 0.2% of the total heat generated in the calorimeter heater winding. This stray heat is accounted for by a wiring arrangement such that one potential lead is at the calorimeter end of the circuit and one at the shield end. The heater potential leads and all of the thermometer leads are 44 swg double rayon insulated manganin.

2. 3. 4 The Adiabatic Shield

The adiabatic shield F is made entirely from copper and can be split into three parts:

- the inner vacuum flange on the cryostat, with integral helium³ pot and thermal jaws;
- the demountable shield base flange;
- the shield heater cylinder.

The inner vacuum flange and helium³ pot were soldered onto their new pumping tubes, and the thermal jaws were treated as mentioned in section 2. 2. 4. Refurbishment of the rest of the shield consisted of complete rewiring, and provision of new vacuum lead-throughs and electrical distribution rings.

The calorimetric leads cable C is soldered to contacts on a Tufnol insulated distribution ring located on the interior of the shield base flange. The cable wires then pass to a similar distribution ring on the exterior via a 10-pin cryogenic vacuum lead-through. On the exterior, the wires change to the more durable 32 swg manganin required for connections to the shield heater cylinder.

The shield heater cylinder weighs 385 g and measures 20 cm long, with o.d. 55 mm, and wall thickness 2 mm. It has internal fittings which locate the tensioning screws used to suspend the calorimeter.

The outer surface of the cylinder has 15 vertical grooves which are used to thermally anchor the wires of the calorimetric cable.

The shield was stripped to the bare copper metal and thoroughly polished with wire wool. The surface was given two coats of GE7031 varnish and baked to provide a hard insulating shell. Lengths of 32 swg manganin wire were then embedded into the vertical grooves and a further two coats of varnish applied. Copper studded Tufnol distribution rings were positioned at the top and bottom of the cylinder and the wires soldered to their respective studs. The surface was wound with one layer of Micropore 3M surgical tape, coated with varnish and lightly baked to provide further electrical insulation before winding of the shield heater.

The shield heater was made from 32 swg manganin wire wound non-inductively and without gaps over the whole of the prepared surface. Approximately 80 metres of wire were used and this produced a heater resistance of 500 ohms at room temperature. Later a further 200 ohms of manganin wire was wound onto the surface of the helium³ pot to ensure that the inner vacuum flange was also adiabatically controlled. This was connected in series with the main heater to give a total resistance of 700 ohms.

2. 3. 5 The Differential Thermopile

The junctions G of the differential thermopile were made from double rayon insulated 44 swg manganin and 40 swg constantan wires, the bare ends of which were twisted together and soldered.

Initially GE7031 varnish was used to insulate the junctions and fix them to thin copper foil heat-sinks. This, however, contracted at low temperatures and peeled off the copper surface. A more durable fixture was made with Ecco Bond 286 epoxy adhesive which was recommended for its low temperature properties by Prof. R. G. Scurlock of the Cryogenic Advisory Unit, Southampton University.

Originally three junctions each were attached to lugs on the external surfaces of the adiabatic shield and the calorimeter vessel. This led to rather complex wiring at the shield-base lead-through, and more importantly resulted in a small but permanent offset from null in the adiabatic control circuitry (see Chapter 3). The problem was latterly overcome by fixing the shield junctions to the internal wall of the shield (as indicated in Figure 2A) which is the true adiabatic surface with respect to the calorimeter. This arrangement also simplified the wiring by reducing the number of thermopile wires emerging at the shield-base from 6 to 2.

A further 44 swg manganin wire soldered to the underside of the copper foil at the calorimeter end is used as the thermal switch indicator lead. This maintains electrical contact with the calorimeter vessel and is connected to a simple voltmeter circuit (see Appendix). The circuit is made when the thermal jaws bite onto the calorimeter vessel to cause cooling, and it is broken when the vessel is thermally isolated.

2.3.6 Further Wiring

Initially the gap from the top of the shield to a Tufnol distribution ring on the base of the internal vessel K was bridged with 36 swg manganin wire. However, during calibration runs below 4.2 kelvin (see Chapter 4) temperature instability was attributed to the thermal conductivity of these wires, and latterly the gauge was changed to 40 swg to significantly reduce thermal transfer and achieve stability.

At the distribution ring, the wires were changed to 36 swg enamelled copper wound round the vessel and varnished in place to thermally anchor at the temperature of the pumping pot.

Connections from the middle flange to outer flange lead-throughs, and thence to the economiser vessel, were made with 36 swg manganin wire. From this point the leads cable P was formed from

36 swg copper and passed to the cryostat top-plate through a tube filled with oil for insulation. The fine gauge cable was then distributed to the screened cables of the measurement instrumentation via an earthed casing attached to the experimental rig.

2. 4 THE CRYOSTAT VACUUM SYSTEM

2. 4. 1 The Experimental Rig

The experimental rig consists of:

- the cryostat;
- the cryostat vacuum system;
- the gas handling system.

These were all mounted on a mild steel framework (6' long, 2.5' wide, 10' high) which was solidly bolted to the floor and ceiling to dampen vibrations.

The cryostat was mounted at the front of the rig to allow easy access for a hydraulic fork-lift truck, used to raise a platform holding the stainless-steel and glass dewars. Once the dewars are in place around the cryostat, the platform can be fixed and the truck removed. The fork-lift is also used to raise the steel liquid helium transfer dewar to an adequate height for syphoning.

The rig was equipped with a No Volts Release/Earth Leakage protection unit to ensure complete electrical safety.

2. 4. 2 The Main Vacuum Lines

Figure 2B shows the vacuum and exchange gas systems serving the three vacuum chambers (F, L, M - Figure 2A) of the cryostat. The arrangement is adaptable, allowing complete independence of the chambers as required during calorimetric runs, but also allowing coupling of the chambers via the exchange gas system when fast

cooling is desired. All permanent vacuum pipework was made with standard Yorkshire copper tubing and brazed joints. The vacuum seals, components and equipment were obtained from Edwards High Vacuum Company. Demountable vacuum joints were made with Klein flanges, stainless steel centrings and Viton O-rings suitable for pressures down to 10^{-9} mbar. These allowed quick connection of the cryostat to the main vacuum system and also to test-apparatus. Floor mounted direct-drive rotary pumps were used to help minimise vibrations.

The high vacuum was achieved with water-cooled diffusion pumps fitted with bi-metallic fail-safe switches to avoid overheating during a break in the water supply. The pumps were filled with Silicone 704 fluid because its low vapour loss, low thermal degradation, and long term chemical stability would produce a generally rugged vacuum system capable of withstanding the rapid removal of large volumes of exchange gas.

For reasons of economy, Penning gauges, rather than ionisation gauges, were fitted to monitor the high vacuum, and SP25K diaphragm valves were used in preference to the more expensive all-metal bellows valves. The high vacuum components could all maintain better than 10^{-9} mbar.

In Figure 2B, the inner chamber/adiabatic shield is served by an EO2 diffusion pump and liquid nitrogen cold trap which combine to give an ultimate vacuum of 3×10^{-7} mbar at a pumping rate of 150 litres/sec. The high vacuum is monitored by a CP25K/Penning 1002 gauge down to 10^{-8} mbar. This is backed by a single stage E1M5 rotary pump which easily betters the critical backing pressure of 0.6 mbar. Alternatively, the critical pressure can be maintained in the 6×10^{-3} cubic metres of backing volume which can be baked and pre-evacuated to 10^{-8} mbar. This is monitored by a PRH10K Pirani gauge and Pirani 1001 controller, and can provide several hours of noiseless running with the rotary pump switched off.

The middle and outer chambers of the cryostat are evacuated by two F203 diffusion pumps fitted with H5L2 water-cooled baffles with integral cantilever isolation valves. This combination achieves an ultimate pressure of 3×10^{-7} mbar at a pumping rate of 70 litres/sec. Each pump is served by 1.5×10^{-2} cubic metres of backing volume, and the critical backing pressure of 0.35 mbar is easily bettered by a two-stage E2M5 rotary pump.

The helium exchange gas system is evacuated by any of the main vacuum lines. It comprises of a 1 litre capacity helium reservoir fed from a main cylinder, and the pressure is monitored to 1 atmosphere by a capsule dial gauge. Delivery of gas to the cryostat is via an LV10K fine control needle valve capable of sealing to 10^{-12} mbar. The equilibrium exchange gas pressure in each chamber is recorded by a PRL10K Pirani low pressure gauge of range 10^{-8} to 100 torr.

Figure 2B**THE MAIN VACUUM LINES**

⊘	Isolation valves
DP	Diffusion pump
NT	Liquid nitrogen trap
WB	Water-cooled baffle/isolation valve
PG	Penning gauge-head
PR	Pirani gauge-head
BV	Backing volume with heater
AV	Air admittance valve
FT	Foreline trap
NV	Fine control needle valve
CNV	Coarse needle valve
DG	Capsule dial gauge
HE	Helium ⁴ exchange gas reservoir

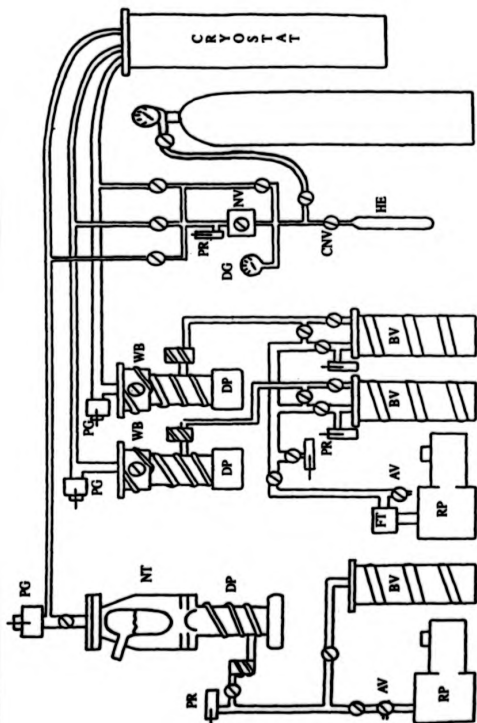


Figure 2B - The Main Vacuum Lines

2. 4. 3 The Gas Handling System

Figure 2C is of the gas handling system for the helium³ isotope intended for use in the evaporation pot (J - Figure 2A) and also as the exchange gas in the calorimeter vessel.

The advantage of helium³ is that whereas helium⁴ undergoes a lambda-transition at 2.17 kelvin^o which results in a highly adsorped super fluid film, the same transition does not occur until 0.1 kelvin with helium³. Therefore, in the pumped-liquid range of temperature, helium³ has a vapour pressure approximately 70 times^o that of helium⁴ and thus produces more efficient heat exchange. The main disadvantage of helium³ is its expense (£400/litre at 2 atmospheres), and completely independent all-glass handling systems are required to avoid contamination and losses.

The glass line is made from 0.2 mm capillary fitted with matching high vacuum capillary taps to minimise dead space. Evacuation is by a three-stage mercury-in-glass diffusion pump fitted with a liquid nitrogen trap, and backed with an E1M5 rotary pump. The vacuum is monitored by a CP25K Penning gauge.

Supply of helium³ gas is from a 1 litre lecture-bottle and the gas pressure is recorded by a PRL10K low pressure Pirani. The exchange gas may be transferred either to the utility port (for filling the calorimeter vessel) or to the evaporation pot by the piston action of the mercury reservoir. This pressure chamber is made from 10 mm wall Pyrex glass and filled with 5 litres of double distilled mercury. Pressure from a nitrogen cylinder applied via the three-way stopcock passes the mercury into two glass cylinders and compresses the exchange gas into the required chamber. Each cylinder is fitted with a ball-valve to check the flow of mercury, and the glass tubing is spiralled to cushion against the movement of the pistons. The reservoir and cylinders were placed over a metal tray and encased in a perspex box for added safety.

Figure 2C**THE GAS HANDLING LINE**

⊙	Isolation valves
MR	Mercury reservoir/pressure chamber
SC	Three-way stopcock
CT	Catchpot tray
GS	Glass spirals
PC	Piston cylinders
BV	Ball valve
PG	Penning gauge head
PR	Pirani gauge head
LB	Lecture bottle
UP	Utility port
NT	Liquid nitrogen trap
DP	Diffusion pump
PP	Rotary pump
IPL	Internal vessel pumping line
SVG	Swept volume gasometer
DPP	Drainage pressure-port

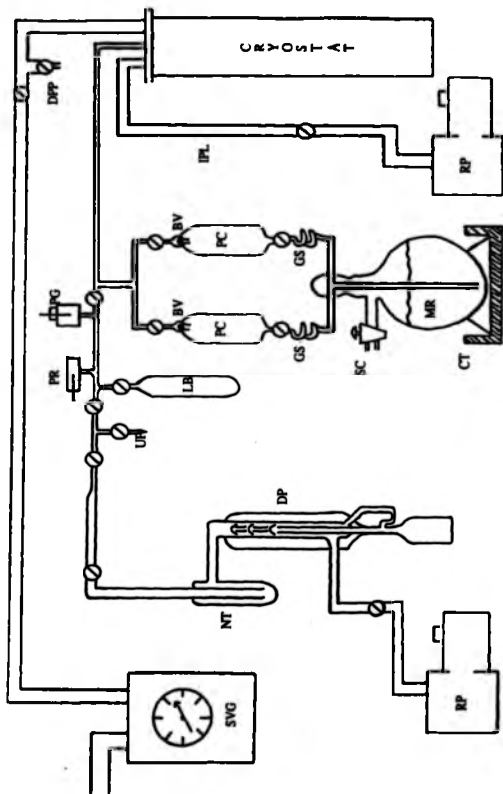


Figure 2C - The Gas Handling Line

Figure 2C also shows the internal vessel pumping line which is simply a double-stage E2M5 rotary pump throttled by an SP25K diaphragm valve to produce the fast pumping rates (up to 280 litres/sec) required for cooling to the lowest temperatures. Also illustrated is the gasometer line used to gauge the rate of refrigerant boil-off, and the drainage pressure-port through which the inner glass dewar can be pressurised to syphon out liquid nitrogen prior to operation at liquid helium temperatures.

2. 4. 4 The New Leak Detector/Analyser

All vacuum lines were initially tested with the Edwards LT104 helium leak detector. However, this unit was only on loan and also, due to its pneumatic automation, was rather prone to breakdown. The author, therefore, constructed a new manual leak detection system. This was based on the newly available ARGAs residual gas analyser, which utilised a compact quadrupole mass spectrometer (Vacuum Generators Ltd.) programmable up to 80 mass units.

Figure 2D shows the simple differential pumping system of two opposing rotary pumps, an EO2 diffusion pump and customised cold trap which ensure that the maximum operating pressure for the ARGAs (10^{-3} mbar) is always bettered, even for large leaks. The programmable features of the unit prove most useful in differentiating between external leaks to atmosphere and internal leaks to refrigerant as well as detecting outgassing of cleaning solvents.

TP Test Port
 RGA Residual Gas Analyzer
 CT Nitrogen Cold Trap
 DP Diffusion Pump
 FC Fan Cooler
 QSV Quarter Swing Valve
 PR Pirani Gauge Head
 RP Rotary Pump

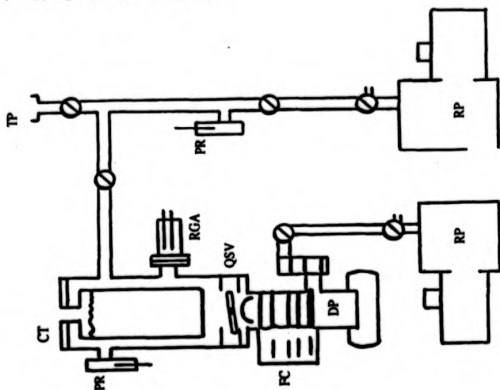


Figure 2D - Leak Detector Analyser

CHAPTER 3
INSTRUMENTATION

CONTENTS	PAGE
3. 1 THE SEMI-AUTOMATIC SYSTEM	46
3. 1. 1 Introduction	
3. 1. 2 The Calorimetric Method	
3. 1. 3 Computer Control	
3. 1. 4 The Data-latching Interface	
3. 1. 5 The Process Control Loop	
3. 2 PRECISION THERMOMETRY	60
3. 2. 1 The Germanium Thermometer	
3. 2. 2 Automatic AC Potentiometry	
3. 3. 3 Real-time Temperature Monitoring	
3. 3 ENERGY INPUT AND ADIABATIC CONTROL	73
3. 3. 1 The Calorimeter Heater Circuit	
3. 3. 2 The Adiabatic Shield Control Circuit	
3. 3. 3 The Shield Heater Power Supply	
3. 3. 4 Refrigerant Level Monitoring	

3.1 THE SEMI-AUTOMATIC SYSTEM

3.1.1 Introduction

As stated in Chapter 2, low temperature adiabatic calorimetry combines the techniques of precision thermometry, accurate measurement of energy input, and reduction of heat leak by adiabatic control. The sections which follow deal with the instrumentation and methods used in this laboratory to meet these requirements. The general principles of each system are summarised. Specific instrument settings and performance during calorimetry are dealt with in Chapter 4.

Overall, a system for semi-automated calorimetry was developed by the author with assistance from the University Electronics Workshop and the Microprocessor Group. Where possible, commercially available instruments were used and these were adapted and linked by commissioned circuitry as required.

Computer control was incorporated with the emphasis on software and the minimum of hardware. This was achieved using a program controlled data-latching interface constructed by the microprocessor technicians, with all of the process control software written by the author.

The instrumentation and methods for resistance thermometry duplicate those of Cryogenic Calibrations Ltd. (Aylesbury) who supplied and calibrated the germanium sensor.

The system for adiabatic control draws upon methods used in the Inorganic Chemistry Laboratory (Oxford) by Dr. L. A. K. Staveley.

3. 1. 2 The Calorimetric Method

Figure 3A illustrates the established calorimetric method of determining a heat capacity point by measurement of the temperature rise dT for a given electrical energy input dE .

The sensor temperature is monitored at regular time intervals to assess the equilibration of the calorimeter vessel. Thermal equilibrium is achieved when the observed temperature drift is linear and in the range $\pm 10^{-3}$ to $\pm 10^{-4}$ degrees per minute. The calorimeter heater is then switched on, and the foredrift temperatures extrapolated to obtain the starting temperature T_i . After an appropriate heating period, t , the heater is switched off and the afterdrift monitored to determine the final temperature T_f . The afterdrift then serves as the foredrift for the next point.

Adiabatic conditions are maintained throughout the heating and equilibration periods so that there is negligible heat loss, and the heat capacity can, therefore, be calculated from the applied dE and the observed dT with a minimum of corrections. Detailed calculations are given in Chapter 4.

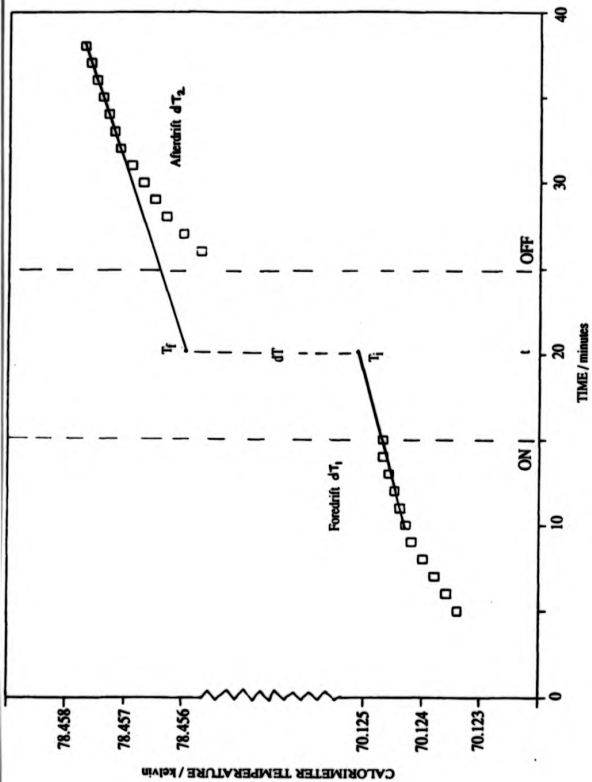


Figure 3A - Calorimetric Method

3. 1. 3 Computer Control

A brief survey of the literature^{17, 18} revealed that even in recent years calorimetrists had mainly relied upon manual methods of temperature monitoring and data collection. Usually the potential difference across the thermometer was meticulously recorded on data sheets, and the assessment of linear drift was made graphically for each point. The conversion of raw data to absolute temperature was then carried out at the end of experimental runs by comparison with temperature charts or by computation.

The relatively slow development of automated and computer controlled systems may be attributed to several factors. Firstly, most low temperature laboratories had been long established and employed relatively old instrumentation which usually proved incompatible with computer interfaces. Often development was not pursued due to the lack of time, funds and expertise, and also due to a lack of motivation.

The latter factor was partly justified by the view that low temperature calorimetry did not readily lend itself to automation, and that a great deal of time and money would be expended to achieve results which could be obtained manually. This was particularly true in laboratories where technicians were available to give assistance, and much of the labour of manual adiabatic calorimetry was reduced to several routine operations which could be performed comfortably and reliably.

As the low temperature laboratory at Stirling was to be newly constructed, this allowed for a fresh approach and provided an opportunity to incorporate automatic data collection and semi-automatic process control. This development was made viable because, in the past ten years, microcomputers had become less expensive and more adaptable, and expertise in interfacing was also readily available. In addition, a degree of automation was regarded as essential since the experiments would be run by one person;

therefore, it was important to minimise labour where possible.

Figure 3B is a schematic outline of the semi-automatic system which was developed in this laboratory. Specific details of the thermometry, energy input and adiabatic control components of the system are given later in this chapter.

In general terms, the system provides automatic thermometry, a semi-automated energy input process and fully automated maintenance of adiabatic conditions. The processes of thermometry and energy input are passive and must be initiated and synchronised by computer control. The adiabatic controller, however, is a continuously active unit which independently responds to and cancels out any temperature imbalance between the shield and the calorimeter vessel. The only manual tasks required are programming of the desired energy input and switching of range settings during the course of an experimental run. The operator is prompted to perform these tasks at the appropriate times, and is then free to monitor the whole experiment. In addition, the operator can manually override each process for troubleshooting purposes.

At the planning stage of the system, two fundamental decisions were made:

- (a) semi-automation was the most feasible method;
- (b) the semi-automated process should be software driven rather than hardware driven.

Development of a fully automated and integrated system was assessed to be impractical since it would have resulted in a complex and expensive interfacing project. It would also have placed severe restrictions on the range of instrumentation within budget. Similarly, a system, which was mainly software driven, was favoured because it would reduce the need for specialised micro-processing knowledge. It would also result in a style of computer control which was more user friendly and more adaptable than a dedicated hardware based system.

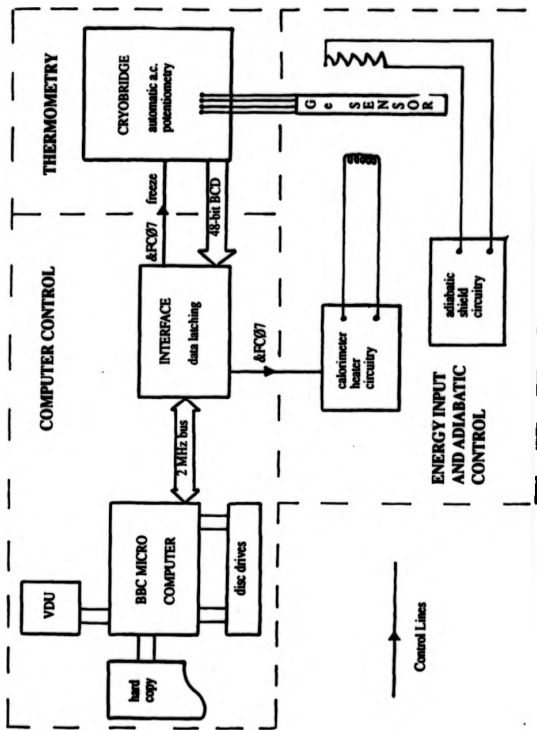


Figure 3B - Schematic Outline of Semi-automatic System

The computer control unit was based on the BBC Master 128K Microcomputer which was the most economical (£500) and versatile available. Additionally, Acorn had incorporated several design features, more commonly found in expensive computers, which rendered the BBC highly suitable for software driven interfacing.

In particular, the 65C12 microprocessor chip used in the BBC Master is capable of memory mapped interfacing. With this method, the chip identifies all of the input/output components, including interface registers, as discrete locations entered in the memory addressing space. Any interface register may, therefore, be made to function by simply incorporating its unique address code into the process control software. This type of communication is organised by the microprocessor bus structure which comprises of the address, data and control buses.

Through the address bus, the microprocessor may select any memory location, or any page of memory, and allocate it for use. Data may then be transferred via the bi-directional data bus on which the processor transmits data during write operations and receives data from the addressed locations during read operations. Since the bi-directional data bus is common to all of the memory and interface devices, it must operate on tri-state logic; the three states being:

- binary high;
- binary low;
- high impedance.

The high impedance state is the stand-by condition for all devices until specifically selected by the processor via the address bus. The transfer of data is implemented by the control bus which activates the read/write mode. This synchronises all bus operations and all data transactions at a frequency of 2MHz as determined by the master clock of the central processing unit.

The major benefit of using the microprocessor bus structure is that

it provides these essential organisational and interfacing functions as an integral part of the computer. This can considerably simplify intermediate interface hardware and lead to more direct coupling of the computer with external instruments.

3. 1. 4 The Data-latching Interface

The above listed computer facilities were put to good use and, as shown in Figure 3B, instrument control was achieved by assigning only two control lines. Also, data collection was fully automated through data-latching interface and a 48-bit path from the thermometry data source. In each case, control and latching was implemented through the bi-directional data bus in response to commands from the process control software.

The data-latching interface was required because frequency variations ruled out a direct coupling method between the data bus and the thermometry unit. As detailed in section 3. 2, thermometry was carried out using a Cryobridge self-balancing a.c. potentiometer and a germanium resistance thermometer. The Cryobridge is equipped with a parallel output port which is a source of binary coded decimal (BCD) data. Normally, BCD is an acceptable form for direct transmission to the microprocessor via its address and data buses. However, the frequency of Cryobridge output signals is mainly determined by the bridge balancing time. The minimum balancing time, using the germanium thermometer, was 40 milliseconds, thus producing data at a maximum frequency of 25 Hz. Since the operating frequency of the bi-directional data bus is 2 MHz, the computer can process information 80,000 times faster than the bridge can supply it. This can lead to the bus misreading data at the instant of cyclic change in the Cryobridge output.

The data-latching interface overcomes this synchronisation problem by instantaneously *freezing* the balancing process of the bridge. The frozen signal is then read to a storage buffer which only changes under program control, thus making data continuously available to the data bus.

The circuitry to achieve this is illustrated in simplified form in Figure 3C. The construction was based on the Intel 8212 chip which is a fully parallel 8-bit data register and buffer. The 8212 is specifically designed for input/output applications with microprocessors. It consists of an 8-bit latch with tri-state buffers plus control and device selection logic which allows direct connection to the microprocessor bi-directional data bus. A full pin-out and logic diagram of the 8212 is provided in the Appendix.

The input/output state of the buffer is switched by the mode control pin 2. When pin 2 is low, the input mode is enabled and the storage registers are primed to capture data from the Cryobridge. However, data may only be captured when the 8-bit latch is synchronised by the strobe function at pin 11. The signal to activate the strobe is provided by the 74103 1-bit latch which is memory mapped to the BBC. When the 74103 is addressed by the process control software, it applies a logical 0 signal to the Cryobridge pin D and *freezes* the bridge at balance for a period of one second. Simultaneously, the 74103 signals the strobe pin 11 to synchronise the data latch and capture data from the Cryobridge. Once captured, the data is continuously available on the buffer until the input mode is reactivated by the program. At the end of the one second *freezing* period, the program releases the bridge and a high signal on pin 2 switches the buffer to output mode. The BBC then reads the data onto its bi-directional data bus by applying a memory address code to the device selector pins 1 and 13 of the 8212 storage register. The raw data is then mapped to the memory workspace where it is immediately uptaken by the software for real-time conversion to absolute temperature and subsequent drift analysis.

Note that for simplicity only one 8212 storage register is shown in Figure 3C. In practice, six 8212 latches were required to accommodate the 48-bit BCD output from the Cryobridge. These were hardwired to the bridge output pins with each latch reading two 4-bit display decades as described in section 3. 2. 3. Also the second control line from the interface was assigned to activate the calorimeter heater circuitry as detailed in section 3. 3.

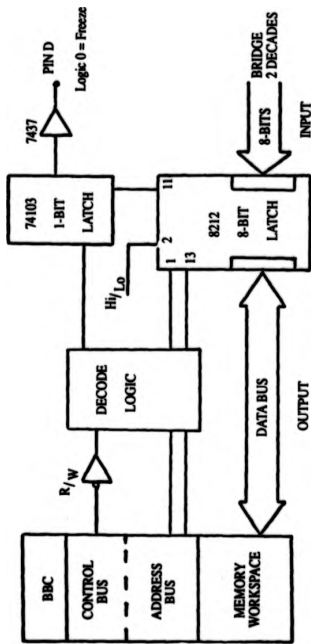


Figure 3C - Circuitry for Data to be continuously available to the Data Bus

All interface registers were mapped to BBC memory page FCXX. The specific address codes used in the process control software are

Table 3C - Cryobridge/BBC Interface Memory Map Page FCXX		
Address Code	Read/Write	Function
&FC00	R	Bridge data register 1
&FC01	R	Bridge data register 2
&FC02	R	Bridge data register 3
&FC03	R	Bridge data register 4
&FC04	R	Bridge data register 5
&FC05	R	Bridge data register 6
&FC06	W	Bridge freeze control
&FC07	W	Calorimeter heater

listed in Table 3C along with the function of each device.

3.1.5 The Process Control Loop

As narration of every individual step of the process control software would become pedantic and convoluted, clarity is best served by the

general explanation given below. However, if necessary, the reader may obtain a more specific understanding from the annotated listing of the program which is provided in the Appendix. The program is written in BBC BASIC language which allows a modular structure, with each module referred to as a procedure.

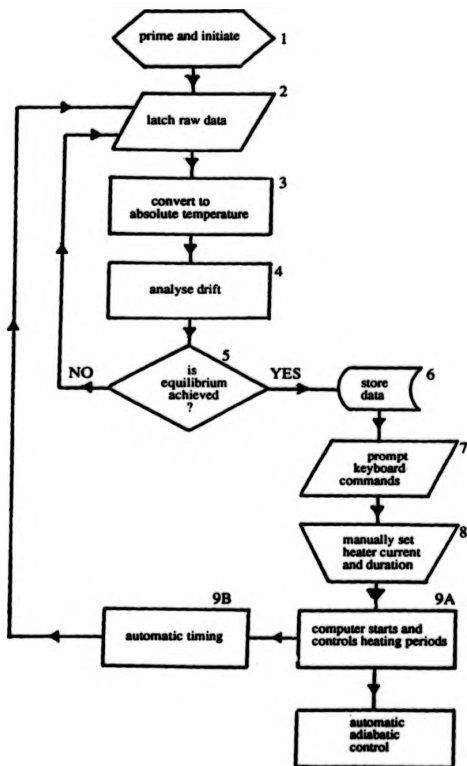
The semi-automatic process may be summarised with the aid of Figure 3D. Essentially this process control loop is a logical breakdown of the calorimetric method outlined in sub-section 3. 1. 2, but with the incorporation of procedures for program controlled interfacing and real-time display of absolute temperature.

In procedure 1, the program firstly reads a thermometry calibration file required during temperature conversion. It then assigns the address codes of Table 3C to each of the data latches and primes the interface to accept data.

The program then initiates the temperature monitoring cycle which comprises procedures 2 → 3 → 4 → 5 → 2. During this cycle, the Cryobridge is frozen and raw data latched onto the interface registers as described in sub-section 3. 1. 4. The program then reads each register and converts the raw BCD data to 8-bit binary which is multiplied out to produce a decimal value of the thermometer resistance.

With procedure 3, the program converts this resistance value to absolute temperature by comparison with the values in the thermometry calibration file and by polynomial calculation. The calculations to generate absolute temperatures in real-time are detailed in section 3. 2.

In procedure 4, the absolute temperatures obtained from six temperature monitoring cycles are analysed by least squares. The loop iterates until six consecutive temperatures display a linear drift of approximately 10^{-3} to 10^{-4} kelvin degrees per minute, at which point equilibrium has been achieved.

**Figure 3D - The Process Control Loop**

When the equilibrium condition has been verified at procedure 5, an audible alarm is sounded to attract the operator. The program immediately stores the starting temperature T_1 and the foredrift dT_1 to memory and branches to the interactive procedures 7 and 8. The operator is prompted to type in the desired heater current and duration, and then to manually set the exact current value on the dials of the calorimeter heater power supply. The program then prompts the operator to start the heating period by pressing the spacebar key.

In procedures 9A and 9B, the program reacts to depression of the spacebar by addressing the calorimeter heater circuit with code &FC07. This simultaneously switches on the heater and an external timer for the programmed period. At this point, the adiabatic controller independently responds and remains continuously active throughout the experimental run as explained in section 3. 3.

At the end of the heating period, the program returns to the temperature monitoring cycle to determine the equilibrium final temperature T_2 and the afterdrift dT_2 . These values are then stored and can also serve as the starting temperature and foredrift for the next heating period.

At the end of an experimental run, the values of T_1 , T_2 , dT_1 , dT_2 , i and t are transferred to analysis files for calculation of the heat capacity as detailed in Chapter 4.

3. 2 PRECISION THERMOMETRY

3. 2. 1 The Germanium Thermometer

The temperature dependence of the electrical resistance of doped germanium has been used for precision thermometry at low temperatures for many years. The thermometers which produce the best sensitivities in the range from 1 to 100 kelvin have been identified⁴⁹ as those with arsenic as the primary dopant. The resistance/temperature relationship of these thermometers tends to be rather complex because different conduction mechanisms dominate in different temperature ranges.⁵⁰ In general, behaviour below 10 kelvin is dependent upon impurity conduction which has a low activation energy. By 40 kelvin the activation energy has risen considerably and impurity conduction by excited states of the arsenic donors takes place. At higher temperatures, the dominant mechanism is thermal excitation of free carriers in the bulk germanium.

The useful working range of the thermometer is determined by the degree of doping since the resistance at liquid helium temperatures is acutely dependent on the exact amount of arsenic in the germanium lattice. The critical concentration of arsenic doping is that at which a Mott transition⁵¹ (free electron conduction) occurs, resulting in a low resistance at 4.2 kelvin and generally poor sensitivity above 20 kelvin with the sensor resistance rapidly attaining a constant value. Below the critical concentration an excessively high and unstable resistance value may be obtained at 4.2 kelvin. The level of doping for a low temperature sensor is, therefore, usually set within very narrow limits just below the critical concentration. The impurity level is varied between these limits to produce a variety of thermometers with sensitivities to suit particular temperature ranges.

As described in Chapter 2, the calorimeter vessel was fitted with a copper block which could accommodate two germanium thermometers - the intention being that one thermometer should cover below 4.2 kelvin, and the other from 4.2 to 100 kelvin to provide adequate sensitivity over the whole range.

A suitable pair of thermometers was donated by the Inorganic Chemistry Laboratory, Oxford. The first of these, a type CG1, had been supplied by Lake Shore Cryotronics Inc. of Ohio in 1963. This thermometer had been subjected to several recalibrations throughout the years, one of which was carried out at the National Physical Laboratory from 0.49 to 4.25 kelvin. During initial testing at Stirling, however, the thermometer proved to be unreliable and it transpired that it had been damaged during later calibrations at higher temperatures.

The second thermometer was a type CR2500L manufactured by Cryocal Inc. of Riviera Beach, Florida. Fortunately, this was of a modern design, using an intermediate level of arsenic to produce a general purpose sensor of adequate sensitivity throughout the whole range from 2 to 100 kelvin. The form of the sensitivity function $\frac{dR}{dT}$ is indicated in Figure 3E. Although the sensitivity is significantly reduced above 70 kelvin, the sensor resistance has not reached a constant value by 100 kelvin and remains within the maximum resolution of the Cryobridge (see Chapter 4).

Additionally, Cryocal avoided piezo-resistive variations²² by using bulk doped single crystal germanium, and thus ensured a high degree of reproducibility (less than 1 millikelvin shift) on repeated thermal cycling. The thermometer also supports a four-terminal bridge-shaped sensor element as recommended for precision potentiometry.²²

Due to the loss of the CG1 thermometer, calorimetry could only be performed with confidence in the 2 to 100 kelvin range. Therefore, the pursuit of cryostat temperatures below 2 kelvin by evaporation of helium²³ was postponed indefinitely.

Cryocal 250BL

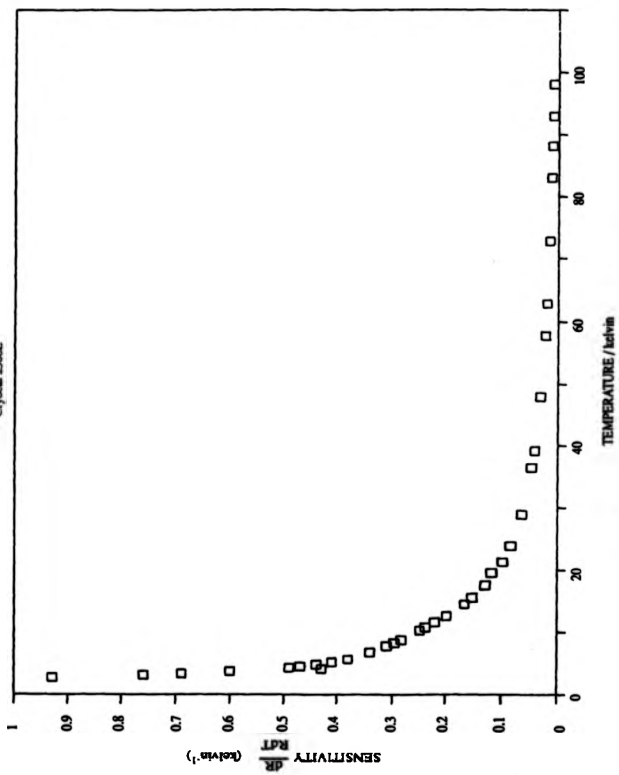


Figure 3E - Thermometer Sensitivity

The CR2500L thermometer had been calibrated by Dr B. W. Ricketson of Cryogenic Calibrations Ltd using a Cryobridge potentiometer to determine the 25 Hz a. c. resistance. The calibration table listing 57 temperatures from 2 to 100 kelvin is reproduced in the Appendix. In summary, the resistance varies through the range from approximately 6 Ω at 100 kelvin, 8 Ω at 77 kelvin and 390 Ω at 10 kelvin, rising to 2.8 k Ω by 4.2 kelvin and 17.5 k Ω at 2 kelvin.

The calibration down to 20 kelvin was against temperatures obtained from germanium, rhodium-iron and platinum thermometers whose own calibrations were accurate to ± 5 millikelvin of the IPTS(68) temperature scale. Below 20 kelvin, the calibration was against a National Physical Laboratory helium⁴ gas thermometer related to the boiling point of hydrogen using the IPTS(68) value of 20.28 kelvin. The accuracy of the calibration was certified to be ± 8 millikelvin. It was also certified that there were enough calibration points to obtain interpolated temperatures with an accuracy better than ± 0.01 kelvin up to 40 kelvin, and ± 0.025 kelvin up to 100 kelvin.

The distinct disadvantage of germanium thermometry is that the resistance/temperature relationship cannot be accurately expressed in simple analytic form. For precision thermometry, computer fitting must be employed and the relation closely approximated in polynomial form.

Blakemore, Winstel and Edwards⁴ have shown that the use of a single polynomial of the form

$$\text{Log}_{10} R = \sum_{i=0}^n A_i (\text{Log}_{10} T)^i \quad (1)$$

over the entire range from 1 to 100 kelvin can produce spurious oscillations with a mean deviation of 0.3% of the absolute temperature. This is inadequate for precision thermometry, and improvement is made by fitting over contracted and overlapping temperature ranges. The same paper reports adequate solutions from separate fits of equation (1) in the temperature ranges from 1 to 20 kelvin and 15 to 100 kelvin.

However, a superior procedure for the CR2500L sensor was suggested by Dr Ricketson.²² This added a third temperature range in recognition of the three overlapping conduction mechanisms which exist. The polynomial fitting was undertaken by P. R. Clayton of the Inorganic Chemistry Laboratory (Oxford) in conjunction with Dr Ricketson at the time of purchase of the thermometer.

The eight calibration points above 65 kelvin were fitted to the equation

$$R = A + BT^{-m} + CT^n \quad (2)$$

Initial guesses of the parameters A, B, C, m, n obtained from Dr Ricketson were refined by iterative least squares and converged to values given in Table 3F. This polynomial represents the data to within ± 1.6 millikelvin, with a mean deviation of 0.6 millikelvin.

The eighteen calibration points in the range 16 to 65 kelvin were fitted to the function

$$\text{Log}_{10} T = \sum_{i=1}^8 B_i [\text{Log}_{10}(R - A)]^i \quad (3)$$

in which the constant A was fixed by the value of parameter A of equation (2). With coefficients listed in Table 3F, the fit is better than ± 2 millikelvin, with a mean deviation of 0.8 millikelvin.

The thirty-three points in the low temperature range from 2 to 16 kelvin were fitted to equation (1) above, as suggested by Blakemore *et al.* The optimized coefficients are again shown in Table 3F. The maximum and mean deviations were found to be ± 2 and 0.9 millikelvin respectively.

These polynomials were all inspected by the author and were found to generate accurate temperatures as claimed. In particular, the overlap of equations (1) and (3) was examined, and it was found that, although there was no intersection, the functions ran very close with the derived temperatures at $R = 125\Omega$ being 15.8570 kelvin and 15.8573 kelvin respectively. Also equations (2) and (3) intersected

at 65.2308 kelvin with respective gradients of -5.485 kelvin/ohm and -5.493 kelvin/ohm. The validity of the calibration functions was therefore verified and they were used for all thermometry carried out in this laboratory.

Table 3F - Thermometer Calibration Functions

(1)		2 to 16 Kelvin	
	$\text{Log}_{10}R = \sum_{i=0}^8 A_i (\text{Log}_{10}T)^i$	A0 = 5.293407282 A1 = - 4.604301690 A2 = 6.785182928 A3 = -15.97228431 A4 = 22.78870807 A5 = - 8.600981650 A6 = -14.30638135 A7 = 15.60664217 A8 = - 4.394662565	
(2)		≥ 65 Kelvin	
	$R = A + BT^{-m} + CT^n$	A = 3.610677 B = 2.639594 × 10 ⁶ C = 9.072157 × 10 ⁻⁷ m = 2.008286 n = 2.659374	
(3)		16 to 65 Kelvin	
	$\text{Log}_{10}T = \sum_{i=0}^7 B_i [\text{Log}_{10}(R - A)]^i$	A = 3.6107 B0 = 2.243988 B1 = - 6.346392 × 10 ⁻¹ B2 = 2.133545 × 10 ⁻¹ B3 = - 2.170376 × 10 ⁻¹ B4 = 1.440569 × 10 ⁻¹ B5 = - 5.572205 × 10 ⁻² B6 = 1.156558 × 10 ⁻² B7 = - 9.232629 × 10 ⁻⁴	

3. 2. 2 Automatic AC Potentiometry

The obvious way to achieve precision thermometry in this laboratory was to duplicate the techniques of Cryogenic Calibrations Ltd. Hence the model 103 Cryobridge (supplied by Automatic Systems laboratories) was obtained for a.c. potentiometry with the CR2500L sensor. The Cryobridge has been specially designed for automatic resistance thermometry and is particularly useful with germanium thermometers.

Firstly, the Cryobridge operates with a very low current which minimises power dissipation within the sensor. This avoids errors due to self-heating, the magnitude of which can be greatly enhanced by the low thermal conductivity of germanium¹⁰.

Secondly, it employs a four lead null balance potentiometric method, such that no current flows in the potential leads during measurement. This is particularly important in determining the true voltage drop across a germanium sensor since the lead resistances are often comparable with the sensor resistance.

Thirdly, the bridge circuitry can preferentially resolve the very small thermometer potential in the presence of mains interference.

The bridge circuitry is shown schematically in Figure 3G. The circuit is an inductive arm ratio comparator. It is symmetrical and thus the two resistances to be compared, R_1 and R_2 , are interchangeable.

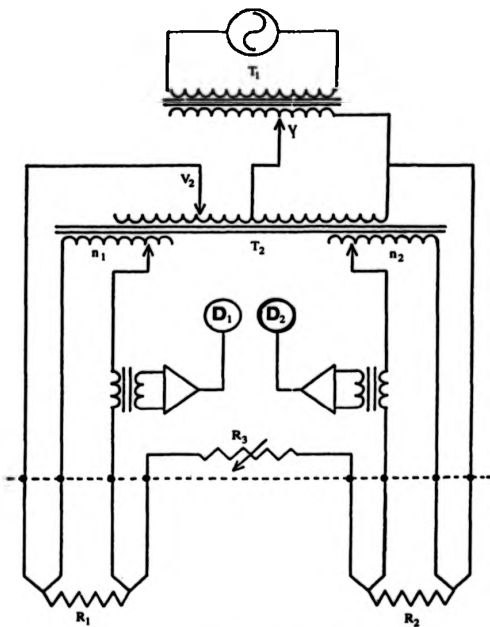


Figure 3G - The Cryobridge Circuitry

Power is from the transformer T_1 which steps down the mains supply to half frequency, providing a low noise source from which the two carrier voltages V_1 and V_2 can be tapped. The carrier supply V_1 determines the full scale voltage drop across R_1 and R_2 in series, and may be set at any of ten values from 10 microvolts to 300 millivolts. The drive voltage V_2 can be varied from 0 to 9.9 times V_1 to compensate for potential drops in the bridge circuit resistance R_2 , and in the leads of R_1 and R_2 . This ensures that the full scale setting of V_1 is always dropped across R_1 and R_2 , so that the voltage drop across each resistor can be accurately calculated from the ratio of the relative potentials n_1 and n_2 at balance. Thus with a resistance thermometer, the current and power can always be readily calculated and adjustment made to minimise the dissipation.

The relative potentials are separated out by the two-stage transformer T_2 which acts as an inductive divider, forming the two inductive arms of the bridge. The primary winding of T_2 sets the applied voltage V_1 , and on transfer to its multiple secondary winding this voltage is accurately divided into 10^6 equal parts. During measurement any potential difference in the arm made up of R_1 and the secondary n_1 is registered as an imbalance by detector D_1 . D_1 is an integrating phase-sensitive detector which sums the bridge imbalance signal for an adjustable period which is a multiple of the mains frequency. The detector quantises the imbalance signal into digital form which is then used by a digital servo to adjust the number of turns n_1 to achieve balance. A similar adjustment to n_2 is initiated by the imbalance signal at D_2 . Both detectors can discriminate against a constant background mains interference up to 5000 times the imbalance signal. Errors due to noise are thus negated in normal operation.

The Cryobridge balancing frequency is determined by the integrating period of the detectors. The highest detector sensitivity is obtained by integrating over the longest available period, 160 milliseconds, which gives a detector bandwidth of 6.25 Hz. With a germanium thermometer, however, this setting reduces the

balancing speed to the point where the imbalance cannot be nullified during normal calorimetry. Hence, a bandwidth of 25 Hz is adopted as a suitable compromise between sensitivity and balancing time. The digital servo thus balances the thermometer and a standard resistor at 25 Hz, simultaneously making the relative potentials n_1 and n_2 available to the display decodes in digital form and to the output port latches in BCD form. The potentials are displayed as six-figure numbers with the usual digital accuracy of ± 2 in the lowest decade.

At balance, the sensor resistance may be determined from the relation:

$$\frac{R_s(\text{sensor})}{R_s(\text{standard})} = \frac{n_1}{n_2}$$

In practice, due to the wide range of sensor resistance (17,500 Ω to 6 Ω), four different standard resistors were required to ensure accurate comparison throughout the range. Wilkins wire wound standard resistors of nominal d.c. resistance 10 000 Ω , 1000 Ω , 100 Ω and 10 Ω were connected to the R_s terminals of the Cryobridge via a high quality selector switch and screened cables. The resistances were maintained at 25.0°C \pm 0.1°C in a thermostatted oil bath. Due to the discrepancies which can arise between a.c. and d.c. measurements⁶⁷ the resistors were recalibrated at 25 Hz a.c. using the Cryobridge. The standard for this was a Wilkins type 5684C a.c./d.c. transfer resistor which had recently been calibrated at 99.9998 Ω \pm 3 ppm by H. Tinsley & Co. The determined a.c. values of the standards are shown in Table 3H. These values were used in all calculations of sensor resistance.

Also shown are the thermometer currents and power dissipations for the CR2500L sensor used with the Cryobridge. The process control software was equipped with a routine which prompted the operator to select the correct standard resistor for each temperature range, thus ensuring that full resolution and minimum power dissipation was always maintained.

**Table 3H - Standard AC Resistance
Thermometer Current and Power with the Cryobridge**

STANDARD AC RESISTANCE (Ohms)	TEMPERATURE RANGES (Kelvin)	THERMOMETER CURRENT (μ Amperes)	POWER DISSIPATION (Watts)
9998.616	2	0.3	6×10^{-9}
	4.2	1.0	4×10^{-8}
1002.207	4.2	3.3	4×10^{-4}
	10	10	5×10^{-3}
100.041	10	25	3×10^{-7}
	30	100	4×10^{-7}
9.997	30	200	2×10^{-6}
	100	700	4×10^{-6}

3. 2. 3 Real-time Temperature Monitoring

As stated, the Cryobridge displays the two relative potentials n_1 and n_2 to six decades. Each decade has a corresponding quad (4-bit) latch at the bridge output port. The 8212 registers of the data-latching interface can accommodate 8 bits, hence each 8212 was hardwired to two quad latches. Thus only six 8212 registers were required to read the full Cryobridge display as described in section 3.1. The BCD output is transferred to the BBC memory workspace where it is passed to the process control software. The pairs of 4-bit BCD digits are separated by logical MASK and SHIFT operators as detailed in the program listing. Each 4-bit digit is converted to binary and multiplied out to give standard decimal values of n_1 and n_2 . The potential ratio is then multiplied by the value of the relevant standard resistor. The resultant sensor resistance is converted to temperature using the thermometer calibration functions listed in Table 3F. These were incorporated into the process control software as separate procedures (see program listing) to produce a continuous real-time display of the calorimeter temperature.

The procedure to generate temperatures in the range from 16 to 65 kelvin is simple since equation (2) gives the temperature

explicitly. However, for equations (1) and (3) real-time solution requires interpolation and iteration.

Whenever a thermometer resistance, R_t , of 9.6637 Ω or less is registered on the Cryobridge, the software branches to the procedure for temperatures above 65 kelvin. This is an iterative loop using equation (3) in the form:

$$T_{i+1} = \left[\frac{B}{R - A - CT_i} \right]^{\frac{1}{n}}$$

The procedure contains a routine which makes a linear approximation between the calibration points above 65 kelvin to provide the initial guess of T_i corresponding to R_t . This is a good approximation since there is a low degree of curvature in this region. Iteration is complete when subsequent values of the function

$$F(T) = CT^n + BT^{-n} + (A - R)$$

have converged to give

$$F(T_{i+1}) - F(T_i) \leq 10^{-4} \text{ kelvin degrees.}$$

Similarly with resistances greater than 125 Ω , the software branches to the procedure for temperatures in the 2 to 16 kelvin range. The iteration in this procedure uses the Newton-Raphson formula which may be expressed as:

$$T_{i+1} = T_i - \frac{F(T_i)}{F'(T_i)}$$

Equation (1) of Table 3F is therefore converted to natural logs and expressed as

$$F(T) = A\theta - 0.4329 \left[\ln R - \sum_{i=1}^k A_i (\ln T)^i \right]$$

with

$$F'(T) = \frac{0.4329}{T} \left[\sum_{i=1}^k A_i i (\ln T)^{i-1} \right]$$

Due to the high curvature in this temperature range, a simple linear interpolation between the thirty-three calibration points provides a poor initial guess for T_1 which results in slow convergence. This was overcome by calculating 300 (R,T) data pairs from equation (1) at intervals of 0.05 kelvin and storing on a separate file. This file has already been referred to in the priming of the process control loop (Figure 3D). Linear interpolation between these data pairs then produced initial values of T_1 which were within 0.1% of the final value and rapidly converged such that

$$T_{i+1} - T_i \leq 10^{-6} \text{kelvin degrees.}$$

All of the procedures resulted in convergence within one second and thus all further work in this laboratory was carried out with the significant advantage of instant visual display of temperature.

3.3 ENERGY INPUT AND ADIABATIC CONTROL

3.3.1 The Calorimeter Heater Circuit

The heat capacity of most substances increases by a factor of 1000 to 10 000 in the range from 2 to 100 kelvin. Thus to provide adequate power, the current to the calorimeter heater winding must vary by a factor of at least 100. In view of this, a model 109 precision d.c. current calibrator was obtained from Time Electronics Ltd. This solid state device was factory calibrated and guaranteed to supply a stable current accurate to 0.03% of the set value. Currents are set manually using five decade switches and five range selectors to provide full-scale values of 99.99 μ A, 999.99 μ A, 9.999 mA, 99.999 mA and 1 amp.

To maintain stability throughout a normal day's work, the calibrator should not be switched off. Hence the supply terminals were connected to the heater winding via the switch circuitry shown in Figure 3I. The switches are all of the make-before-break type to preserve continuity of the supply. With this arrangement, the set current is supplied to a dummy load until heating is required. Heating can be initiated by the software through the solid state relay (address code &FCØ7) or by manual operation of switch S₁. In each case, switching the heater on simultaneously starts the clock and diverts the current from the dummy load. In the software mode, however, the heating period is pre-programmed and timing is provided by the internal BBC clock. Whereas in manual mode the clock is an external Thorn/EMI scaler timer which merely records elapsed time. This apart, the software and manual heating methods are identical.

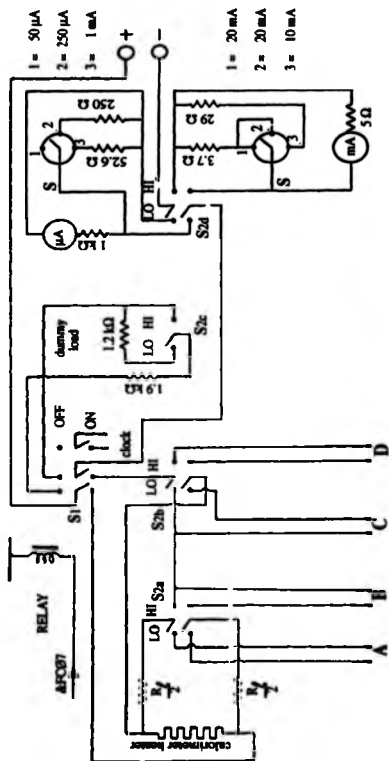


Figure 31 - Calorimeter Heater Switching Circuit

The remainder of the circuitry is provided mainly for the convenience of the operator. The four tier rotary wafer switch S_2 separates the circuit into LO and HI power modes. The LO setting selects microamp currents for calorimetry below 20 kelvin, whilst the HI setting selects the milliamp ranges for higher temperatures. A visual indication of the current is given by the microammeter or milliammeter as selected by the fourth tier $S2d$. The full scale reading of each meter can be varied by means of the shunt resistors set with switch $S8$.

The third tier $S2c$ changes the dummy load from 3.1 k Ω to 1.9 k Ω which approximates the total resistances (including external leads) of the heater circuitry at helium and nitrogen temperatures respectively.

The first two tiers $S2a$ and $S2b$ switch in the pairs of leads A, B, C, and D. These were built into the circuit to provide permanent terminals for easy connection of measurement instrumentation. The terminals were used with a precision d.c. potentiometric bridge and a digital voltmeter during calibration of the heater resistance as described in Chapter 4.

3.3.2 The Adiabatic Shield Control Circuit

During a heating period and on the approach to thermal equilibrium, radiative heat transfer is nullified by an automatic system which maintains the adiabatic shield at the same temperature as the surface of the calorimeter vessel. Sophisticated methods to achieve this have been developed (in particular by Westrum, Furukawa and McCullough²⁰ at the National Physical Laboratory), but essentially the methods all take the following form.

A temperature difference between the shield and the calorimeter generates an e.m.f. in the junctions of a differential thermopile. The signal is amplified, displayed on a chart and used to control the power supply to the shield heater winding. Heat is supplied to the

winding until the thermopile signal is cancelled and adiabatic conditions prevail.

The adiabatic control system constructed in this laboratory is illustrated in Figure 3J. This retains the essentials of the NPL and other methods, but uses simpler apparatus suggested by Dr L. A. K. Staveley from his experience in the Inorganic Chemistry Laboratory.

The fine wires of the manganin/constantan thermopile emerge at the cryostat top-plate and are soldered to contacts in a screened junction box. Here the wires change to heavy duty coaxial cables which pass to a three-way switch with silver plated wiping contacts to avoid any spurious e.m.f.

Setting (1) of the switch isolates the control unit from the thermopile and is used in extreme conditions to quickly shut down the circuit.

Setting (2) is used to attenuate the thermopile signal in conditions where a large temperature imbalance exists.

Setting (3) is for normal use and directly connects the thermopile signal to the preamplification stage of the circuit.

A type 6214 Tinsley photocell galvanometer amplifier was used as the preamplifier. This device rotates an internal mirror through an angle in proportion to the magnitude of the thermopile signal. The mirror deflects a light beam across an amplifying photodiode array to produce the output current. The benefit of this instrument is that the optical method displays superior stability, with the absence of zero-drift and almost no current noise. Indeed the only noise source was found to be mechanical vibration of the mirror and this was avoided by mounting the preamplifier separately from all other apparatus. Additionally, the amplifier has the facility for either current or voltage feedback with variable input impedance. Since the thermopile circuit resistance was 150 Ω , the amplifier was set for maximum voltage feedback which gave an input resistance of

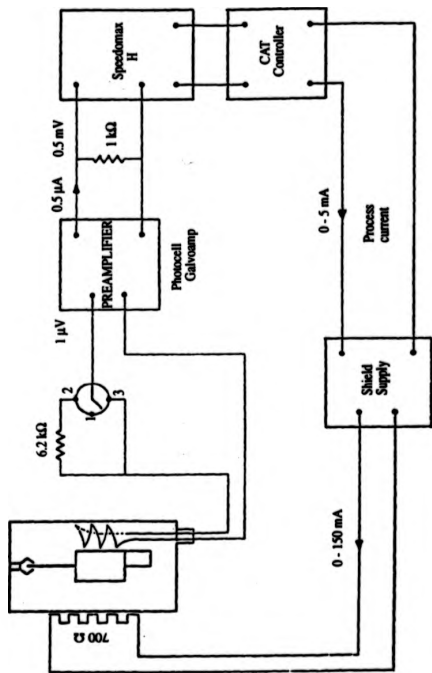


Figure 3J - The Adiabatic Control System

at least 1.5 k Ω , thus avoiding input attenuation of the thermopile signal. Direct measurement showed that the amplifier provided an output current of 0.5 μ amps per μ volt input, and this was passed through a 1 k Ω resistor to give an output voltage of 0.5 millivolts. Thus the voltage gain in the preamplification stage is 500.

The amplified thermopile signal passes to a Leeds & Northrup Speedomax H (model S) recording amplifier and controller. This visually displays the temperature difference as a deviation of the recorder pen from the centre-zero on a chart with full-scale deflections of ± 5 millivolts. The pen movement is controlled by a calibrated transmitting slidewire which also forms part of an internal bridge circuit.

At this stage the temperature differential sensed by the thermopile has been converted to a bridge imbalance signal. The imbalance signal is amplified and transmitted to an integral Leeds & Northrup series 80 current adjusting type (CAT) controller. In response to the bridge imbalance this unit produces a process-controlling current (0 to 5 mA) which may be used to regulate the shield heater power supply.

The process current is the sum of three terms and in theory it may be represented by an equation for damped oscillations such as

$$F(x) = Ax + B\left(\frac{dx}{dt}\right) + C\left(\frac{d^2x}{dt^2}\right)$$

where x is the deviation from the balance point.

In practice, the three terms are referred to as **Proportional**, **Reset**, and **Rate** controlling actions.

Proportional action provides a process controlling current which is proportionate to the magnitude of the temperature imbalance. The proportion is quantified as a percentage of full-scale through which the recorder pen must move to vary the process current from

minimum to maximum. Thus for a proportional band of 10%, the recorder pen need only move 0.5 millivolts for the process current to rise from 0 to 5 milliamps. A narrowing of the proportional band (i.e. reducing the percentage setting) causes greater proportional action and increases the sensitivity of the controller response. However, even at maximum sensitivity, the finite response time means that proportional action always lags behind the temperature imbalance. This is referred to as "following", and its accumulation can lead to a small but permanent drift away from balance. Reset action is required, therefore, to correct the process current and ensure that balance is achieved.

Reset action cyclically integrates the imbalance signal to determine the magnitude of the correction. It then repeatedly applies the correction but in proportion to the speed $\frac{d}{dt}$ with which the imbalance changes. This results in a gradual change in the process current until the balance point is reached.

The Rate control corresponds to the second derivative of the imbalance with time. Rate only becomes significant very close to balance and provides a measure of the acceleration of the recorder pen to or from the balance point. It corrects the process current in proportion to the acceleration. By so doing, Rate in effect tries to anticipate the power requirement to reduce time lag at the beginning of a heating period and to avoid overshoot on the approach to balance.

The optimum setting of each control term is dependent on the thermal characteristics of the cryostat and can only be determined by trial and error as described in Chapter 4. The optimum set of terms is that which results in smooth adjustment of the process current and thus steady control of the shield power supply. The process current may also be varied by manual control, and its approximate value is indicated on an output current meter.

3. 3. 3 The Shield Heater Power Supply

Figure 3K shows the circuitry of the shield power supply. The heater current is provided by a Kingshill 100 volt stabilised d.c. source which is regulated by a bipolar transistor. The d.c. source is connected across a 5 k Ω potentiometer to allow adjustment (0 to 100 volts) of the bias potential at the emitter junction. This sets the maximum heater current which can be drawn and thus allows appropriate power ranges to be selected for high and low temperature control.

When set at 100 volts, the current can be regulated up to 200 mA to provide high power for control above 20 kelvin. At lower temperatures, the power requirement rapidly falls off, due to the reduced heat capacity of the shield, and the bias potential is reduced to provide low power with a maximum output current of 15 mA.

The regulating transistor forms an emitter-follower circuit which means that the output current from the emitter is directly controlled by (or follows) the base potential. In this case, the regulator responds to the potential derived from the process current of the CAT controller which enters the circuit via the variable (2.5 k Ω) potentiometer. The setting of this potentiometer determines the sensitivity of the response. On selecting low or high power, the response is manually adjusted such that the maximum process current of 5 mA from the CAT controller results in maximum output current (15 mA or 200 mA respectively) being supplied to the heater. These adjustments ensure that the current is correctly regulated in each power range. During adjustment, the dummy load is selected to avoid uncontrolled heating of the shield.

Once the initial power adjustments have been made, the Leeds & Northrup controller can be relied upon to automatically maintain the temperature of the adiabatic shield to within a few millikelvin of the calorimeter over a prolonged period.

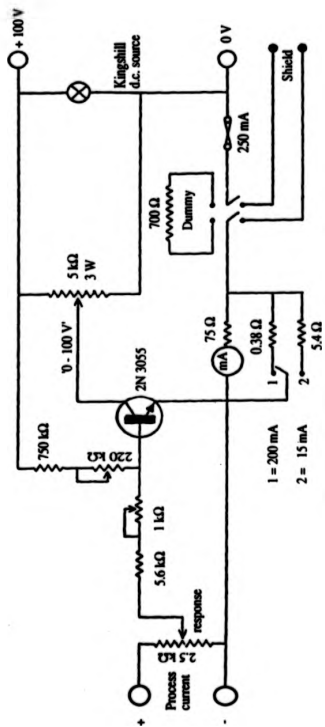


Figure 3K - The Circuitry of the Shield Power Supply

3. 3. 4 Refrigerant Level Monitoring

As illustrated in Chapter 2 (Figure 2A), liquid helium sensors were positioned at five levels in the cryostat. The sensors were purchased from the Clarendon Laboratory, Oxford where they had been developed. The author is grateful to Mr John Crosier, the Chief Electronics Technician, for specially preparing the sensors and providing the detector circuitry shown in Figure 3L.

The sensors are silicon transistors operating as forward biased diodes with a supply current of 1 milliamp. The protective casing of the transistor has been drilled to expose the semiconductor junction.

On contact with liquid helium, the resistance of the junction increases and the potential across the diode changes from approximately 2.5 volts to 3 volts. This fluctuation triggers the bistable transistor circuit to light the LED indicating liquid helium. When contact with liquid helium is broken, the circuit flips back to indicate that the sensor is surrounded by gas.

The five sensors are served by separate bistable detectors and LEDs each providing continuous monitoring of the refrigerant level. The sensors were initially tuned with the aid of a vibrating helium dipstick to verify the liquid level.

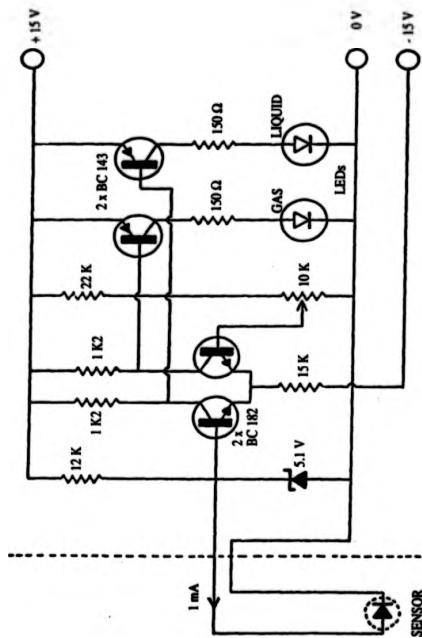


Figure 3L - The Detector Circuitry

CHAPTER 4
OPERATION AND CALIBRATION

CONTENTS	PAGE
4.0 INTRODUCTION	86
4.1 OPERATION OF THE CRYOSTAT	88
4.1.1 Routine Assembly	
4.1.2 Cooling with Liquid Nitrogen Refrigerant	
4.1.3 Cooling with Liquid Helium	
4.2 INSTRUMENT SETTINGS AND PERFORMANCE CHECKS	95
4.2.1 The Cryobridge and the Thermometer	
4.2.2 The DC Source and Timer	
4.3.3 The Adiabatic Control Circuit	
4.3 CALIBRATION	107
4.3.1 Resistance of the Calorimeter Heater	
4.3.2 Heat Capacity Calculations	
4.3.4 Heat Capacity of the Empty Calorimeter	
4.3.4 The Heat Capacity of Benzoic Acid	

4.0 INTRODUCTION

By this stage of the project, the construction of the cryostat, vacuum systems and instrumentation had all been completed. Semi-automatic control had also been incorporated and the general operating principles were broadly outlined. The objectives of the first phase of development had been achieved, therefore, and clearly the next major objective was calibration of the apparatus.

However, before calibration could begin an extensive period of familiarisation and testing was required so that practical working methods could develop through "hands on" experience of the apparatus. During this time, the best methods for routine assembly and cooling of the cryostat were determined. Suitable instrument settings were also identified, the limits of performance noted, and methods adopted which worked within these limits.

The transition from a collection of apparatus to a fully working unit which produced meaningful heat capacity results proved to be a lengthy one. At different times, each component of the apparatus displayed its own particular teething problems, and the greatest difficulty lay in having all of the components simultaneously in good working order. Initially, progress was made through simple bench testing of the instrumentation. This was followed by trial runs using liquid nitrogen and then liquid helium during which the resistance of the calorimeter heater was determined as a function of temperature.

The first attempts at heat capacity measurements were carried out on the empty calorimeter vessel. These ran smoothly above 50 kelvin but measurements with liquid helium were severely hindered due to repeated failure of the cryostat. It was at this late stage that the second reconstruction of the cryostat was undertaken using seamless bellows

and a tinned internal vessel as was described in Chapter 2. Following this the measurements with the empty calorimeter vessel were completed without further incident.

Finally, the heat capacity of a standard thermometric sample of benzoic acid was determined to complete the calibration of the apparatus and validate the methods.

4.1 OPERATION OF THE CRYOSTAT

4.1.1 Routine Assembly

The following methods were used in the assembly of the empty calorimeter vessel and cryostat prior to the initial cooling trials and calorimetric runs. Details of sample filling are given in the section on benzoic acid.

During assembly of the calorimeter vessel, the weights of silver tubing and solder were recorded to enable correction for the small variations which occur in different assemblies. The copper cap for sealing the vessel was tinned with hard solder. A length of silver tube was then passed through the cap and soldered into place with high melting (183°C) Pb/Sn solder. The lips of the vessel filling-port were tinned and the cap and tube sealed into place with a good fillet of the low melting (80°C) indium based solder. A glass socket with a capillary neck was slid over the silver tube and fixed into place with black wax. The greased socket was then fitted into the utility port (UP) of the glass vacuum line shown in Figure 2C. After leak testing with the helium detector, the vessel was evacuated to 6×10^{-6} millibar over 24 hours.

Beginning just above the copper sealing cap, a 2 cm length of the silver tube was crushed using flat-nosed crimping pliers. A cut was then made at the centre of the crimped section, and the cut end immediately sealed with indium solder.

With practice, the above sealing method proved to be reliable. However, on the first few attempts, air had obviously leaked into the vessel. Therefore, to avoid any uncertainty, the following test was carried out after every assembly of the empty vessel. The completed calorimeter

vessel was sealed into a vacuum chamber attached to a rotary pump. The chamber was evacuated for two hours and then repressurised with helium gas. After a further two hours, the calorimeter vessel was removed and placed in another chamber served by the helium leak detector. If no helium was detected, then the vessel was considered to be leak-free and the assembly routine continued.

The four nylon loops on the calorimeter vessel were each hooked onto their tensioning screws. The screws were then guided into their housings on the inner vacuum chamber and fixed with locking nuts. The tension in the loops was adjusted such that the copper heat exchange tube on top of the calorimeter vessel was positioned exactly in the radial centre of the cylinder with no free play, as shown in Figure 2A. Only in this position can the thermal jaws fully grip the tube and cause efficient heat exchange. At this stage, the thermal switch indicator lead was temporarily connected up, the inner chamber was pushed onto its cryostat flange, and the action of the thermal jaws was tested. Once the continuity of the circuit had been proven, the cylinder was removed from the cryostat and the assembly proceeded.

The wires forming the calorimetric cable were individually soldered to the lead-through pins on the shield base. Each circuit was checked for continuity, independence and isolation from earth. The shield base was then sealed onto the cylinder with the low melting indium solder, and the electrical circuitry was rechecked. After this, the top of the shield was soldered to a test flange on the leak detector and the base seal was helium tested. Following successful sealing of the base, the emerging wires were connected to the lower distribution ring of the shield and further electrical checks were made at the upper distribution ring.

At this point, the calorimeter vessel was successfully mounted and sealed inside the adiabatic shield, and the upper lip of the shield was cleaned and tinned prior to indium soldering onto its cryostat flange. The inner vacuum chamber was then fully leak tested on the cryostat. The cryostat wiring was completed by connecting from the upper ring of the shield to the Tufnol ring on the internal vessel. All circuits were then tested, firstly by multimeter, and secondly by seeking a positive response to switching on the instrumentation.

Prior to fitting the middle vacuum can, the two distribution rings on the surface of the adiabatic shield were wound with a layer of Micropore 3M paper tape to cover the solder points. This precaution was taken because electrical problems had previously arisen due to splashes of solder when sealing the middle can. The middle can and flange were cleaned and tinned and the can was preheated to assist the flow of the indium sealant. The middle chamber was then leak tested for external leaks via the flange seal, and also for any internal leakage from the internal pumping vessel and the inner chamber which were pressurised with helium for this purpose. Once the chamber was tested, the flange was cleaned, sprayed with acetone, and blow-dried to remove any traces of flux and moisture.

The outer vacuum can was then sealed and leak tested in a similar manner, and the liquid helium depth sensors were fixed to positions 3, 4 and 5 as shown in Figure 2A. The outer flange was then cleaned and sprayed with acetone followed by chloroform to aid drying. Particular attention was paid to drying the lead-throughs and the bronze bellows to avoid freezing problems during cooldown. The assembly routine was then completed with a final electrical check on all circuits.

4. 1. 2 Cooling with Liquid Nitrogen as Refrigerant

Following successful assembly and leak testing, the cryostat was connected to the vacuum system by means of its flexible connectors. The whole system was evacuated initially by rotary pump to 0.1 millibar, and then overnight by diffusion pump to at least 5×10^{-6} millibar. The glass dewar was also evacuated to 10^{-6} millibar and leak tested the following morning. This was routinely carried out prior to each cooling of the cryostat.

The cooling procedure began by placing the glass dewar inside the protective stainless-steel dewar and half filling with liquid nitrogen. The dewars were slowly raised around the cryostat using the hydraulic fork-lift. Once in position the rubber Leiden seal was rolled over the neck of the cryostat, and the dewar was filled with liquid nitrogen from a funnel through the syphon entry tube.

During the immersion of the cryostat, and at all subsequent stages of the cooling, each of the Penning gauges was closely monitored to detect any leaks which opened up when in contact with the refrigerant. When no leakage occurred, the pressure in the outer chamber rapidly dropped to around 5×10^{-6} millibar and continued to improve due to efficient cryopumping on the cold surfaces. The operation of the thermal jaws was then tested by winding the thermal-switch on and off several times. If the switch operated properly and no leakage was observed, the jaws were wound tightly onto the copper cooling tube of the calorimeter vessel. The internal pumping pot (Figure 2A) was then filled with liquid nitrogen by opening the needle valve and slowly throttling the E2M5 rotary pump shown in Figure 2C. The pot was usually filled after three minutes throttling, as indicated by the presence of liquid nitrogen in the flexible connector above the top-plate causing the surrounding air to liquefy. Once this was observed, the rotary pump was switched off and the internal assembly could be left to cool to 77 kelvin by conduction through the thermal switch in approximately twelve hours. This method was normally employed overnight to achieve a very stable temperature measurement when checking the performance of the thermometer (see section 4. 2. 1).

On most occasions, however, faster cooling was required and helium exchange gas was used in addition to the thermal switch. Once the internal vessel had been filled with liquid nitrogen and cryopumping had been observed in the outer can, the line isolation valve was closed and exchange gas was admitted via the fine control needle valve (Figure 2B) to a pressure of 50 torr. When this had cryopumped the surface of the middle can, helium was admitted at about 20 torr to the middle chamber. The inner vacuum was then monitored and, when the pressure dropped to 5×10^{-6} millibar, exchange gas was bled into the inner chamber to a pressure of 10 torr to assist cooling of the calorimeter vessel. By this method, the interior of the cryostat would cool to 77 kelvin within four hours.

To enable cooling below 77 kelvin, the exchange gas in the outer can was now pumped out and the can evacuated to at least 10^{-6} millibar. The economiser vessel was then filled with liquid nitrogen to minimise heat transfer down the cryostat tubes. The E2M5 rotary pump serving the internal vessel was switched on again to ensure that the vessel was filled with liquid nitrogen. The cryostat needle valve was then closed and the throttle valve fully opened to maximise the pumping rate and solidify nitrogen in the vessel. Pumping was maintained to sublime the nitrogen and cool the internal assembly. The calorimeter vessel was normally cooled to 55 kelvin within three hours, and at this point the helium exchange gas in the inner chamber was pumped away and the chamber evacuated by diffusion pump. The exchange gas pressure in the middle chamber was also reduced to about 5 torr which provides the heat leak necessary for the adiabatic shield as explained in section 4. 2. 3. The calorimeter continued to cool via the thermal switch and, after a further two hours, the temperature stabilised between 50 and 53 kelvin. The thermal switch was then opened to isolate the calorimeter vessel. Typical conditions may be summarised as follows:

Thermometer reading	50 - 53 kelvin
Thermal drift	0.5 millikelvin/minute
Inner chamber pressure	5×10^{-6} millibar
Middle chamber pressure	5 torr helium ⁴ exchange gas
Outer chamber pressure	10^{-5} millibar
Thermal switch	Off.

Thus, the cryostat was now ready *either* for heat capacity measurements above 50 kelvin *or* to begin the cooling procedure with liquid helium.

4. 1. 3 Cooling with Liquid Helium

The interior of the cryostat was cooled to approximately 52 kelvin as detailed above. Once this had been achieved the calorimeter vessel was thermally isolated and the exchange gas was pumped

out of the middle chamber. Evacuation of all chambers was carried out overnight and the internal vessel was continuously pumped to sublime away the remaining nitrogen. By the morning the pressure in all cans was better than 10^{-5} millibar and the internal temperature had normally risen to around 55 kelvin. The rotary pump serving the internal vessel was switched off and the outlet valve to the gasometer (Figure 2C) was closed.

With the liquid transfer syphon fixed into the cryostat, liquid nitrogen was syphoned out of the glass dewar by applying pressure to the drainage pressure pot (DPP, Figure 2C). This also precooled the syphon prior to liquid helium transfer. Once the glass dewar was empty, the drainage port was closed, the gasometer was reopened and the drained liquid nitrogen was used to replenish the stainless-steel dewar and the economiser vessel. A Statebourne 30 litre liquid helium storage dewar (model SD30) was then carefully raised by fork-lift until the syphon was immersed in liquid helium. This caused rapid boiling and the helium vapour further cooled the syphon and the dewar. After the initial boiling had subsided, the storage dewar was steadily pressurised until liquid helium flowed into the glass dewar. An indication of the rate of transfer was gained from the volume swept by the gasometer, and the liquid level was monitored by the liquid helium depth sensors. As soon as the lowest sensor showed that the outer can was in contact with liquid, exchange gas was admitted to the outer and middle chambers to a pressure of approximately 20 torr, and the thermal switch was closed. High vacuum was always maintained in the inner chamber to avoid the problem of helium adsorption onto the surface of the calorimeter vessel. The liquid transfer was continued slowly until the gasometer indicated that rapid boiling had ceased. The liquid level was then raised above the highest helium sensor and was maintained between sensors 1 and 2 whilst liquid was throttled into the internal pumping vessel. The thermal switch then cooled the calorimeter vessel to 4.2 kelvin within 3 to 4 hours, and normally 11 to 12 litres of liquid helium had been used to achieve this.

Through experience, it was found that temperature stability below 4.2 kelvin could only be achieved when the pressure in the outer can was at least 10^{-4} millibar. Higher pressures resulted in inadequate insulation for the internal pumping vessel and a rapid return to 4.2 kelvin. Due to helium adsorption, pressure reduction was slow with 10^{-4} millibar only being achieved after 2 hours pumping. The internal vessel was then refilled by throttling for 2 minutes, the needle valve was closed, and the pumping rate maximised to solidify helium. This cooled the calorimeter to 2 kelvin within 1 hour. The exchange gas in the middle chamber was then pumped away and the thermal switch was opened to isolate the calorimeter. The temperature usually stabilised within 10 to 15 minutes, after which heat capacity measurements could commence. Typical cryostat conditions at this stage were:

Thermometer reading	2 to 2.2 kelvin
Inner chamber pressure	$< 10^{-6}$ millibar
Middle chamber pressure	10^{-5} millibar
Outer chamber pressure	5×10^{-5} millibar
Liquid helium level	Above sensor 2
Thermal switch	Off.

4. 2 INSTRUMENT SETTINGS AND PERFORMANCE CHECKS

4. 2. 1 The Cryobridge and the Thermometer

The Cryobridge settings were determined from the operating instructions manual¹⁰ in conjunction with recommendations for germanium thermometry outlined in the technical brochure of Cryogenic Calibrations Ltd.¹¹ These specified two main requirements for good performance:

- Firstly, the current supplied to the thermometer must be controlled at a level which does not cause more than 1 millikelvin of self-heating in the sensor.
- Secondly, the setting of the Cryobridge detector sensitivity must complement the sensitivity of the thermometer such that a temperature change of 1 millikelvin can be resolved throughout the whole temperature range.

The first requirement was met simply by observing the maximum power dissipation allowed by Cryogenic Calibrations. The carrier supply voltages were set at

$$V_1 = 3 \text{ millivolts, and}$$

$$V_2 = 1.4 \times V_1$$

which ensured that the voltage drop across the sensor and the standard resistor were always of the same order of magnitude and, therefore, equally resolved. Table 4A shows that the thermometer currents resulting from these settings always produced

a power dissipation which was less than the allowed maximum. Self-heating was thus maintained below 1 millikelvin throughout the whole temperature range.

The settings to achieve 1 millikelvin resolution were determined from the thermometer sensitivity curve, the form of which was illustrated in Figure 3E in Chapter 3. The higher the thermometer sensitivity, the lower the number of significant figures which must be read by the Cryobridge. For example, at 4.2 kelvin the magnitude of the thermometer sensitivity function $\frac{dR}{dT}$ is approximately 0.5. To detect a 1 millikelvin change this requires resistance resolution $\Delta R = 0.5 \times dT = 0.5 \times 0.001 = 5 \times 10^{-4}$. Hence the bridge must always read at least four figures, and five figures will always be sufficient. The Cryobridge resolution was therefore set to five decades since this would always resolve the range from 4.2 to 10 kelvin.

Table 4B shows the thermometer sensitivity and the number of decades of resolution which were set in each temperature range. As mentioned in Chapter 3, the thermometer sensitivity significantly reduces above 70 kelvin. However, as can be seen, the resistance resolution required at 100 kelvin is $\Delta R = 8 \times 10^{-4}$ which remains within six decades.

In addition, the *Resistance Range* dial of the Cryobridge was adjusted as shown in Table 4B such that the range setting matched the order of magnitude of the thermometer resistance. This effectively tuned the Cryobridge detector sensitivity to that of the thermometer. All settings were adjusted manually following a prompt from the computer software, and with these settings 1 millikelvin resolution was maintained over the whole temperature range.

On two occasions during the initial cooling trials, all of the cryostat chambers were evacuated and the internal vessel was filled with liquid nitrogen. The thermal jaws were wound tightly onto the cooling tube of the calorimeter vessel and the apparatus was left overnight to equilibrate at the temperature of the refrigerant. Each morning, the equilibrium temperature was recorded by the

Cryobridge, and a measurement of atmospheric pressure was taken from a Fortin barometer. The measurements of 77.286 kelvin at 756 mm Hg, and 77.303 kelvin at 757 mm Hg compare favourably with values of 77.283 kelvin and 77.295 kelvin respectively which were obtained from tables.⁶¹ The measurements are both within the ± 0.025 kelvin accuracy quoted for the thermometer calibration (Chapter 3) and thus indicate satisfactory performance.

Strictly, the accuracy of measurement should be checked at a fixed point such as the argon triple-point. However, as the cryostat had no facility to precisely regulate the vapour pressure, purchase of an argon triple-point cell would have been required. These were available from the National Physical Laboratory, but the cost was prohibitive. Also, it was desirable to avoid the potentially damaging rewiring of the thermometer to the cell. In view of this, the accuracy of the factory calibration was accepted as it was carried out using a Cryobridge and standards traceable to NPL. In addition, heat capacity measurements were planned using a standard thermometric sample of benzoic acid, and thus the whole system would be validated prior to measurements on unknowns.

TABLES 4A, 4B: CRYOBRIDGE SETTINGS

detector bandwidth: 25 hz

carrier supply: $V_1 = 3$ millivolts; $V_2 = 1.4 \times V_1$

resistance standards: external

Table 4A - Power Matching

Sensor temperature (K)	Resistance (ohms)		Sensor current (μ amps)	Power dissipation (watts)	
	sensor	standard		sensor	allowed
2	17 500	9998.616	0.1	1.8×10^{-10}	10^{-8}
4.2	2 800		0.2	1.5×10^{-10}	
4.2	2 800	1000.207	0.8	1.8×10^{-9}	10^{-7}
10	390		2	1.6×10^{-9}	
10	390	100.041	6	1.4×10^{-8}	10^{-7}
30	32		23	1.7×10^{-8}	
30	32	9.997	71	1.6×10^{-7}	10^{-6}
100	6.5		188	2.0×10^{-7}	

Table 4B: Sensitivity and Resolution Matching

Sensor temperature (K)	Sensor resistance (ohms)	Resistance range (ohms)	$\frac{dR}{dT}$ (K)	$\frac{dR}{R}$	Resolution decades
2	17 500	10 000	1.5	1.5×10^{-3}	4
4.2	2 800	1 000	0.5	5×10^{-4}	5
10	390	100	0.2	2×10^{-4}	5
30	32	10	0.05	5×10^{-5}	6
100	6.5	10	0.008	8×10^{-4}	6

4. 2. 2 The DC Source and Timer

The model 109 d.c. current calibrator supplying the calorimeter heater was bench tested prior to use. For this purpose the calibrated Wilkins resistor ($99.9998\Omega \pm 3$ ppm) was wired in series with the supply. The voltage dropped across the resistor was measured by the null balance method using a six decade Pye precision potentiometric bridge (resolution 0.1 μ volts), Scalamp galvanometer and preamplifier. The galvanometer drift was measured as 0.00001 volts per minute and the bridge was always balanced within one minute.

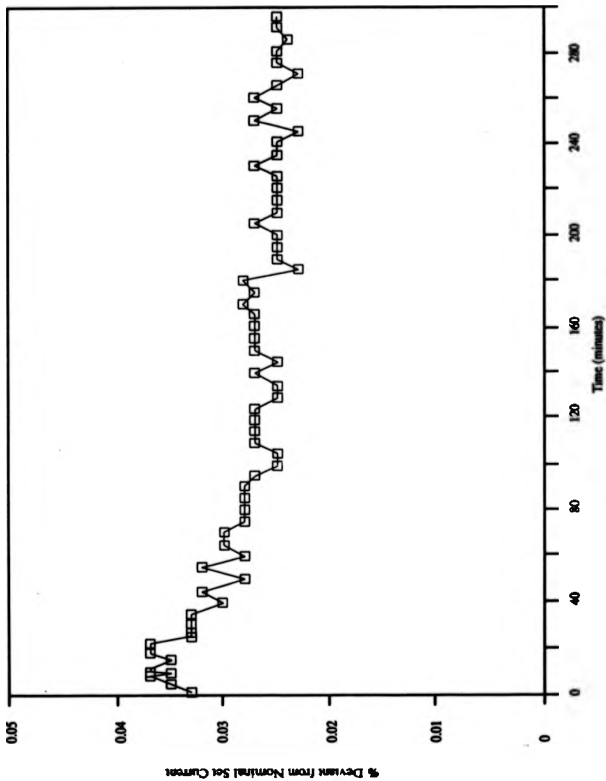
During the first series of tests, the supply accuracy was found to be closer to 0.05% than the specified accuracy of 0.03%, and the unit was returned to Time Electronics for recalibration. On return, the variation in current was measured as less than 0.03% in the ranges below 1 milliamp. However, above 1 milliamp the supply required a "warm up" period of one hour before accuracy better than 0.03% was achieved. Also, the maximum drive voltage of the instrument was found to be 15 volts and, as the load resistance due to the calorimeter heater was approximately 2000 ohms, this meant that the maximum supply current which could be drawn without error was 6.5 milliamps. Graph 4C shows the percentage variation for a current of 6 milliamps over a five hour period. To avoid deviations greater than 0.03% the d.c. source was always switched on and passed through the dummy load (Figure 3I) for at least one hour prior to commencing calorimetric measurements.

As explained in Chapter 2, heating of the calorimeter was usually software initiated, and the duration determined, by the BBC clock. This type of clock utilises a quartz oscillator chip which, although providing excellent precision, can be prone to inaccuracy. Therefore, the timing of this clock was checked against the Thorn/Emi scaler timer (accuracy ± 2 milliseconds) which was intended for use during manual heating periods. This revealed that there was a systematic error in the oscillator. The error was cumulative, but well behaved, and was readily quantified by a linear least-squares fit (correlation

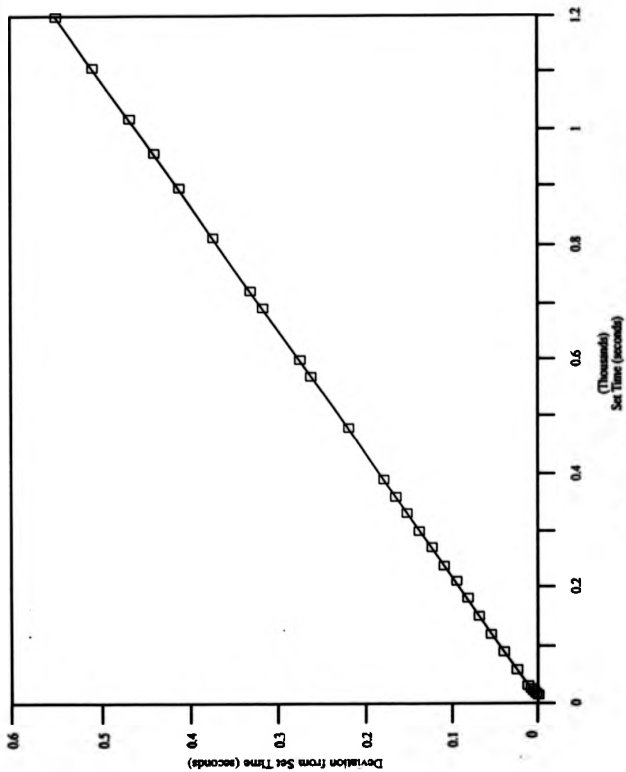
coefficient 0.9999) as shown in Graph 4D. The timing was corrected using the formula:

$$\text{HEATING PERIOD t(seconds)} = (1.00046 \times \text{SET TIME}) - 0.0035.$$

With this correction incorporated into the control-software, the heating period was always timed with an accuracy of ± 2 milliseconds.



Graph 4C - D.C. CURRENT CALIBRATOR
Variation of Drawn Current with Time



Graph 4D - Correction of BBC Oscillator Time
Timing of Heating Period

4. 2. 3 The Adiabatic Control Circuit

The function of the adiabatic control circuitry (Figure 3J) has been described in section 3. 3. 2. The precision of the control is determined by two factors. These are firstly the accuracy with which temperature imbalance between the calorimeter and shield can be detected, and secondly the response of the C.A.T. controller to cancel this imbalance.

Detection of temperature imbalance is limited by the sensitivity of the differential thermopile and by the resolution of the Speedomax "H" recorder. The detection circuitry was designed to produce a voltage gain of 500 at the preamplification stage. Thus a 1 microvolt signal from the thermopile becomes a 0.5 millivolt input to the Speedomax. A preamplification gain of 1000 was also tested but was unstable, and the gain of 500 proved to be the best compromise between stability and sensitivity.

The null-balance mechanism of the Speedomax has a quoted deadband of $\leq 0.15\%$, and the error in the null-point can thus be ± 7.5 microvolts for the ± 5 millivolt span instrument. Dividing by the preamplification gain, this means that thermopile signals of magnitude less than 0.015 microvolts will not be resolved. Since the sensitivity of each thermocouple rises from 0.66 microvolts per kelvin at 2 kelvin to 19 microvolts per kelvin at 100 kelvin,²³ the sensitivity of the three junction thermopile rises from approximately 2 microvolts per kelvin to 60 microvolts per kelvin. Hence, the 0.015 microvolt detection limit equates to a temperature imbalance of ± 8 millikelvin and 0.3 millikelvin when controlling at 2 kelvin and 100 kelvin respectively. Therefore, on cooling from 100 kelvin to 2 kelvin, the accuracy with which the shield and calorimeter can be made isothermal decreases by one order of magnitude. This, however, is more than compensated for by the effect of radiative heat transfer (proportional to T^4) decreasing through several orders of magnitude. The detection accuracy is thus sufficient for adiabatic control throughout the whole temperature range.

The response of the C.A.T. controller is dependent on the settings of the Proportional, Rate and Reset dials. As explained in section 3. 2. 2, these three terms are independent and must be tuned through trial and error. Prior to tuning, the cryostat was cooled to 77 kelvin. The inner chamber was evacuated and exchange gas was retained in the middle chamber at a pressure of 3 torr to provide a heat leak for the adiabatic shield. To balance out the cooling caused by this exchange gas, the controlling slidewire of the Speedomax "H" was adjusted so that the calorimeter would appear to be slightly hotter than the shield and a small current would pass through the shield heater even when there was no signal from the thermopile. A further adjustment was then made so that the current to the shield was immediately switched off if the shield became hotter than the calorimeter. The author is grateful to Mr. John Anderson of Leeds and Northrup for making these adjustments and for his advice on finding the best set of control terms as described below.

The adiabatic control circuitry was switched on and the calorimeter was heated in the range from 77 to 100 kelvin using a current of 6.5 milliamps. By operating in the highest temperature range and using the maximum rate of heating, the C.A.T. tuning was determined under the most rigorous operating conditions which would be encountered. Thus the set of terms producing smooth control for these conditions would also be suitable for the whole range of operation.

The tuning began by adjustment of the Proportional dial to the narrowest band (10%) which avoided oscillation in the trace of the Speedomax "H". Reset action was then gradually increased to return the trace closer to the null point. Once oscillation appeared, the Reset was fixed (15%) and the Proportional band was increased until the oscillation disappeared (20%). The maximum Rate setting which minimised overshoot of the null point was then determined (0.1).

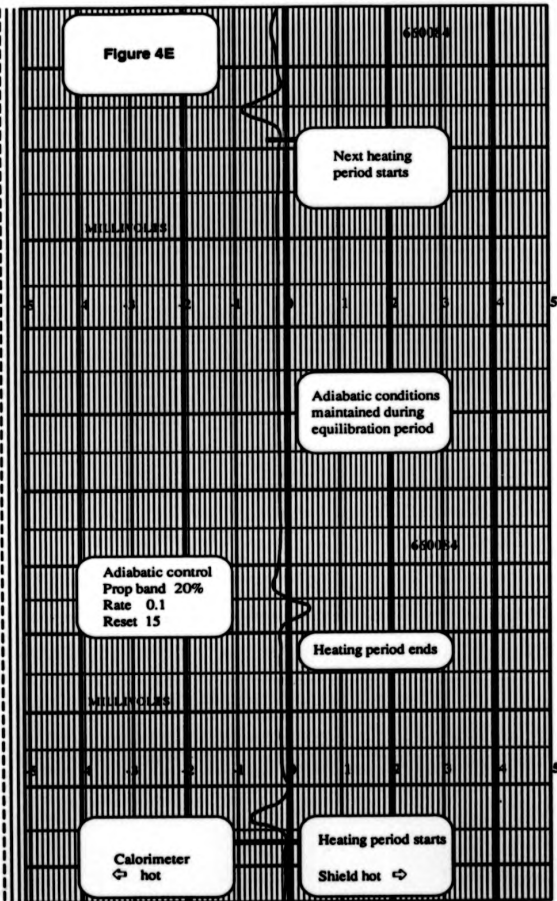
Figure 4E illustrates the control achieved with the terms set at 20%, 0.1 and 15 during a heating period of 5 minutes at 6.5 milliamps above 90 kelvin. The characteristics of the trace may be explained as follows. Firstly, the true null point does not coincide with the centre-

zero of the chart due to the slidewire adjustment described above. With the trace at the true null point (-0.2 millivolts) the temperature imbalance between the shield and calorimeter is the detection limit of 0.3 millikelvin. The current in the shield due to the offset from centre-zero is just enough to cancel the shield heat-leak at this point. If the trace becomes more positive than the null point then the shield is hotter than the calorimeter and the shield current immediately switches off. Conversely, a more negative trace means that the calorimeter is hotter and the controller increases the current to the shield.

When the calorimeter heater is switched on, the thermal inertia of the adiabatic shield results in a small temperature lag between the surfaces of the shield and the calorimeter vessel. After 30 seconds, the temperature difference has peaked at approximately 20 millikelvin and it is automatically reduced to null by the controller within one minute, so producing the negative peak on the recorder trace. Null balance is then maintained until the end of the heating period.

When the calorimeter heater switches off, the surface temperature of the calorimeter vessel decreases as thermal energy is conducted into the sample and to the thermometer. In this case, the thermal lag makes the shield slightly hotter than the calorimeter, the shield current switches off, and the heat-leak cools the shield. The temperature differential again peaks at 20 millikelvin and is nullified in approximately one minute. The controller then maintains null balance during the equilibration period of the calorimeter and until a further heating period commences.

The set of control terms thus produces a smooth response with compensating positive and negative temperature peaks associated with the adiabatic shield. Therefore, there is no nett thermal transfer between the shield and calorimeter, and adiabatic conditions are maintained such that the thermal drift of the calorimeter at equilibrium is typically better than 1 millikelvin per minute.



4.3 CALIBRATION

4.3.1 Resistance of the Calorimeter Heater

The resistance of the calorimeter heater as a function of temperature was determined prior to attempting any heat capacity measurements. A current of 100 microamps from the d.c. calibrator was passed through the heater in series with a Wilkins standard resistor ($99.9998\Omega \pm 3$ ppm). Voltage measurements were then made at terminals A and C of the heater circuitry as shown on Figure 3I. The Pye precision potentiometric bridge was again employed for null-balance measurement; thus no current flowed in the potential leads and there was no need to account for their resistance.

As the calorimeter gently warmed, its temperature was displayed by the computer at one minute intervals and, after a little practice, the manual balancing of the bridge was timed to coincide with this display. The heater resistance at each temperature was then calculated by multiplying the voltage ratio by the standard resistance. The experimental values are listed in Table 4F, and regular smoothed values are shown in Table 4G.

Figure 4H illustrates the resistance versus temperature relationship of the heater. The resistance decreases from 2028.470Ω at 100 kelvin to 2026.307Ω at 77 kelvin, and to 2023.285Ω by 50 kelvin. The monotonic decrease in this temperature range can be attributed to reduced scattering of the conduction electrons by phonons, and is typical of most alloys. However, with most alloys the resistance would continue to drop and attain a residual value which is temperature independent. As can be seen, the heater resistance approaches a shallow minimum of 2019.949Ω at 19.43 kelvin, but then rises

steeply to a value of 2028.981Ω by 2 kelvin. This behaviour is known as the *Kondo Effect*²² and it occurs because the heater is made from Karma alloy (76% Ni, 20% Cr, remainder Fe, Al) which is a dilute magnetic alloy.

It is known that some ions (such as Cr, Fe²⁺) which in isolation have a magnetic electronic shell can retain a fraction of their magnetic moment in a dilute solid solution with another metal. These dilute magnetic alloys have localised magnetic moments which can act as scattering centres for conduction electrons. The conduction electron becomes magnetised in the vicinity of the magnetic ion, and with this induced magnetisation it can undergo a further exchange interaction with another magnetic ion. Kondo showed that at low enough temperatures an anomalously high scattering probability of the magnetic ions can be caused by this exchange coupling. The shallow minimum around 19 kelvin in the resistance versus temperature curve is therefore a balance between the diminishing phonon scattering resistivity and the onset of resistivity due to the magnetic scattering which becomes dominant below 19 kelvin.

The smooth curve shown in Figure 4H was obtained by polynomial least squares fitting. The polynomial overlap method was employed in which data was split into three overlapping ranges from 2 to 40 kelvin, 10 to 60 kelvin, and 30 to 100 kelvin. A degree-10 polynomial fits the range up to 13.007 kelvin where it intercepts a degree-4 polynomial at $R_h = 2020.502\Omega$, with the gradients in the overlap region being $-0.190\Omega / \text{kelvin}$ and $-0.187\Omega / \text{kelvin}$ respectively. The degree-4 polynomial then fits the data up to 46.880 kelvin where it intercepts a degree-2 function at $R_h = 2022.902\Omega$ with the respective gradients being $0.120\Omega / \text{kelvin}$ and $0.124\Omega / \text{kelvin}$. The maximum deviation in this data is 0.03% and the polynomial forms are free from oscillation in each of the quoted ranges. The polynomial coefficients are listed in Table 4I, and they were incorporated into the software to determine the energy input to the calorimeter as part of the heat capacity calculations which are described in section 4. 3. 2.

**Table 4F - Experimental Values for the
Calorimeter Heater Resistance**

TEMPERATURE (K)	RESISTANCE (OHMS)	TEMPERATURE (K)	RESISTANCE (OHMS)
2.146	2028.416	21.663	2020.038
2.185	2028.375	21.739	2020.146
2.348	2027.778	23.315	2020.158
2.500	2027.400	23.692	2020.246
2.795	2027.454	25.786	2020.258
2.835	2027.273	26.123	2020.445
3.046	2027.083	28.333	2020.558
3.081	2026.917	28.943	2020.796
3.332	2026.615	31.747	2020.938
3.337	2026.462	34.626	2021.358
3.830	2025.880	37.184	2021.678
3.887	2025.667	39.514	2021.998
4.180	2025.375	43.123	2022.518
4.229	2024.897	46.367	2022.658
4.250	2024.497	53.953	2023.721
4.381	2024.430	54.362	2023.799
4.482	2023.884	54.951	2023.858
4.999	2023.284	55.015	2023.899
5.239	2023.646	56.334	2024.020
5.586	2023.884	57.447	2024.118
6.179	2022.285	58.588	2024.341
6.460	2022.497	60.445	2024.521
8.235	2022.116	61.168	2024.738
8.980	2021.996	63.805	2024.938
9.029	2021.816	65.815	2025.059
9.546	2021.716	69.376	2025.500
10.145	2021.520	70.472	2026.680
11.479	2020.946	73.438	2026.080
11.780	2020.916	76.235	2026.239
12.983	2020.396	77.559	2026.419
14.399	2020.096	78.453	2026.461
15.633	2019.996	79.813	2026.561
16.630	2020.030	82.441	2026.721
16.981	2020.019	86.010	2027.099
17.173	2019.908	88.436	2027.458
17.520	2019.998	91.318	2027.718
18.463	2019.946	94.166	2028.020
18.660	2019.797	96.075	2028.039
19.690	2019.938	97.799	2028.379
19.956	2019.996	99.020	2028.399
		100.410	2028.419

**Table 4G - Regular Smoothed Values for the
Calorimeter Heater Resistance**

TEMPERATURE (K)	RESISTANCE (OHMS)
2	2028.981
4	2023.175
6	2023.028
8	2021.817
10	2021.110
12	2020.667
14	2020.332
16	2020.092
18	2019.972
20	2019.952
22	2020.015
24	2020.143
26	2020.322
28	2020.538
30	2020.782
32	2021.041
34	2021.308
36	2021.576
38	2021.841
40	2022.097
42	2022.343
44	2022.579
46	2022.805
48	2023.041
50	2023.285
55	2023.884
60	2024.465
65	2025.029
70	2025.574
75	2026.101
80	2026.611
85	2027.102
90	2027.576
95	2028.032
100	2028.470

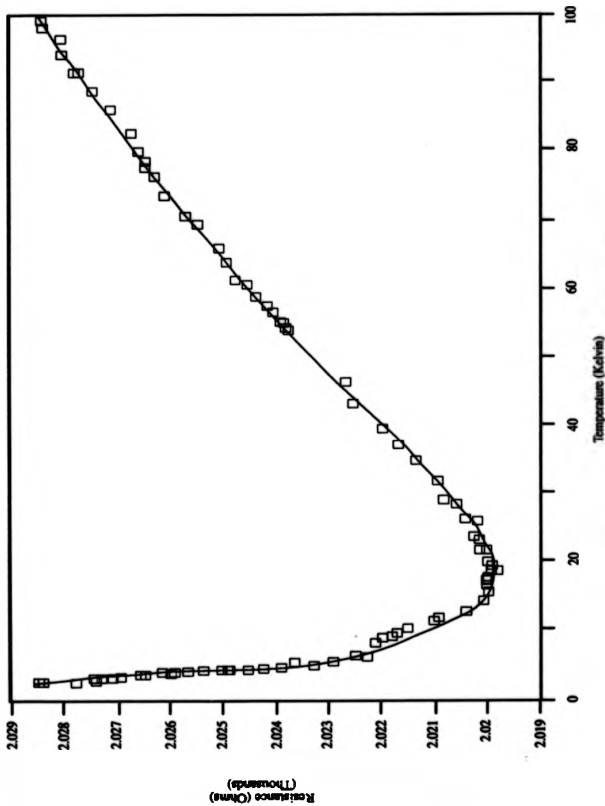


Table 4I - Polynomial Forms of the Heater Resistance

$2^{\circ}\text{K} \leq T \leq 13.007^{\circ}\text{K}$	$\text{Rh} = \sum_{n=0}^{10} \text{A}_n \cdot T^n$ <p> A0 = 2035.58515 A1 = -4.26061029 A2 = 0.557718056 A3 = -4.31718743 $\times 10^{-2}$ A4 = 2.07867078 $\times 10^{-3}$ A5 = -6.3633581 $\times 10^{-5}$ A6 = 1.25523044 $\times 10^{-6}$ A7 = -1.58624805 $\times 10^{-8}$ A8 = 1.23884653 $\times 10^{-10}$ A9 = -5.43926092 $\times 10^{-13}$ A10 = 1.02607295 $\times 10^{-13}$ </p>
$13.007^{\circ}\text{K} < T \leq 46.880^{\circ}\text{K}$	$\text{Rh} = \sum_{n=0}^4 \text{A}_n \cdot T^n$ <p> A0 = 2027.3264 A1 = -0.958024577 A2 = 4.15495166 $\times 10^{-2}$ A3 = -6.86597261 $\times 10^{-4}$ A4 = 4.12282596 $\times 10^{-6}$ </p>
$46.880^{\circ}\text{K} < T \leq 100^{\circ}\text{K}$	$\text{Rh} = \sum_{n=0}^2 \text{A}_n \cdot T^n$ <p> A0 = 2016.3113 A1 = 0.157369769 A2 = -3.57804605 $\times 10^{-4}$ </p>

4.3.2 Heat Capacity Calculations

As explained in section 3.1.5, during a calorimetric run the process-control software monitors the Cryobridge output and records the foredrift and afterdrift (d_f and d_a), starting temperature and final temperature (T_i and T_f), heater current i and heating period t for each heat capacity point. The data is then transferred to a file on floppy disc and from this it can be read into programs to calculate the heat capacity results.

The calculations follow the standard method of data treatment outlined by McCullough.²⁶ The experimentally observed mean heat capacity may be expressed as

$$C(obs) = \frac{\Delta E}{\Delta T}$$

at the mean temperature

$$T_m = \frac{T_i + T_f}{2}$$

The energy input is $E = i^2 R h t$ where the value of the heater resistance Rh is calculated at T_m using the polynomial forms of $Rh(T)$.

In calculating the value of the temperature interval a correction for temperature drift is made by taking the algebraic mean of the foredrift and afterdrift, such that

$$\Delta T = (T_f - T_i) - \left[\frac{t(d_f + d_a)}{2} \right]$$

The values of the observed mean heat capacity can then be corrected for curvature to determine the true observed heat capacity at T_m using the equation

$$C(true) = C(obs) - \left[\frac{(T_f - T_i)^2}{24} \right] \cdot \frac{d^2 C(obs)}{dT^2}$$

which is derived from the cubic form of the heat capacity.

In the case where the calorimeter vessel contains a chemical sample, the sample heat capacity is calculated from

$$C(\text{sample}) = C(\text{true}) - \left[C(\text{vessel}) + \sum C_i M_i + \frac{3PV}{2T_m} \right]$$

The term $C(\text{vessel})$ is the heat capacity of the empty calorimeter vessel as determined by the calibration measurements of section 4.3.3. The summation term $\sum C_i M_i$ accounts for any variability of the calorimeter mass which is due to the use of different masses of solder and silver tubing in each assembly of the calorimeter vessel. The solder heat capacities were determined by summing the heat capacities of the component metals²⁶ in the correct proportions. These values were then polynomial fitted in the ranges from 1 to 15 kelvin and 15 to 100 kelvin to allow corrections to be made throughout the whole temperature range. The polynomials are listed in the Appendix.

The term $\frac{3PV}{2T_m}$ corrects for the heat capacity of helium³ exchange gas which is present at pressure P in the free volume V of the calorimeter when it contains a chemical sample. The correction assumes perfect gas behaviour throughout the entire operating range.

The sample heat capacity is then smoothed by iterative least-squares to obtain a best polynomial fit of the form

$$C(\text{smooth}) = \sum a_i T_m^i$$

The best fit is that which minimises the sum of squares

$$W_i [C(\text{sample}) - C(\text{smooth})]^2$$

The weighting $W_i = \frac{1}{C(\text{sample})_i}$ ensures that the smaller heat capacities are adequately represented, and thus the minimisation is valid over the whole temperature range.

Finally the smoothed values of the sample heat capacity are converted to molar form.

4.3.3 Heat Capacity of the Empty Calorimeter Vessel

The empty vessel was evacuated for 24 hours to 8×10^{-6} mbar. It was then sealed with 0.0981 grams of crimped silver tube, 0.0485 grams of Sn/Pb solder and 0.2539 grams of indium based solder. The cryostat was then assembled and cooled as previously described.

The calibration run in the 50 to 100 kelvin range was completed without difficulty. Heating currents ranged from 3 to 6 milliamps for periods of 120 to 360 seconds. In this range, the equilibration periods increased from 6 to 12 minutes and the adiabatic controller operated smoothly as shown in Figure 4E.

The first attempt to calibrate in the liquid helium range was severely hindered by fracture of the phosphor-bronze bellows and leakage from the internal pumping vessel. This caused continuous cooling of the adiabatic shield which in turn caused a large negative temperature drift at the end of a heating period and a steady decline of the calorimeter towards 4.2 kelvin. Thus, the calorimeter could not be operated adiabatically and it was necessary to replace the bellows and fully coat the pumping vessel with a layer of solder. This amounted to a partial reconstruction and rewiring of the cryostat which took several weeks to achieve satisfactorily. Following this the calibration from 2 to 50 kelvin was completed successfully. In this range, the heating currents rose from 100 microamps to 3 milliamps for heating periods of 60 to 180 seconds, with the calorimeter rapidly equilibrating in 2 to 5 minutes.

The experimental results are listed in Table 4J. The data was again split into three overlapping temperature ranges and fitted to the functions (1), (2) and (3) shown in Table 4K.

Below 3.4583 kelvin, the data may be represented by the expression

$$C_p = aT + bT^3 + cT^6 \quad (1)$$

which is the general form for a metallic conductor. The aT term is

the electronic heat capacity and the higher terms approximate the lattice heat capacity. Estimates of the parameters a and b were obtained by plotting the experimental results in the form \bar{C}_v versus T^3 and drawing a straight line through the data at the lowest temperatures as shown in Graph 4L. This made the assumption that the vessel heat capacity would follow the Debye T^3 law which is a good first approximation at the lowest temperatures. These first estimates were then successively iterated in a minimisation program to determine the optimised values of Table 4K. The optimised function has a correlation value of 99.7% which signifies a good fit.

As can be seen from Graph 4M, function (1) shows rapid divergence from the experimental values from 5 kelvin upwards. It was found that function (2) gently crossed function (1) at 3.4583 kelvin (0.008043 JK^{-1}) and provided the best fit to the data up to 34.260 kelvin where it was intersected by polynomial function (3). The experimental points and smoothed curve are illustrated by Graphs 4N and 4O.

**Table 4J - Experimental Values for the
Empty Calorimeter Vessel Heat Capacity**

T/K	C_p/JK^{-1}	T/K	C_p/JK^{-1}	T/K	C_p/JK^{-1}
2.068	0.0033	20.325	0.5225	89.453	7.300
2.186	0.0039	22.094	0.644	90.273	7.354
2.282	0.0040	24.012	0.789	91.502	7.365
2.672	0.0050	26.234	0.989	92.148	7.481
2.920	0.0059	28.930	1.302	93.284	7.514
2.958	0.0060	32.242	1.709	94.765	7.688
3.209	0.0068	35.699	2.008	97.415	7.868
3.464	0.0081	39.519	2.482	98.723	7.857
3.721	0.0092	41.308	2.640	100.020	7.986
4.236	0.0114	43.543	2.982		
4.442	0.0122	45.232	3.130		
5.462	0.0186	48.060	3.532		
6.362	0.0263	50.448	3.824		
7.288	0.0383				
7.784	0.0442				
9.172	0.0697	52.710	4.093		
9.622	0.0781	55.285	4.396		
11.064	0.1105	58.736	4.712		
12.234	0.1442	60.080	4.882		
13.138	0.1708	62.364	5.160		
14.294	0.2147	67.028	5.560		
15.382	0.2567	70.884	5.798		
16.428	0.3060	74.901	6.167		
17.493	0.3578	79.376	6.536		
18.765	0.4256	84.354	6.832		

Table 4K - Polynomial Functions for the Empty Calorimeter Heat Capacity

$$2^{\circ}\text{K} \leq T < 3.4583^{\circ}\text{K} \quad C_p = aT + bT^2 + cT^3 \quad (1)$$

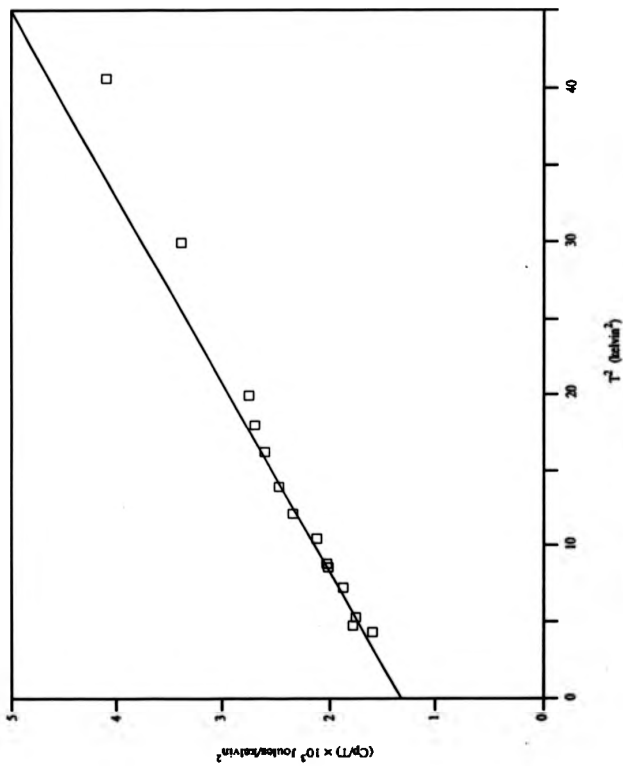
$$\begin{aligned} a &= 1.32063744 \times 10^{-3} \\ b &= 7.87127369 \times 10^{-9} \\ c &= 4.45371828 \times 10^{-7} \end{aligned}$$

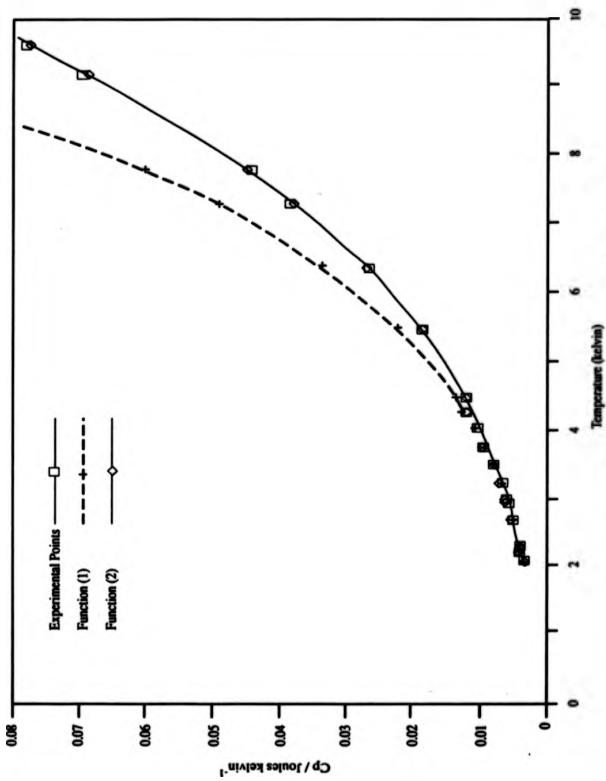
$$3.4583^{\circ}\text{K} \leq T \leq 34.260^{\circ}\text{K} \quad C_p = \sum_{i=0}^8 A_i T^i \quad (2)$$

$$\begin{aligned} A_0 &= -1.58642559 \times 10^{-2} \\ A_1 &= 1.74418567 \times 10^{-2} \\ A_2 &= -5.81868843 \times 10^{-3} \\ A_3 &= 1.05188457 \times 10^{-3} \\ A_4 &= -8.45752074 \times 10^{-6} \\ A_5 &= 3.90673037 \times 10^{-6} \\ A_6 &= -9.9767813 \times 10^{-6} \\ A_7 &= 1.30271939 \times 10^{-9} \\ A_8 &= -6.78818145 \times 10^{-12} \end{aligned}$$

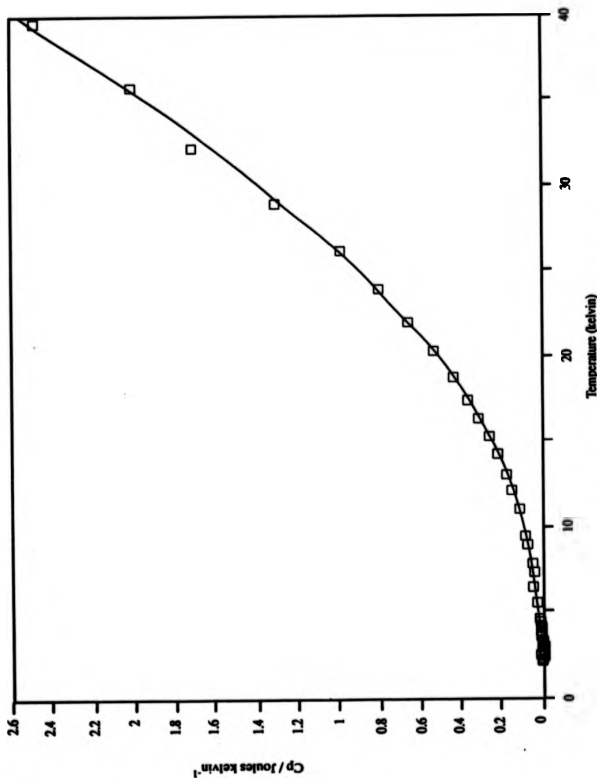
$$T > 34.260^{\circ}\text{K} \quad C_p = \sum_{i=0}^6 A_i T^i \quad (3)$$

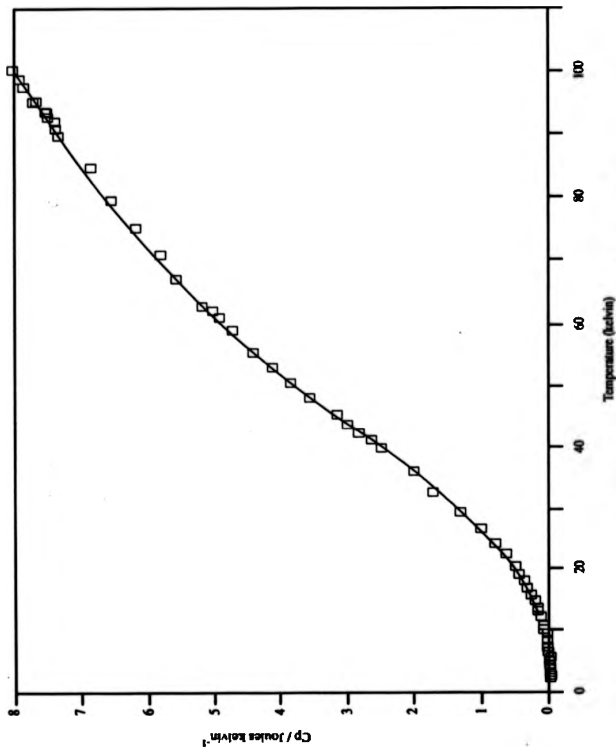
$$\begin{aligned} A_0 &= -11.28591020 \\ A_1 &= 1.31237511 \\ A_2 &= -6.09393334 \times 10^{-2} \\ A_3 &= 1.556565039 \times 10^{-3} \\ A_4 &= -2.10339453 \times 10^{-5} \\ A_5 &= 1.42976171 \times 10^{-7} \\ A_6 &= -3.85440846 \times 10^{-10} \end{aligned}$$





Graph 48M - Empty Calorimeter Heat Capacity
From 2 to 10 kelvin





Graph 40 - Empty Calorimeter Heat Capacity
From 2 to 100 kelvin

4. 3. 4 The Heat Capacity of Benzoic Acid

The sample of benzoic acid used in this run was certified by the National Chemical Laboratory for use as a thermochemical standard. It was obtained from B. D. H. (batch number 0194690) and the calorific value was quoted as 26435.1 ± 2.9 joules per gram.

The sample arrived in the form of tablets. These were broken into granules and 17.2083 grams (0.1409 moles) were loaded into the calorimeter. The vessel cap and silver tubing were soldered into place and the assembly was evacuated to 10^{-5} millibar through the utility port on the gas handling line (Figure 2C). The line was then isolated and helium exchange gas was bled into the assembly via a fine control needle valve to a pressure of 3 torr. The vessel was then sealed, leak tested and placed into the cryostat in the usual manner.

Heat capacity measurements were first carried out using nitrogen as a refrigerant. In this run, the lowest temperature achieved by subliming nitrogen was 54.8 kelvin and the measurements commenced at 56.107 kelvin. This was due to inexperienced operation of the cryostat when it contained a chemical sample. The liquid helium run was therefore extended up to 62 kelvin to ensure that the full range was covered. The experimental results are listed in Table 4P and are illustrated by Graphs 4R and 4S. The data was smoothed by least squares fitting and the mean deviation from the smoothed values was 1.6%. Table 4Q shows the smoothed values generated at regular temperature intervals.

Graph 4T compares the heat capacity values obtained in this laboratory with those of other workers. The smoothed values of Table 4Q are used as the baseline and the other values are plotted as deviations from this. Above 20 kelvin, the most reliable data available is that of the National Bureau of Standards⁷. This was obtained with a sophisticated calorimeter employing several radiation shields. For results above 60 kelvin, the accuracy is claimed to be $\pm 0.3\%$, whilst below 60 kelvin it reduces to $\pm 1\%$. Below 20 kelvin, the N.B.S. values were calculated by Debye

extrapolation and they are plotted merely to illustrate the deviation which can be inherent in such approximations.

The most reliable experimental data available below 20 kelvin is that of Sklyankin²⁰ and of Clay²¹, both of whom used simple manually operated calorimeters for which the primary operating range was from 4 to 20 kelvin. These observers obtained very similar values with the estimated accuracy better than $\pm 1.5\%$ in both cases.

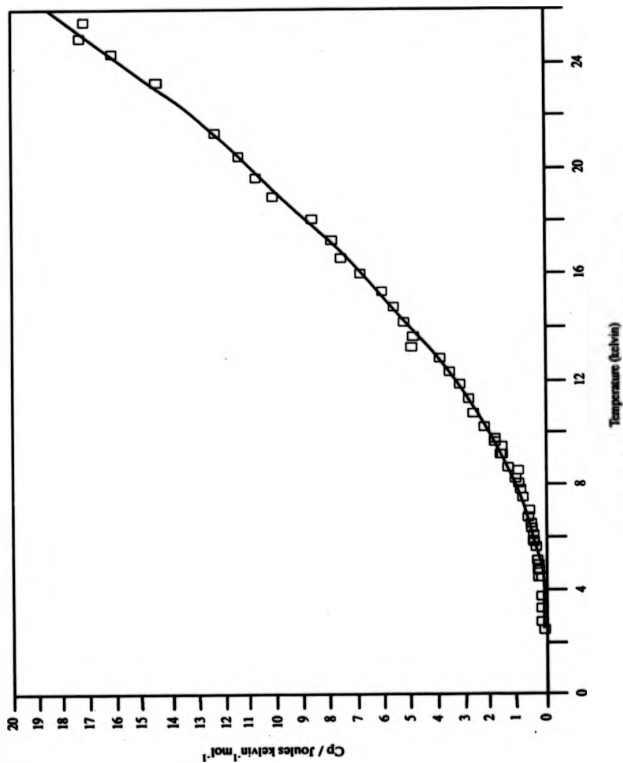
As shown by Graph 4T, the values obtained in this laboratory from 30 kelvin upwards are consistently low when compared with N.B.S. values. Below 30 kelvin, there is no systematic trend and the data shows scatter and greater uncertainty due to the rapidly diminishing absolute heat capacity. Overall, the data obtained in this laboratory is generally within $\pm 2\%$ of the other values. At the outset of this work, an accuracy of $\pm 1\%$ had been anticipated. This was probably a rather ambitious target for a new laboratory in a department with no other low temperature activity. Therefore, the achievement of measurements accurate to $\pm 2\%$ is quite gratifying and generally validates the apparatus and the methods of operation.

Table 4P - Experimental Results for the
Heat Capacity of Benzoic Acid

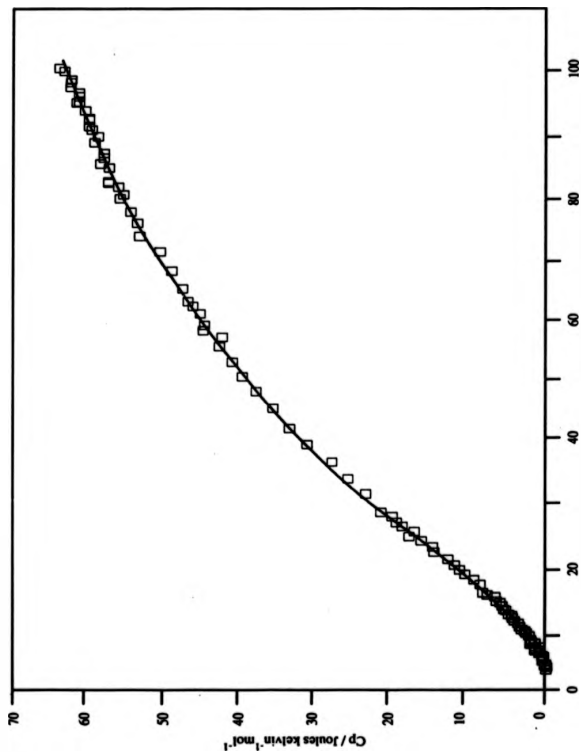
T/K	$C_p/JK^{-1} \text{ mol}^{-1}$	T/K	$C_p/JK^{-1} \text{ mol}^{-1}$	T/K	$C_p/JK^{-1} \text{ mol}^{-1}$
2.547	0.0427	18.849	10.248	75.584	53.608
2.808	0.0570	19.174	10.268	77.465	54.288
3.219	0.0888	19.596	10.849	78.041	54.959
3.767	0.1049	20.351	11.616	79.469	55.839
4.468	0.1684	20.670	11.840	80.192	55.441
4.560	0.1789	21.240	12.451	81.278	55.891
4.613	0.1856	22.478	13.980	82.173	57.309
4.733	0.2013	23.153	14.652	84.273	57.260
4.911	0.2152	24.256	16.250		
5.085	0.2426	24.554	16.135	84.954	58.651
5.798	0.3817	25.470	17.060	86.963	58.865
5.918	0.3926	26.704	19.020	88.308	58.910
6.261	0.4509	28.113	19.917	88.950	58.908
6.491	0.5183	28.749	21.224	89.059	59.406
6.741	0.6104	30.040	21.341	90.907	59.927
7.007	0.6490	31.185	23.683	92.833	60.340
7.510	0.8268	33.184	24.600	94.732	61.605
7.759	0.8952	33.830	25.914	96.096	61.283
8.007	0.9972	35.906	27.288	96.607	61.195
8.165	1.1057	36.618	28.057	98.459	62.208
8.539	1.1996	38.343	29.508	98.723	62.050
9.111	1.5663	39.418	31.244	100.281	63.670
9.388	1.6835	41.308	32.146		
9.632	1.8584	42.184	33.382		
9.685	1.8313	44.725	35.608		
10.180	2.2470	48.058	37.914		
10.704	2.6473	52.090	41.002		
11.229	2.8712	55.285	42.829		
11.762	3.2669	58.148	45.001		
12.286	3.6122	60.689	45.673		
12.759	4.0149	62.762	47.065		
13.640	4.9245				
14.121	5.2085				
14.696	5.6403	56.107	42.787		
15.314	6.0676	58.736	44.484		
15.953	7.0357	61.665	46.274		
16.563	7.7376	64.691	47.837		
16.987	8.4585	67.800	49.284		
17.392	8.6673	70.997	50.772		
18.012	8.7140	73.672	53.140		
18.101	9.3485				

Table 40 - Regular Smoothed Values for the Heat Capacity of Benzoic Acid

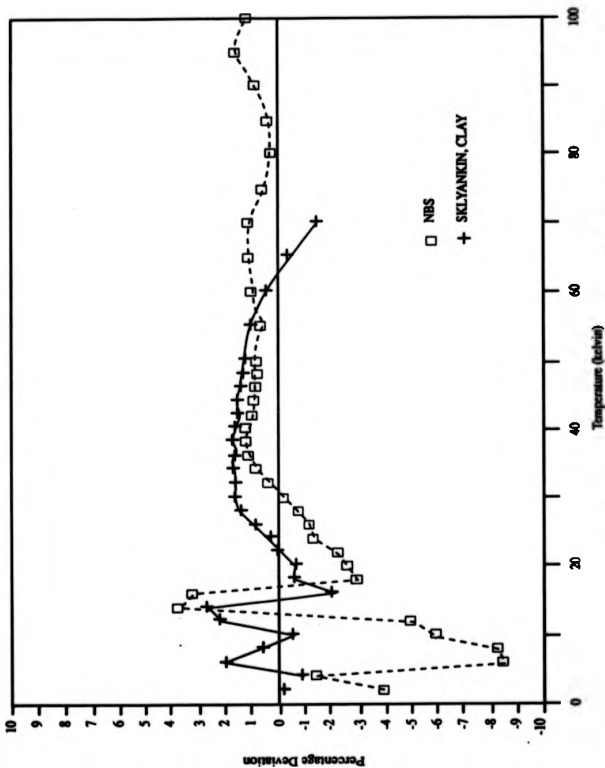
T/K	$C_p/\text{JK}^{-1}\text{mol}^{-1}$
2	0.01621
4	0.12609
6	0.4582
8	1.0821
10	2.0477
12	3.4321
14	5.1242
16	7.0474
18	9.125
20	11.290
22	13.486
24	15.675
26	17.828
28	19.930
30	21.973
32	23.956
34	25.879
36	27.746
38	29.557
40	31.314
42	33.014
44	34.657
46	36.238
48	37.753
50	39.200
55	42.513
60	45.435
65	48.098
70	50.663
75	53.224
80	55.702
85	57.881
90	59.588
95	61.036
100	63.160



Graph 4R - Heat Capacity of Benzoic Acid
From 2 to 25 kelvin



Temperature (kelvin)
Graph 4S - Heat Capacity of Benzoic Acid
From 2 100 kelvin



Graph 4T - Comparison With Other Workers
 Heat Capacity of Benzoic Acid

CHAPTER 5**HEAT CAPACITY STUDIES**

CONTENTS**PAGE**

5. 1	ORIENTATIONAL DISORDER	182
5. 1. 1	The Site Model of Orientational Disorder	
5. 1. 2	Complex Salts and the Schottky Anomaly	
5. 1. 3	Previous Studies of Ammine Salts	
5. 2	CHLOROAMMINE COBALT(III) COMPLEXES	189
5. 2. 1	Proposals	
5. 2. 2	Chloropentaammine Co (III) Dichloride	
5. 2. 3	Trans-dichlorotetrammine Co (III) Dichloride	
5. 3	DISCUSSION	182

5.1 ORIENTATIONAL DISORDER

5.1.1 The Site Model of Orientational Disorder

Orientational disorder can arise in a crystalline solid when diatomic or polyatomic molecules or ions are able to randomly occupy two or more distinguishable orientations in the crystal lattice. The theoretical treatment of this disorder is based on the site model.⁷ In this model, each molecule (or ion) occupies one of a number of orientations at its lattice site. Each orientation corresponds to the minimum of a potential well, and the number of allowed orientations is related to the symmetry operations of the crystal space group and the molecular point group.

The molecules librate in their potential wells until they gain enough energy to jump over the potential barrier into another orientation. A distinguishable orientation occurs when the crystal space group allows a reorientation with symmetry elements which do not form a subgroup of the molecular point group. If the reorientational symmetry coincides with a symmetry element of the molecule, each jump results in a new but indistinguishable orientation, and no disorder is introduced.

The site model assumes a rigid lattice, with each molecule subject to a static potential generated by nearest-neighbour interactions. This ignores the fact that the libration of the molecules causes the potential field to fluctuate dependent on the degree of thermal agitation.

Experimentally, the onset of disorder may be observed as a thermal anomaly in the heat capacity curve of the solid. The disorder may be classified as dynamic or static, although the terms are used rather loosely, and the distinction generally depends on the degree of thermal

motion and the rate at which reorientation occurs. For example, at temperatures near to the onset of free rotation, the molecules may undergo torsional oscillations through a large angle and a significant number may have enough energy to surmount the potential barrier. Above the barrier, the disorder is clearly dynamic and involves several degrees of freedom. Conversely, when the thermal energy is low compared to the barrier height, the molecules are restricted to small amplitude librations. In this case, a negligible number of transitions are observed and the disorder is regarded as static.

The reorientation rate and the class of disorder are thus dependent on the temperature range being observed and on the depth of the potential well.

For most substances, the height of the potential energy barrier between orientations is much greater than the thermal energy of a molecule at or below room temperature. Therefore, at low temperatures few molecules are able to surmount the barrier at any given time and the duration of a jump has been estimated as 10^{-12} to 10^{-13} of a second.⁷¹ This means that the dynamics of reorientational motion become relatively insignificant at low temperatures, and the lower the temperature the more applicable is the static treatment of disorder.

Low temperature study of the orientational disordering of whole molecules has normally been confined to small hydride species such as CH_4 ⁷² and NH_3 .⁷³ However, when bound to a central atom, the restricted rotation of these groups can have interesting consequences, resulting in a special form of orientational disorder at very low temperatures.

For this reason the remainder of this chapter is mainly concerned with the restricted rotation of coordinated NH_2 in ammine salts.

5.1.2 Complex Salts and the Schottky Anomaly

Order-disorder phenomena have been observed in complex salts with the general formulae $M(NH_3)_6X_2$ and $M(NH_3)_6X_3$. Even when the anion X is monatomic, the nature of the polyatomic cation allows two possible ways for orientational disorder to arise.

In the first case, whole cations may undergo reorientation in the crystal lattice. Secondly, within each cation, disorder may be introduced due to torsional displacements of the ammonia ligands about the M-N axes.

Both types of motion evolve over a broad temperature range and can occur simultaneously. For example, as the temperature increases above 100 kelvin, whole cations may commence step-wise rotational diffusion which can gradually develop into three-dimensional tumbling by 300 kelvin.

Also over the same temperature range, the ammonia ligands within the cation transform from torsional oscillators to one-dimensional free rotors.

Due to the combination of motions, it can be very difficult to provide an exact description of the development of the disorder. However, it is sometimes possible to resolve the contribution from each type of motion if the behaviour at low temperatures is known.

Generally, below 100 kelvin, motion involving the whole cation has been frozen out and the motion of the ammonia ligands is confined to libration in a potential well. Dependent on the nature of the crystal lattice, the transformation from rotor to oscillator may occur smoothly through independent ligand motion, or it may occur as a critical phase transition involving cooperative ligand motion.

In either case, the amplitude of oscillation decreases as the temperature decreases until the ligands occupy their ground state librational energy level. At this stage all classical motion may be regarded as having ceased.

However, reorientational ordering persists by means of quantum mechanical tunnelling of the potential barrier. Through this the protons may transfer between equivalent orientations, which on its own would provide no disorder. However, the coupling between orientation and nuclear spin results in the librational energy levels being split into sub-level states which are discretely quantised by their different total nuclear spin. The splitting between these internal energy levels is small and normally the protons are distributed according to Boltzman statistics. At a sufficiently low temperature, usually below 1 kelvin, the upper levels of the librational ground state are vacated in favour of the lower levels. Provided that rapid spin conversion can occur, the "additional" heat capacity due to repopulation of the upper levels may appear as a Schottky anomaly in low temperature measurements.

The form of the Schottky heat capacity may be derived from first principles as follows.

For a set of internal energy levels ϵ_i of degeneracy g_i , the partition function may be written as

$$q = \sum_i g_i e^{-\beta \epsilon_i}, \quad \text{where } \beta = \frac{1}{kT}$$

From this the Schottky heat capacity may be expressed as

$$\frac{C_{\text{Schottky}}}{R} = \frac{q''}{q} - \left(\frac{q'}{q}\right)^2 \quad (1)$$

At temperatures well above the maximum in the Schottky anomaly, the exponents tend to unity. Thus for a two level splitting of energy $\Delta E = \epsilon_1 - \epsilon_2$, the partition function and its derivatives reduce to

$$q = g_1 + g_2, \quad q' = g_1 \beta \epsilon_1 + g_2 \beta \epsilon_2, \quad q'' = g_1 (\beta \epsilon_1)^2 + g_2 (\beta \epsilon_2)^2$$

By substitution and rearrangement equation (1) then becomes

$$\begin{aligned} \frac{C_{\text{Schottky}}}{R} &= \frac{g_1 g_2}{(g_1 + g_2)^2} \cdot (\beta \Delta E)^2 \\ &= \frac{g_1 g_2}{(g_1 + g_2)^2} \left(\frac{\Delta E}{kT} \right)^2 \end{aligned} \quad (2)$$

Equation (2) reveals the $\frac{1}{T^2}$ dependence of the Schottky specific heat at temperatures well above the maximum in the anomaly. This is referred to as the "high temperature tail" of the anomaly. Provided that the tail can be well resolved, a value for the splitting energy ΔE can be calculated and from this the magnitude of the potential barrier may be determined. Details of these calculations are given in section 5.3.

5. 1. 3. Previous Studies of Ammine Salts

The ammine salt which has been most thoroughly studied at low temperatures is probably the hexaammine nickel (II) iodide, $\text{Ni}(\text{NH}_3)_6\text{I}_2$.^{74,75,76} This salt has a lambda-type transition at 19.8 kelvin which results from the mutually cooperative rearrangement of the six ammonia ligands in each cation. The phenomenon is lattice induced and has been ascribed to the reduction of symmetry (from face centred cubic, high temperature phase) which occurs as the temperature is lowered.^{77,78}

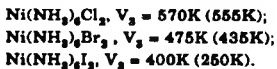
Being a paramagnet, the salt also shows a magnetic transition to an antiferromagnetically ordered state; the Néel temperature being 0.3 kelvin. There is also a Schottky anomaly associated with the hindered rotation of the NH_3 ligands. Coincidentally, the maximum contribution from this transition also occurs at 0.3 kelvin, causing considerable overlap of the magnetic and Schottky specific heats.

Related salts have also been studied, but generally the treatment is not as extensive and is limited by the temperature range. For example, the heat capacities of the series $\text{M}(\text{NH}_3)_6\text{I}_2$

(where $M = \text{Ni, Co, Mn, Zn, Cd}$ and Ca) have all been measured).²⁹ However, the work concentrates on the lambda-transition which is present in all six compounds. In the order given, the transition temperature increases from 20 to 52 kelvin, the transition broadens and the accompanying entropy gain ΔS_t increases to the considerable value of $29.8 \text{ JK}^{-1} \text{ mol}^{-1}$ for the Ca salt.

The most notable work from which barrier heights have been determined is that of van Kempen *et al* ³⁰, who cooled below 1 kelvin by adiabatic demagnetisation, and obtained heat capacities for the isomorphous series $\text{Ni}(\text{NH}_3)_6\text{X}_2$, ($\text{X} = \text{Cl, Br, I}$). The deuterated form of the iodide salt was also considered. In this form, only the magnetic transition was clearly resolved, but there was an indication that the Schottky effect may occur well below 0.3 kelvin; the deuteron being less able to tunnel than the proton.

Latterly, these experimental results were complemented by a theoretical investigation by Bates and Stevens.³¹ This represented the molecular interactions by a point charge electrostatic model. The energy barriers within the crystals were computed by evaluating the intra-cluster interaction between protons on the same cation, plus the interaction between protons on nearest-neighbour $\text{Ni}(\text{NH}_3)_6^{2+}$ clusters. A barrier height of around 280 kelvin was calculated for the intra-cluster interaction. The contribution from nearest-neighbours was calculated to be 280K for the chloride, 190K for the bromide and 120K for the iodide. The additional small contribution from the eight nearest-neighbour halide ions around each cation was also taken into account. This resulted in total maximum barrier heights as follows:



The bracketed values are those determined experimentally by van Kempen.³⁰ The agreement with experiment is particularly good for the chloride, and it is also reasonable for the bromide.

Comparison of the iodide values is intriguing, however, since even the intra-cluster contribution is greater than the experimental value.

Some interest has also been shown in hexammine cobalt (III) salts. A magnetic resonance study by Murray and Waugh²² indicates continuous reorientational motion in the series $\text{Co}(\text{NH}_3)_6\text{X}_3$, with $\text{X} = \text{Cl}, \text{Br}, \text{I}, \text{NO}_3, \text{BF}_4$ and PF_6 . This involved proton and ^{19}F line-width studies as well as second moment studies from 90 to 400 kelvin. The proton second moment studies show that at 90 kelvin the ammonia ligands are rapidly reorientating about the Co-N axes. All of the salts displayed a very broad line-width transition up to 300 kelvin, at which point rapid three-dimensional tumbling of the cations is indicated. Tumbling of the BF_4^- and PF_6^- counterions has already begun by 90 kelvin.

Further studies have concentrated on the chloride salt. A deuteron magnetic resonance study by Ito and Chiba²³ showed that below 170 kelvin only the C_3 axis reorientation of the ND_3 group is present; all other motion of the $\text{Co}(\text{ND}_3)_6^{3+}$ ions having been frozen out. The hindered rotation of NH_3 ligands in $\text{Co}(\text{NH}_3)_6\text{Cl}_3$ about their threefold axes was also confirmed by the NMR investigation of Kim²⁴, and was found to persist down to 4.2 kelvin.

The heat capacity of $\text{Co}(\text{NH}_3)_6\text{Cl}_3$ was measured by P.R. Clayton and R.D. Weir²⁵ using two calorimeters in the range from 2 to 310 kelvin. There was no evidence of cooperative NH_3 reorientation of the type found in the hexammine metal (II) halides. Instead the NH_3 ligands transformed smoothly and uncooperatively resulting in a Schottky anomaly, the tail of which was well resolved in the 2 to 7 kelvin region. From this the height of the threefold potential barrier was estimated to be $V_3 = 560$ kelvin. The similarity of this value with that of $\text{Ni}(\text{NH}_3)_6\text{Cl}_3$ ($V_3 = 555\text{K}$) was shown to be due to the similar nearest-neighbour metal atom distances in the two salts; which average out at 7.116Å for Ni - Ni and 7.166Å for Co - Co.

5.2 CHLOROAMMINE COBALT(III) COMPLEXES

5.2.1 Proposals

Although several studies have been outlined in section 5.1, these have mainly been carried out in isolation. Therefore, there has been little systematic or correlated investigation of the factors which influence the rotational barrier. The basis of current knowledge is the reasonably satisfactory agreement of Bates and Stevens' electrostatic model with the experimental results of van Kempen. The conclusions from this are summarised below.

The major influence on the barrier height is the intra-cluster interaction of protons within the same cation. The magnitude of this can be related to the mean distance between the central ion and the nitrogen atoms of the ammonia ligands.

The next most important interaction is that between nearest-neighbour cations. This is mainly determined by the nearest-neighbour metal atom distances, which may in turn be influenced by the nature of the halide counterions. However, the direct interaction between nearest-neighbour halide ions is regarded as relatively unimportant.

The proposal of this laboratory was to break new ground by studying variation of the intra-cluster interaction. This would be achieved by carrying out low temperature heat capacity measurements on compounds in which the ammonia ligands could be substituted in a systematic way.

It was decided that the chloroammine cobalt (III) complexes would be the most promising. Firstly, Co(III) has the definite

advantage of being diamagnetic, forming low spin complexes with the inert d^6 configuration. This rules out the occurrence of any magnetic transition which could obscure the tail of a Schottky anomaly. Secondly, the hexaammine salt, $\text{Co}(\text{NH}_3)_6\text{Cl}_2$, had already been studied with no evidence of lattice induced effects and the Schottky tail had been well resolved.

The intention was to select compounds from the series $[\text{CoCl}_n(\text{NH}_3)_{6-n}]\text{Cl}_{3-n}$ which includes *cis* and *trans* tetrammines and *mer* and *fac* triammines. These cobaltammines were central to the development of coordination chemistry by Werner. Consequently, they have been extensively studied with respect to their ligand substitution reactions and isomerism.¹⁰ Several thermal decomposition studies have been carried out, most notably by Wendlandt,^{11,12} and the direction of isomerisation in the solid state (*trans* to *cis*) has also been determined by Watt and Butler.¹³ Heats of formation and solution, plus relative thermal stabilities have also been addressed.^{11,12} There has been considerable investigation of infra-red spectra and lattice vibrations.^{13,14,15} In particular the work of Fujita¹⁶ highlights the presence of weak hydrogen bonding between inner-sphere NH_3 ligands and outer-sphere halide ions.

An interesting study of the effect of substituting halide ions for NH_3 ligands in the inner coordination sphere has been reported by Fluck and Burger¹⁷ using X-ray photoelectron spectroscopy. The study indicates that in moving from $[\text{Co}(\text{NH}_3)_6\text{Cl}_2]$ to $[\text{Co}(\text{NH}_3)_5\text{Cl}]\text{Cl}_2$ there occurs a nett decrease in the strength of the remaining Cobalt-Nitrogen coordinate bonds. Whilst for $[\text{Co}(\text{NH}_3)_5\text{Cl}_2]$ the bond strength is greater than either the hexaammine or pentaammine salts. The data also indicates the greater stability of inner-sphere complexes in agreement with equilibrium studies.¹⁸

There is a paucity of crystal structure data, with only the hexaammine salt being fully characterised.¹⁹ A powder photographic study²⁰ of the pentaammine indicates an orthorhombic unit cell.

The Co-N distance of the NH_3 group coordinated in the trans position to the chlorine atom is 1.91\AA , whilst the four other Co-N distances are 1.97\AA .

No other crystal structures were traced, despite a literature search through the Cambridge Crystallographic Data Centre and a subsequent search of the German Crystal Database. Several attempts were made to obtain sizable crystals by very slow evaporation. All attempts failed, and in each case the salts precipitated as micro-crystalline powders.

Heat capacity measurements were carried out on these very fine powder samples of the pentaammine and the trans-tetrammine salts.

5. 2. 2 Chloropentaammine Co(III) Dichloride

The calorimetric sample of this salt was prepared as follows. 40 grams of NH_4Cl was dissolved in 120 cm^3 of 0.880 ammonia solution. This was placed in an ice bath, and 20 grams of $\text{CoCl}_2 \cdot 6\text{H}_2\text{O}$ was added with stirring until it dissolved. Aliquots of H_2O_2 were added and once oxidation was complete the solution was boiled and then left to cool naturally. The precipitate was dried under vacuum and then recrystallised from aqueous ammonia. The product was washed with dilute HCl and ethanol prior to drying at 100°C for 2 hours.

Elemental Analysis of the dust-like, purple powder produced the following mass percentages:

Co, 23.80 (23.53);	N, 27.58 (27.96);
H, 6.07 (6.04);	Cl, 42.64 (42.47).

The values in brackets are theoretical.

14.877 grams of the salt was loaded into the calorimeter vessel. The vessel was evacuated and then repressurised to 3 torr with helium³ exchange gas prior to sealing. The seals were effected with

0.0471 grams of hard solder, 0.0853 grams of soft solder and 0.1105 grams of silver tubing.

Heat capacity measurements were first carried out in the range from 53 to 100 kelvin. Heating currents of 5 mAmps to 6.5 mAmps were used for periods from 300 to 360 seconds. Equilibration times ranged from 8 to 15 minutes.

For measurements at helium temperatures, the currents varied from 100 μ Amps to 5 mAmps for periods of 60 to 300 seconds. Equilibration times were longer than expected, ranging from 3 to 10 minutes. Fore and after drifts were also predominantly negative, suggesting cooling of the calorimeter. However, the inner vacuum was monitored at a steady 6×10^{-7} mbar, indicating that no leaks had occurred. It was concluded that the very small particle size of the salt had resulted in an inefficient conduction mechanism; by point contact of the crystals with the surface of the vessel. The vessel surface thus remained at a higher temperature for a longer period of time, and the slow heat transfer throughout the sample gave the appearance of cooling.

Graph 5A illustrates the experimental heat capacity curves, and the values are listed in Table 5B. The data was polynomial smoothed with a mean deviation of 1.8% in the range from 30 to 100 kelvin. Below 30 kelvin, the mean deviation increases to 3%.

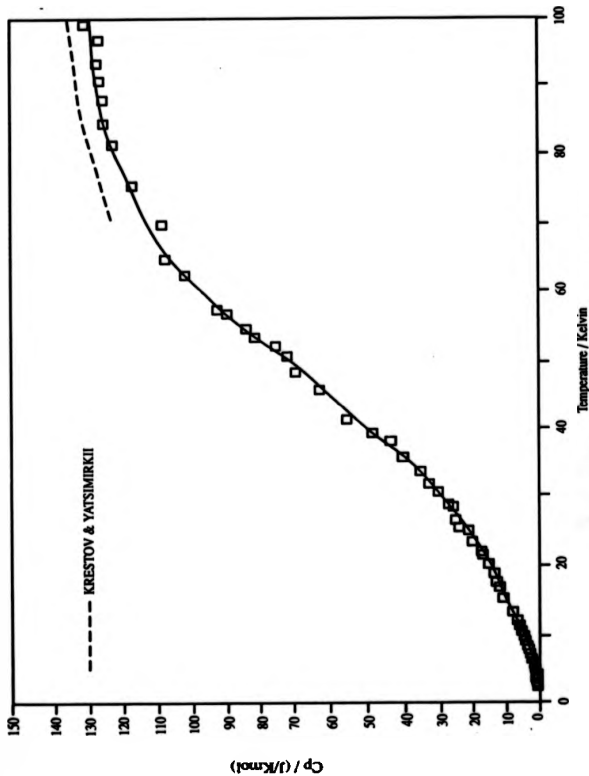
Table 5C shows smoothed values for the heat capacity generated at regular temperature intervals. The thermodynamic functions $H^{\circ}(T) - H^{\circ}(O)$ and $S^{\circ}(T)$ were calculated from the integrals

$$\int_0^T C_p dT \text{ and } \int_0^T C_p T^{-1} dT \text{ respectively.}$$

The Gibbs function was calculated from

$$- \{G^{\circ}(T) - H^{\circ}(O)\} T^{-1} = - \{H^{\circ}(T) - H^{\circ}(O)\} T^{-1} + S^{\circ}(T).$$

Graph 5A also illustrates the smoothed data of Krestov and Yatsimirskii¹⁰⁰ who carried out measurements in the 70 to 310 kelvin range. The data of this laboratory is 1.6% lower than that of the Russians in the 70 to 100 kelvin range.



Graph 5A - Experimental Values of Heat Capacity
 $[\text{Co}(\text{NH}_3)_6]\text{Cl}_2$ From 3 to 100 kelvin

Table 5B - Experimental Values of the Heat Capacity of Chloropentaammine Cobalt(III) Dichloride $[\text{Co}(\text{NH}_3)_5\text{Cl}_2]\text{Cl}_2$ from 3 to 100 kelvin

T/K	$C_p/\text{JK}^{-1}\text{mol}^{-1}$	T/K	$C_p/\text{JK}^{-1}\text{mol}^{-1}$
53.708	76.43	8.312	2.027
56.281	84.19	8.860	2.295
57.582	89.27	9.158	2.482
57.988	91.97	9.209	2.546
62.957	102.42	9.635	2.991
65.759	108.62	10.182	3.462
70.354	109.81	10.710	3.639
75.988	118.88	11.258	4.188
81.929	124.05	11.357	4.500
84.722	126.52	12.092	5.278
87.523	126.86	12.758	6.151
90.480	127.99	13.257	6.728
93.534	129.93	14.430	7.875
96.547	128.70	15.912	10.37
99.186	133.29	17.444	11.65
		17.893	12.68
3.788	0.0466	18.974	13.54
3.867	0.0794	20.520	16.06
3.986	0.1071	21.614	17.37
4.064	0.1278	21.958	17.74
4.086	0.1330	23.403	20.40
4.190	0.1658	25.040	21.88
4.239	0.2159	25.774	24.33
4.585	0.3022	26.805	25.76
4.610	0.3108	28.578	26.35
4.884	0.3886	28.988	28.04
5.085	0.4490	31.423	32.02
5.311	0.4835	33.028	35.65
5.559	0.5923	35.003	38.50
5.809	0.7132	36.614	42.05
6.036	0.8479	37.991	43.24
6.312	0.9878	39.560	48.72
6.459	0.9757	42.614	56.59
7.010	1.299	46.498	63.00
7.188	1.419	48.634	68.73
7.635	1.794	51.249	71.58
7.835	1.891	54.987	81.80

Table 5C - Smoothed Heat Capacity and Thermodynamic Functions of Chloropentaammine Cobalt(III) Dichloride, $[\text{Co}(\text{NH}_3)_5\text{Cl}]\text{Cl}_2$

T/K	CP/JK ⁻¹ mol ⁻¹	H ^o (T)-H ^o (O) Jmol ⁻¹	S ^o (T) JK ⁻¹ mol ⁻¹	-[G ^o (T)-H ^o (O)]T ⁻¹ JK ⁻¹ mol ⁻¹
6	0.8360	6.67	0.8721	
8	1.781	9.18	1.227	0.0793
10	3.274	14.16	1.776	0.361
12	5.191	22.56	2.537	0.657
15	8.636	43.16	4.055	1.18
20	15.25	102.5	7.428	2.30
25	22.34	196.4	11.59	3.73
30	29.85	326.6	16.31	5.43
35	38.39	496.6	21.54	7.35
40	48.53	713.4	27.31	9.47
45	59.85	984.0	33.68	11.82
50	71.63	1313	40.59	14.34
55	83.16	1700	47.96	17.06
60	93.90	2143	55.68	19.97
65	103.41	2637	63.58	23.01
70	111.44	3175	71.55	26.20
75	117.85	3748	79.46	29.48
80	122.69	4350	87.23	32.85
85	126.10	4973	94.78	36.28
90	128.42	5610	102.1	39.74
95	130.11	6256	109.0	43.19
100	131.79	6911	115.8	46.65

5. 2. 3 Trans-dichlorotetrammine Co(III) Chloride

The trans- $[\text{Co}(\text{NH}_3)_4\text{Cl}_2]\text{Cl} \cdot \text{H}_2\text{O}$ salt was prepared by the method of Jorgensen as outlined in *Gmelin's Handbook*.¹⁰ Finely ground $[\text{Co}(\text{NH}_3)_4(\text{H}_2\text{O})\text{Cl}]\text{Cl}_2$ was mixed with concentrated H_2SO_4 and left at room temperature for 2 hours. The mixture was then cooled to 0°C and concentrated HCl was added slowly from a dropping funnel. The solution was then left at room temperature for 2 days by which time the bright green powder product had been precipitated. The product was recrystallised from HCl , washed with ethanol and dried at 100°C for 2 hours. The elemental analysis was as follows:

Co, 23.3 (23.44); N, 22.39 (22.28); H, 5.89 (5.61);
Cl, 42.19 (42.3); Oxygen, by difference, 6.2 (6.4).

16.430 grams of the trans-tetrammine salt was loaded into the calorimeter vessel. The pressure of helium³ exchange gas was increased to 10 torr to assist equilibration. The unit was sealed with 0.1116 grams of hard solder, 0.9992 grams of soft solder and 0.0666 grams of silver tube.

The first attempt at heat capacity measurements was unsuccessful. This was because a large positive temperature drift was encountered below 4.2 kelvin, and a large negative drift was encountered above 4.2 kelvin. The pressure of the inner can was found to be 4.8×10^{-4} mbar, clearly indicating ingress of helium gas. However, no leak could be detected at room temperature and, in an attempt to rectify the fault, all of the joints on the inner vacuum line were coated with fresh solder.

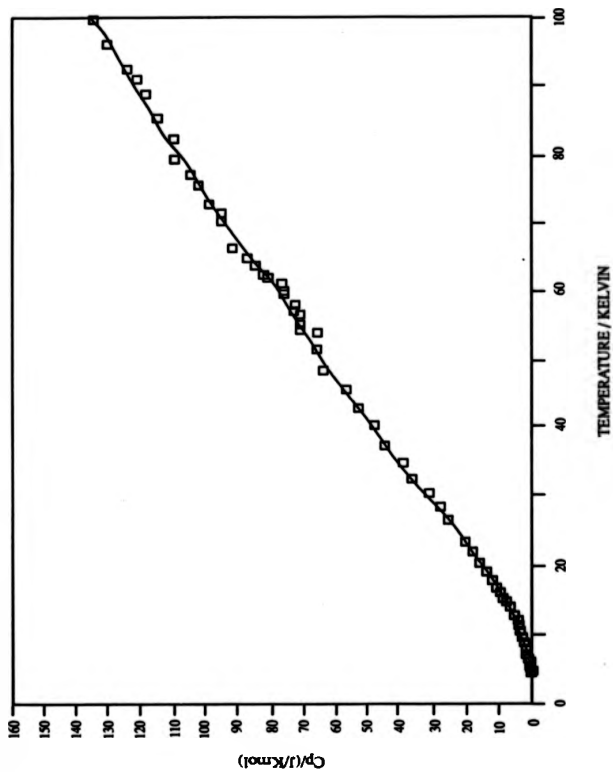
During the subsequent run, the inner vacuum was maintained between 10^{-6} mbar and 9×10^{-7} mbar. Again, however, temperature stability below 4.2 kelvin could not be maintained. Measurements above 4.2 kelvin were subject to negative drift of the same order (1 to 2 millikelvin) as was experienced for the pentaammine salt. There was also a marked improvement in performance with increasing temperature as had been observed for the pentaammine.

The heat capacity results are illustrated by Graph 5D and are listed in Table 5E. Regular smoothed values are available from Table 5F. The mean deviation above 10 kelvin was found to be 1.7%. Below 10 kelvin, the data was subject to a high degree of scatter, with some 6% to 8% deviance observed. For this reason, smoothed values are quoted only for the reliable range above 10 kelvin.

Following completion of the calorimetry, the cryostat was further investigated. Again, no leaks were detected at room temperature. The cryostat was then hooked up to the new leak detector and fully immersed in liquid nitrogen. The residual gas analyser detected nitrogen gas in the inner vacuum chamber and the pressure increased when liquid nitrogen was throttled into the internal pumping pot.

It seems likely that there is a small pinhole leak on the inner line, the likely position of which is on the section of stainless-steel tube which passes through the refrigerant pumping pot (see Figure 2A). The leak is temperature sensitive due to the differential contraction between the copper pot and the steel tube. The temperature instability thus results from ingress of helium gas, causing heating or cooling respectively when the calorimeter is below or above 4.2 kelvin. The situation may have been further aggravated by leakage of gas into the pumping pot via the needle valve, which is surrounded by liquid helium.

Before reliable measurements could be achieved, it would be necessary to replace the inner vacuum line and the pumping pot. Further to this, it would also be preferable to use an increased pressure (50 to 100 torr) of exchange gas in the calorimeter vessel to counteract the poor thermal conductivity of fine powders.



Graph 5D - Experimental Values of Heat Capacity
trans $[\text{Co}(\text{NH}_3)_4\text{Cl}_2]\text{Cl} \cdot 5\text{H}_2\text{O}$, 5 to 100 K

Table 5E - Experimental Values of the Heat Capacity of Trans-dichlorotetrammine Cobalt(III) Chloride $[\text{Co}(\text{NH}_3)_4\text{Cl}_2]\text{Cl} \cdot \text{H}_2\text{O}$ from 5 to 100 kelvin

T/K	$C_p/\text{JK}^{-1}\text{mol}^{-1}$	T/K	$C_p/\text{JK}^{-1}\text{mol}^{-1}$
4.771	0.00076		
4.970	0.0153		
5.115	0.0184	53.774	65.653
5.238	0.0974	55.276	70.526
5.584	0.1199	56.719	70.526
5.686	0.2868	59.485	75.54
5.956	0.3387	60.806	76.60
6.540	0.5756	62.092	80.48
6.865	0.7467		
7.420	1.175		
7.668	1.523	57.376	72.35
7.909	1.862	59.882	75.42
8.644	2.329	62.446	81.15
9.757	2.952	63.692	83.86
10.933	3.492	64.905	86.10
11.340	4.058	66.184	90.49
11.762	4.077	70.186	93.85
12.614	5.106	71.470	94.24
13.060	5.668	72.730	98.09
13.534	6.083	75.363	101.56
14.057	6.658	76.944	104.27
14.658	7.418	79.172	109.29
15.368	8.522	82.232	109.77
16.181	9.394	85.114	114.37
17.081	10.669	88.601	117.85
18.093	11.920	90.854	120.50
19.243	13.632	92.513	123.80
20.500	15.538	95.799	129.26
21.843	17.610	99.439	133.78
23.293	20.014		
24.573	25.587		
28.450	28.253		
30.469	31.437		
32.582	36.430		
34.795	38.720		
37.430	44.403		
40.269	47.860		
42.829	52.866		
45.529	56.332		
48.311	63.455		
51.568	65.152		
54.570	70.865		

Table 5F - Thermodynamic Functions of Trans-dichlorotetrammine Cobalt(III) Chloride; $\text{trans-}[\text{Co}(\text{NH}_3)_4\text{Cl}_2]\text{Cl} \cdot \text{H}_2\text{O}$

T/K	$C_p/\text{JK}^{-1}\text{mol}^{-1}$	$H^\circ(\text{T})-H^\circ(\text{O})$ Jmol^{-1}	$S^\circ(\text{T})$ $\text{JK}^{-1}\text{mol}^{-1}$	$-[G^\circ(\text{T})-H^\circ(\text{O})]\text{T}^{-1}$ $\text{JK}^{-1}\text{mol}^{-1}$
10	2.644	0.236		
15	7.886	25.771	0.844	
20	14.76	81.81	4.021	
25	22.71	175.15	8.153	1.15
30	31.22	309.87	13.04	2.71
35	39.73	487.36	18.50	4.57
40	47.10	704.3	24.28	6.67
45	54.94	959.5	30.28	8.96
50	62.68	1254	36.47	11.40
55	70.31	1586	42.80	13.96
60	77.85	1957	49.25	16.64
65	85.29	2364	55.77	19.39
70	92.62	2809	63.36	22.22
75	99.86	3291	69.0	25.12
80	106.99	3808	75.67	28.08
85	114.03	4360	82.37	31.07
90	120.96	4948	89.09	34.11
95	127.80	5570	95.81	37.18
100	134.53	6226	102.5	40.28

5.3 DISCUSSION

For a solid in which there is no obvious thermal anomaly, the low temperature heat capacity can often be adequately represented by a sum of the lattice contributions in the form

$$C_p = aT^3 + bT^6 + \dots \quad (3)$$

Normally when the heat capacity results below 10 kelvin are plotted in the form $C_p T^{-3}$ versus T^2 , the result is a straight line graph of positive slope, b , starting from a positive intercept a on the $C_p T^{-3}$ axis.

Graphs 5G and 5H respectively show the pentaammine and trans-tetrammine data plotted in this form. Clearly the data does not conform to normal $aT^3 + bT^6$ behaviour. The graphs are, however, fairly similar to that reported for the $\text{Co}(\text{NH}_3)_6\text{Cl}_2$ salt²⁵ which is reproduced in Figure 5K. In all cases, there is a maximum in the heat capacity curve above 4 kelvin, followed by a steady decline. The major difference is that while the rapidly rising Schottky tail is clearly shown below 4 kelvin in the hexaammine data, there is no obvious anomaly in the pentaammine or trans-tetrammine salts. In spite of this, the data was checked for a $\frac{1}{T}$ dependence by investigating the equation $C_p = aT^3 + cT^{-3}$ at the lowest available temperatures. Graphs 5I and 5J show plots of $C_p T^3$ versus T^6 , both of which indicate large negative values for the Schottky coefficient c . It can be concluded, therefore that there is no evidence of a Schottky anomaly for these two compounds in the temperature range covered by these measurements.

If a $\frac{1}{T}$ dependence had been observed along with a positive coefficient c , then the magnitude of the hindering potential could have been quantified by calculations based on the following model.

The ligand motion is assumed to be completely uncooperative and the ligands in each cation are treated as wholly independent torsional oscillators with fixed axes along the Co-N bonds. All of the NH_3 groups are assumed to be subject to a local potential barrier corresponding to the molecular symmetry only.

Consequently, the potential energy function of each NH_3 group has threefold symmetry and may be written as

$$V(\phi) = \frac{1}{2} V_2 (1 + \cos 3\phi) \quad (4)$$

The Hamiltonian operator for libration of a single NH_3 group may be written as

$$H = \frac{-\hbar^2}{8I\pi^2\phi^2} \frac{\partial^2}{\partial \phi^2} + V(\phi) \quad (5)$$

Where I is the moment of inertia of the NH_3 group about the threefold axis ($I = 4.40 \times 10^{-47} \text{ Kg m}^2$).

The Schroedinger equation may be expressed as

$$\frac{\partial^2 \psi}{\partial \phi^2} + (\Omega - 2\alpha \cos 3\phi) \psi = 0 \quad (6)$$

where $\Omega = (E - \frac{1}{2} V_2) \cdot \frac{8I\pi^2}{\hbar^2}$

and $\alpha = \frac{1}{2} V_2 \cdot \frac{8I\pi^2}{\hbar^2}$

This is a Mathieu equation, solutions for which have been tabulated by Gloden.¹⁰⁰ Provided that the energy difference between two consecutive eigenstates can be determined, the value of α may be obtained from the tables and thus V_2 may be calculated.

By analogy with equation (2), derived in section 5. 1. 2, the Schottky heat capacity for a mole of $\text{Co}(\text{NH}_3)_6^{2+}$ ions may be represented by

$$C_{\text{Schottky}} = nR \frac{g_1 g_2}{(g_1 + g_2)^2} \left[\frac{\Delta E}{kT} \right]^2 \quad (7)$$

where n is the number of NH_3 ligands per cation. This may be equated with the experimentally observed anomaly as follows

$$nR \frac{g_1 g_2}{(g_1 + g_2)^2} \left[\frac{\Delta E}{kT} \right]^2 = cT^{-2} \quad (8)$$

In this case, ΔE is the splitting of the librational ground state and thus represents the energy difference between the first and second eigenstates. Evaluation of ΔE requires knowledge of the quantum weights g_1 and g_2 . These have been determined for the NH_3 molecule by E.B. Wilson¹⁰ using group theory as summarised below.

For NH_3 , the protons can have nuclear spin quantum numbers of $\pm \frac{1}{2}$ resulting in an eight-fold degeneracy of the spin wave function on exchange of nuclear coordinates. The exchange of coordinates is equivalent to rotations about the C_3 axis and spans the reducible representation $4A + 2E$. This would be the case in the presence of an infinitely high barrier where tunnelling could not occur. For a finite potential, however, each torsional energy level forms a doublet; the upper level of which is symmetry species E and the lower level symmetry species A . The coupling of the different rotational states with the nuclear spin states must then be accounted for. This yields representations of the form $A \times (4A + 2E) = 4A + 2E$ and $E \times (4A + 2E) = 4A + 6E$.

Since the product of the rotational and nuclear spin wave functions, $\Psi_{\text{rot}} \Psi_{\text{spin}}$, must be totally symmetric, only the contributions from the A species are relevant. Hence the eight-fold degenerate ground state is split into two quartets as illustrated in Figure 5L. The quantum weights are thus $g_1 = g_2 = 4$ and

equation (8) may be reduced to the form

$$\frac{\Delta E}{k} = \sqrt{\left(\frac{0.481}{n} \cdot c\right)} \quad (8)$$

Thus the splitting energy may be evaluated provided that the Schottky coefficient c has been quantified.

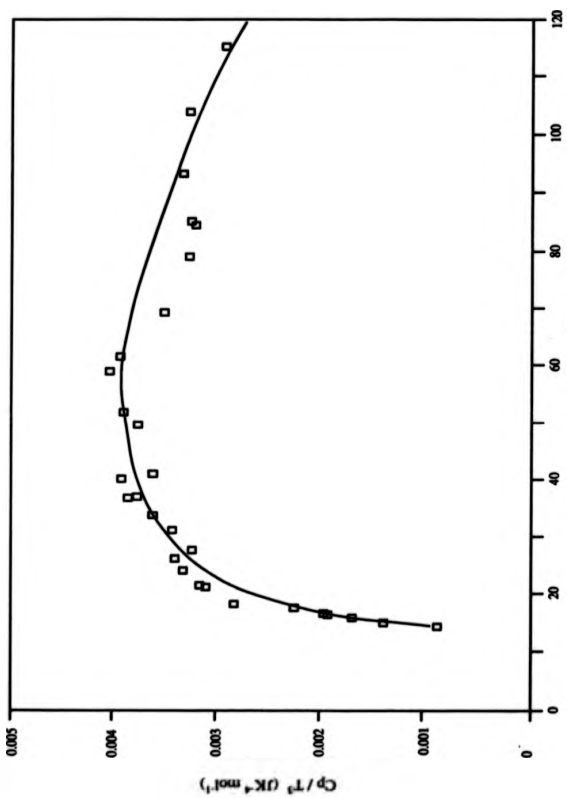
There is no doubt that the probability of observing a Schottky anomaly, and quantifying c , would have been greatly enhanced if the heat capacity measurements had extended well below 4.2 kelvin. In the analysis of the hexaammine salt, $\text{Co}(\text{NH}_3)_6\text{Cl}_2$,¹⁶ the upward turn of the Schottky tail just begins to show around 4.2 kelvin, and the best fit to a $\frac{1}{T}$ dependence occurs in the range from 2 to 3.6 kelvin.

Considering the lowest temperatures achieved in the author's experiments, the absence of Schottky anomalies is not too surprising, particularly for the trans-tetraammine salt, since results were not obtained below 4.2 kelvin.

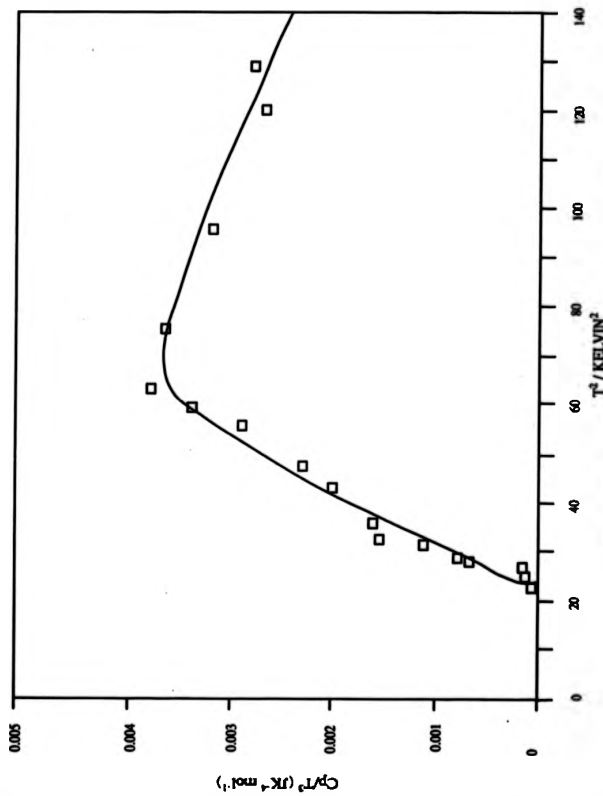
For the pentaammine salt, however, the reported decrease in Co-N bond strength¹⁷ produces an increase in bond length and suggests a lower intracluster barrier compared to the hexaammine. If this was the dominant effect, it would result in a higher splitting energy, ΔE , for the pentaammine. Consequently, the Schottky anomaly and its tail would occur at higher temperatures. This is particularly interesting since there is no evidence of an upward turn in the six pentaammine results in the 3.7 to 4.2 kelvin range. The results are, therefore, more consistent with a pentaammine Schottky anomaly occurring at a lower temperature. This would mean that other interactions must significantly contribute to the total barrier height. There are two possibilities.

Firstly, as a consequence of the increased Co-N bond length, the overall size of a cluster increases. This can result in greater contributions from cluster-cluster interactions.

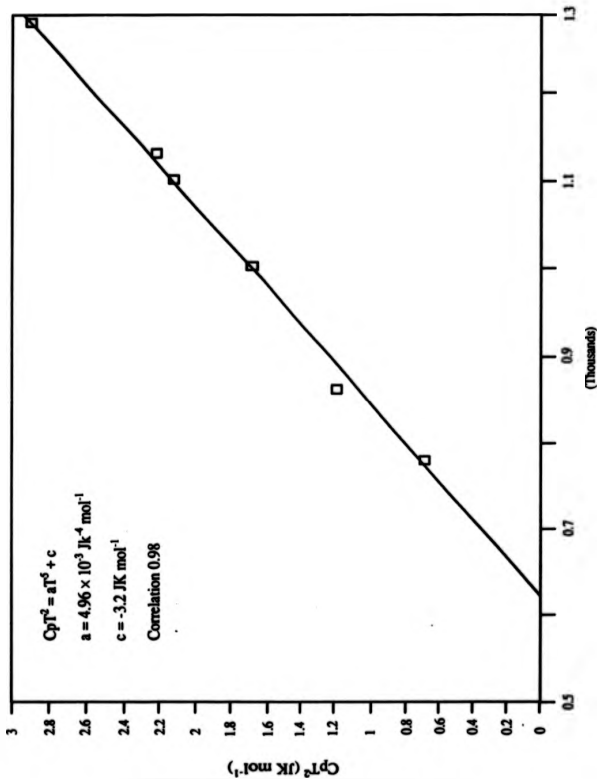
Secondly, it has been reported that the NH_3 rocking mode in the pentaammine has a greater infra-red absorbance frequency than that of the hexaammine salt.²⁴ This may be indicative of a greater contribution from hydrogen bonding in the pentaammine salt.



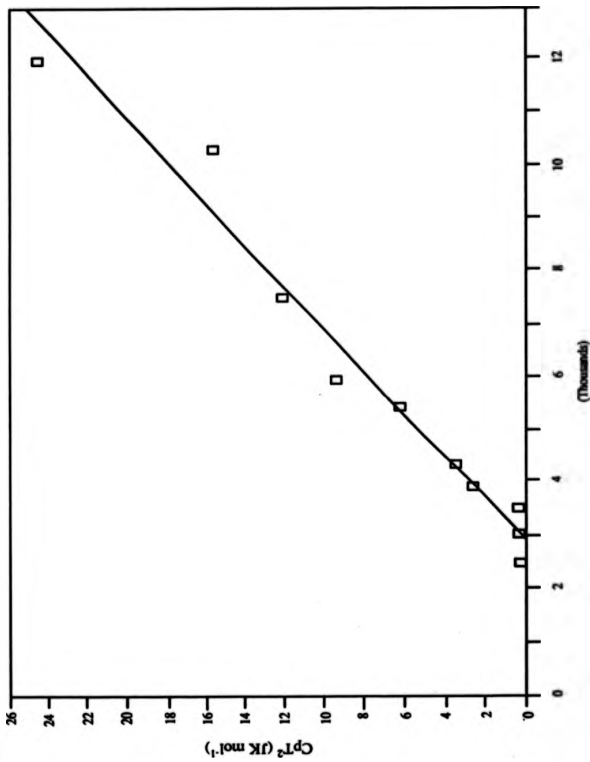
Graph SG - $\text{Co}(\text{NH}_3)_6\text{Cl}_2$, C_p/T^3 versus T^2
From 3.7 to 10.7 kelvin



Graph 5H - $\text{trans}[\text{Co}(\text{NH}_3)_2\text{Cl}_2] \cdot \text{H}_2\text{O}$ C_p/T^2 versus T^2
From 4.7 to 11.3 kelvin



Graph 51 - $[\text{Co}(\text{NH}_3)_6]\text{Cl}_2$, $C_p T^2$ versus T^4
 From 3 to 4.2 kelvin

Graph 5J - trans-[Co(NH₃)₄Cl₂]Cl·6H₂O $C_p T^2$ versus T^2

From 4 to 6 kelvin

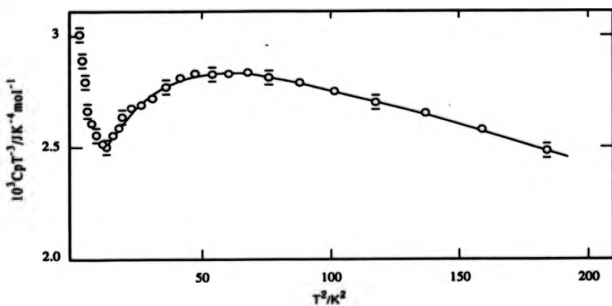


Figure 5K - The Schottky Effect in $Co(NH_3)_6Cl_2$

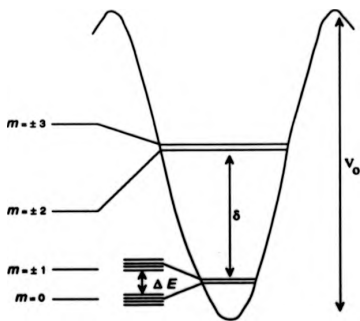
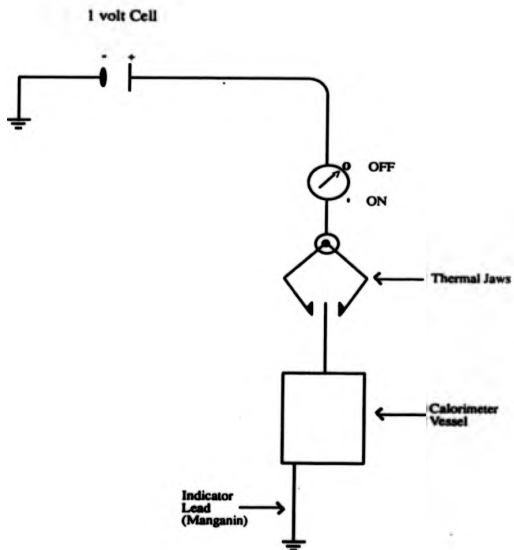


Figure 5L - Schematic of the energy levels of an NH_3 group in a $Co(NH_3)_n^{2+}$ ion.

Splitting as a result of quantum mechanical tunnelling

APPENDIX TO CHAPTER 2

Heat Switch Indicator Circuit

APPENDIX TO CHAPTER 3

Intel 8212 Logic Diagram

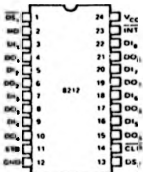
Process Control Software

Thermometer Calibration Certificate

intel

8212 8-BIT INPUT/OUTPUT PORT

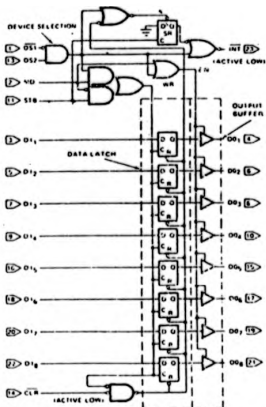
PIN CONFIGURATION



PIN NAMES

Pin No.	Symbol
1	GND
2-12	D ₀ -D ₇
13-14	CS, CS-bar
15-16	OEN, OEN-bar
17-18	OEN, OEN-bar
19-20	OEN, OEN-bar
21-22	OEN, OEN-bar
23-24	OEN, OEN-bar
25-26	OEN, OEN-bar
27-28	OEN, OEN-bar

LOGIC DIAGRAM



CS	CS-bar	CS-bar	DATA	OEN	OEN-bar	OEN-bar	OEN-bar	INT
0	0	0	0	0	0	0	0	0
0	0	0	1	0	0	0	0	0
0	0	1	0	0	0	0	0	0
0	0	1	1	0	0	0	0	0
0	1	0	0	0	0	0	0	0
0	1	0	1	0	0	0	0	0
0	1	1	0	0	0	0	0	0
0	1	1	1	0	0	0	0	0
1	0	0	0	0	0	0	0	0
1	0	0	1	0	0	0	0	0
1	0	1	0	0	0	0	0	0
1	0	1	1	0	0	0	0	0
1	1	0	0	0	0	0	0	0
1	1	0	1	0	0	0	0	0
1	1	1	0	0	0	0	0	0
1	1	1	1	0	0	0	0	0

CS = CHIP SELECT
CS-bar = CHIP SELECT (ACTIVE LOW)
OEN = OUTPUT ENABLE
OEN-bar = OUTPUT ENABLE (ACTIVE LOW)

INTERNAL OR FLOW UP

```

*****PROGRAM CONTROL SOFTWARE*****

10REM Cryobridge data acquisition
20REM plus merger of sorting routine
30REM and convergence routine
40REM*****VERSION 30 RUNNING*****
50CLS
60PROCseefile
70CLS
80PRINT"Above 30 Kelvin...TYPE 1"
90PRINT"10 to 30 Kelvin...TYPE 2"
100PRINT"4.2 to 10 Kelvin...TYPE 3"
110PRINT"2 to 4.2 Kelvin...TYPE 4"
120PRINT
130INPUT"WHICH RANGE IS THE CALORIMETER IN",range
135wait=0
140IF range=1 THEN Rs=9.997
150IF range=2 THEN Rs=100.041
160IF range=3 THEN Rs=1002.207
170IF range=4 THEN Rs=9990.616
175INPUT"USING LIQUID HELIUM OR NITROGEN",cryogen$
176IFcryogen$="HELIUM" THEN wait=40000
177IFcryogen$="NITROGEN" THEN wait=88000
180REM-----
185INPUT"MAX DRIFTRATE =1E-4 OR 1E-5 OR OTHER",max
190REM-----
200I=0
210 HEAT=&FC07
220THEAT=0
230F=0
240change=0
250DIMdrift(6)
260 DIM temp(9)
270DIM resist(9)
280DIM LATCH(5),RK(5),D1X(6),D2X(6)
290REM set up I/O addresses
300FREEZE=&FC06
310FOR I=0 TO 5:LATCH(I)=&FC00+I:NEXT I
320 FREEZE=0
330CLS
340PRINT"NOW LATCHING DATA FROM CRYOBRIDGE"
350REPEAT
360EX=&00020507 :REM NUMBRS FORMAT
370FOR J=1 TO wait: NEXT J
380REM-----
390PROCgetdata
400REM-----
410Rs=(N1/N2)*Rs
420IF Rt<6.3050 THEN CLS :PRINT"CALORIMETER ABOVE 100 KELVIN":PRINTSTRINGS(40,
""):PROChitmp

```

```

4401F R1># 6637 AND R1<# 6637 THEN PROC:tltemp
4401F R1># 6637 AND R1<125 THEN PROC:dltemp
4401F R1># 6637 THEN Ttherm=85 2300
4601F R1<125 THEN Ttherm=1b 857
4701F R1>125 THEN PROC:tltemp
4801F F=1
0901F I(F) Ttherm
4401F F#6 THEN PROC:tltemp
5101F F#6 THEN PROC:dltemp
520PROCcheck
525UNTIL FALSE
530DEFFPROCcheck
4401F F#6A
5601F Ttherm>30 AND R1<# 997 THEN ENDPROC
5601F Ttherm>30 AND R1<# 997 THEN change=10 R1<# 997 PROC:warn
5651F Ttherm>10 AND Ttherm<30 AND R1<# 100 041 THEN ENDPROC
5701F Ttherm>10 AND Ttherm<30 AND R1<# 100 041 THEN change=100 R1<# 100 041 PROC
warn
5751F Ttherm>4 2 AND Ttherm<10 AND R1<# 1002 207 THEN ENDPROC
5801F Ttherm>4 2 AND Ttherm<10 AND R1<# 1002 207 THEN change=1000 R1<# 1002 207
PROC:warn
5851F Ttherm<4 2 AND R1<# 998 616 THEN ENDPROC
5901F Ttherm<4 2 AND R1<# 998 616 THEN change=10000 R1<# 998 616 PROC:warn
595ENDPROC
600DEFFPROCwarn
610REPEAT
620PRINT"EXTERNAL STANDARD MUST BE CHANGED NOW"
630PRINT
640PRINT"TURN SWITCH R2 TO 'change' OIME"
650PRINT"THEN TYPE IN THE VALUE AND PRESS RETURN"
660INPUT"EXTERNAL STANDARD IS NOW #, nominal"
670UNTIL change=nominal
680ENDPROC
710REM -----
720REM Routine to unload bridge interface
730REM*****
740DEF PROCgetdata
750REM latch bridge data
760FREEZE=1
770IN=TIME<100
780REPEAT
790UNTIL TIME>FIN
800REM unload data from registers
810FOR I=0 TO 5
820R(I)=PLATCH(I)
830NEXT I
840REM release bridge
850FREEZE=0
860REM unpeck registers
870REM preserve bottom nybble to make bad digit
880D1(1)=FNbot(R(0))
890D1(2)=FNtop(R(0))
900D1(3)=FNbot(R(1))
910D1(4)=FNtop(R(1))
920D1(5)=FNbot(R(2))
930D1(6)=FNtop(R(2))
940D1(1)=FNbot(R(3))
950D1(2)=FNtop(R(3))
960D1(3)=FNbot(R(4))

```

```

970D2X(4)=FMup(DX(4))
980D2X(5)=FNbot(DX(5))
990D2X(6)=FMup(DX(5))
1000REM add 'em up
1010N1=D1X(1)*100000+D1X(2)*10000+D1X(3)*1000+D1X(4)*100+D1X(5)+10+D1X(6)
1020N2=D2X(1)*100000+D2X(2)*10000+D2X(3)*1000+D2X(4)*100+D2X(5)+10+D2X(6)
1030ENDPROC
1040REM*****
1050REM-----
1060REM Function to get bottom nybble into bot
1070DEF FNbot(X)=X AND &0F
1080REM-----
1090REM Function to get top nybble in bot (must mask and shift right by 4)
1100DEF FMup(X)=(X AND &F0) DIV &0F
1110END
1120REM
1130REM merger of sorting routine
1140REM*****
1150DEFPROCtemp
1160REM 65 to 100 Kelvin
1170Rt=(N1/N2)*Rs
1180 X=0
1190 X=X+1
1200READ temp(X)
1210READ resist(X)
1220IF Rt >resist(X) THEN GOTO 1190
1230T1=temp(X):T2=temp(X-1)
1240R1=resist(X):R2=resist(X-1)
1250 T=Ti*((T1-T2)/(R1-R2))*(Rt-R1)
1260 RESTORE 1270
1270DATA 100.7861,6.3050,95.237,6.5791
1280DATA 90.602,6.8538,85.709,7.1991
1290DATA 80.320,7.6619,75.325,8.1881
1300DATA 70.159,8.8613,65.309,9.6495
1310DATA 65.2306,9.6637
1320PROCiterate
1330ENDPROC
1340REM*****
1350REM merger of convergence routine
1360DEFPROCiterate
1370REM TEMPERATURE TESTING
1380REM FOR delta=<math>\theta</math> CONVERGENCE
1390PRINT
1400PRINT
1410 Tloop=<math>\theta</math>
1420REPEAT
1430Tloop=((2.639594E4)/((Rt-.3.610677)*((.972157E-7)*(T1-.2.659374))))^<math>\theta</math>.497937

```

```

1448 delta=((0.072157E-7)*(Tloop^2.659374))+((0.639594E4)*(Tloop^2.000296))+((
610E77 Rt)
1450IF ABS(delta)>1E-4 THEN T1:Tloop
1460UNTIL ABS(delta)<1E-4 :Ttherm:Tloop
1470PRINT"Therm=",Ttherm
1480ENDPROC
1490REM*****
1500DEFFPROCdrift:
1510A=@:B=@
1520PRINT"LSQ DRIFT ANALYSIS"
1530 FOR F=1 TO 6:PRINTdrift(F):NEXTF
1540FOR F=1 TO 6
1550A:=(A+drift(F)):B:=(B+(F*drift(F))):NEXTF
1560rate:=((2*B)-(7*A))*0.02057: PRINT"driftrate=",rate
1570 IF ABS(rate)<=max THEN PROCheat
1580ELSE:PRINT"rate BAD. NEXT DATA"
1590 FOR F=1 TO 5:drift(F)=drift(F+1):NEXTF
1600F=5:PROCgetdata
1605 VDUI:PRINTdrift(6):VDUI3
1610 IF F<5 THEN PRINT"F=",F
1620ENDPROC
1630REM*****
1640DEFFPROCmidtemp
1650REM 16 to 65 KELVIN
1660Rt:=(N1/N2)*Rs
1670Y=LOG(Rt-3.6107)
1680Ttherm=10^((2.243988)-((0.6346392*Y))+((0.2139545)*(Y^2))-((0.2170376)*(Y^3
)))+((0.1440569)*(Y^4))-((0.05572205)*(Y^5))+((0.01156558)*(Y^6))-((0.232629E-4)
*(Y^7))
1690PRINT
1700PRINT"Therm=",Ttherm
1710ENDPROC
1720REM*****
1730DEFFPROCheat
1740VDU7:VDU7:INPUT"DO YOU WISH HEATING ? ANS. Y OR N".K$
1750IF K$="Y" THENPROCinfo
1760H=@
1770ENDPROC
1780REM*****
1790DEFFPROCinfo
1795 VDUI2:FOR F=1 TO 6:PRINTdrift(F):NEXTF
1796PRINT"DRIFTRATE=",rate
1800I=@:L=@: REM RESET TO ZERO
1810INPUT"SET CURRENT I mA":I
1820INPUT"NOMINAL HEATING PERIOD t seconds":t
1830t=t+100
1840PRINT"TO HEAT PRESS <SPACE BAR>"
1850 IF GET=32 THEN PROCtime

```

```

1100ENDPROC
1170REM*****
1180DEFPROCline
1190PRINT "HEATING PERIOD" , " " , "SECOND"
1900TIME=0.000 "H"AT=1 REPEAT UNTIL TIME<= "H"AT-0.000000 PRINT"AR(17,23),(
TIME/100)*(1.0004599956) 3.47336E 3
1905VIB3
1910ENDPROC
1920REM*****
1930DEFPROCcasefile
1940DIMT(320),R(320)
1950xx=000020547
1960INPUT "TYPE start TO BEGIN PROGRAM".file$
1970that=OPENIN(file$)
1980count=0
1990REPEAT
2000count=count+1
2010INPUTthat,T(count),R(count)
2020PRINT "T=",T(count), "R=",R(count)
2030UNTIL EOFthat
2040CLOSEthat
2050PRINT "END OF FILE"
2060ENDPROC
2070REM*****
2080DEFPROClowtemp
2090R=(N1/N2)*Rn
2100Tloop=0
2110count=0
2120REPEAT
2130count=count+1
2140UNTIL R(count)<Rt
2150T=T(count)
2170A0=5.293407202 :A1=-4.604301600 :A2=6.785102000 :A3=-15.07220431
2180A4=22.78370007 :A5=-8.600981650 :A6=-14.30658135 :A7=15.60664217
2190A8=-4.394602565
2200REPEAT
2210Z=LOGT
2220B=(A0-LOGRt)+(A1*(Z))+(A2*(Z^2))+(A3*(Z^3))+(A4*(Z^4))+(A5*(Z^5))+(A6*(Z^6
))+(A7*(Z^7))+(A8*(Z^8))
2230B=(1/T)*((A1)+(2*A2*Z)+(3*A3*(Z^2))+(4*A4*(Z^3))+(5*A5*(Z^4))+(6*A6*(Z^5))
+(7*A7*(Z^6))+(8*A8*(Z^7)))
2240Tloop=(T-(D/E))
2250IF ABS(Tloop-T)>1E-5 THEN T=(T-(D/E))
2260 UNTIL ABS(Tloop-T)<=1E-5
2270IF ABS(Tloop-T)<=1E-5 THEN Ttherm=Tloop
2280PRINT
2290PRINT "Ttherm=";Ttherm
2300ENDPROC
2310REM*****
>
>

```

***** (N, T) POINT GENERATOR FOR REAL TIME CONVERGENCE*****

```

100 DIM T(120), R(120)
20 count = 0
300 S= 100000000
40 INPUT Tstart, T
50 FOR T=T TO 17 STEP 0.05
60 A0= 5.297407202 A1= 4.604301600 A2= 6.785102920 A3= 15.97220431
70 A4= 22.78670007 A5= 0.600211850 A6= 14.30050135 A7= 15.00064217
80 A8= -4.304002005
90 LOGT
100 R= ((A0)+(A1*(Z))+(A2*(Z^2))+(A3*(Z^3))+(A4*(Z^4))+(A5*(Z^5))+(A6*(Z^6))+(A7
*(Z^7))+(A8*(Z^8)))
110 R= 10^r
120 count = count + 1
130 T(count) = T, R(count) = R
140 PRINT T, R
150 IF T > 17 THEN GOTO 170
160 NEXT T
170 chno = OPENOUT(FILE$, 1) = 0
180 FOR count = 1 TO 320
190 PRINT chno, T(count), R(count)
200 NEXT count
210 CLOSE chno
250 END

```



CRYOGENIC CALIBRATIONS LTD

Ref

Our Ref

PITCHCOTT, Nr. AYLESBURY, BUCKINGHAMSHIRE, HP22 4HT, ENGLAND

TEL 029 864 259 (WHITCHURCH 259)

CALIBRATION NUMBER CCG 418

Thermometer Specification: CryoCal Type CR 2500L, No. 4450

<u>Temperature (Kelvin)</u>	<u>Resistance (ohms)</u>
2.005	17,450
2.221	13,100
2.403	10,600
2.611	8,536
2.809	7,098
3.001	6,045
3.199	5,200
3.422	4,456
3.598	3,981
3.799	3,529
3.992	3,172
4.198	2,846
4.433	2,536.0
4.650	2,292.2
5.010	1,957.3
5.406	1,664.9
5.813	1,424.4
6.194	1,240.3
6.555	1,043.6
7.032	931.9
7.471	809.1
8.010	685.2
8.516	589.6
9.022	510.8
9.529	445.1
10.011	392.42
10.501	347.36
11.031	306.19
12.090	242.43
13.005	201.87
13.923	170.55
15.012	142.21
16.010	122.43
17.088	105.22
17.879	91.05



CRYOGENIC CALIBRATIONS LTD

Your Ref.

Our Ref.

PITCHCOTT, Nr. AYLESBURY, BUCKINGHAMSHIRE, HP22 4HT, ENGLAND

TEL. 029-464 258 (WHITCHURCH 258)

CALIBRATION NUMBER CCG 418

Page 2

<u>Temperature (Kelvin)</u>	<u>Resistance (ohms)</u>
19.038	82.753
20.001	74.391
22.490	58.137
25.069	46.638
27.499	38.893
30.092	32.760
33.061	27.536
35.152	24.669
37.587	21.923
40.712	19.1753
45.457	16.0502
50.313	13.7486
55.112	12.0606
60.416	10.6510
65.309	9.6495
70.159	8.8613
75.325	8.1881
80.320	7.6619
85.709	7.1991
90.602	6.8538
95.237	6.5791
100.781	6.3050

The temperatures were obtained from germanium, rhodium-iron and platinum thermometers whose own calibrations are accurate to $\pm .005K$ of the IPTS (68) down to 20K. Below 20K, the scale has been obtained from a National Physical Laboratory gas thermometer related to the boiling point of hydrogen using the IPTS (68) value of 20.28K. The scale is probably $2.5 \times 10^{-4} \times T K$ in excess of thermodynamic temperature. To obtain the T_{58} Helium Vapour Pressure Scale subtract $.0019 \times T K$ from the given temperature.

The above calibration should be accurate to $\pm .008K$ or $\pm .0005$ ohms. With suitable interpolation procedures there are sufficient points to obtain an accuracy including interpolation of $\pm .01K$ up to 10K and $\pm .025K$ up to 100K.

Checked...*26/11/...*...

APPENDIX TO CHAPTER 4

SOLDER CORRECTIONS: POLYNOMIAL FORMS

$$C_p = \sum_1^4 a_i T^i$$

Hard Solder
1 to 15K

$$\begin{aligned} a_0 &= -1.74167041 \times 10^{-4} \\ a_1 &= 3.13263393 \times 10^{-4} \\ a_2 &= -1.562057 \times 10^{-4} \\ a_3 &= 3.29293593 \times 10^{-5} \\ a_4 &= -1.14806639 \times 10^{-4} \end{aligned}$$

15K to 100K

$$\begin{aligned} a_0 &= -4.16182763 \times 10^{-2} \\ a_1 &= 5.14987422 \times 10^{-3} \\ a_2 &= -6.9296568 \times 10^{-3} \\ a_3 &= 4.66001325 \times 10^{-7} \\ a_4 &= -1.23600768 \times 10^{-9} \end{aligned}$$

Soft Solder
1 to 15K

$$\begin{aligned} a_0 &= -1.67366173 \times 10^{-4} \\ a_1 &= 3.07942791 \times 10^{-4} \\ a_2 &= -1.66407538 \times 10^{-4} \\ a_3 &= 4.00085196 \times 10^{-5} \\ a_4 &= -1.4686858 \times 10^{-4} \end{aligned}$$

15K to 100K

$$\begin{aligned} a_0 &= -3.57706892 \times 10^{-2} \\ a_1 &= 4.30794524 \times 10^{-3} \\ a_2 &= 1.44598001 \times 10^{-3} \\ a_3 &= -2.13925387 \times 10^{-4} \\ a_4 &= 3.81876926 \times 10^{-8} \\ a_5 &= -2.94069799 \times 10^{-10} \\ a_6 &= 8.62080962 \times 10^{-13} \end{aligned}$$

Silver Tube**1 to 15K**

$$a_0 = -2.51648068 \times 10^{-7}$$

$$a_1 = 6.02532727 \times 10^{-6}$$

$$a_2 = -8.22827239 \times 10^{-8}$$

$$a_3 = 1.49324346 \times 10^{-6}$$

$$a_4 = 2.54546892 \times 10^{-8}$$

15K to 100K

$$a_0 = 3.26860123 \times 10^{-7}$$

$$a_1 = -5.64264125 \times 10^{-3}$$

$$a_2 = 3.37385531 \times 10^{-4}$$

$$a_3 = -5.71294431 \times 10^{-6}$$

$$a_4 = 4.24971016 \times 10^{-8}$$

$$a_5 = -1.19209702 \times 10^{-10}$$

REFERENCES

- 1 A. Inaba; *J. Chem. Thermod.* **15**(12): 1137 (1983).
- 2 O'Hare, Hubbard, Flotow; *J. Chem. Thermod.* **16**(1): 45 (1984).
- 3 D.I. Bradley *et al*; *Cryogenics* **22**: 296 (1982).
- 4 A.C. Anderson; *Rev. Sci. Inst.* **41**: 1446 (1970).
- 5 B.D. Josephson; *Phys. Lett.* **1**: 251 (1962).
- 6 J. Clarke, M.B. Ketchen; *Appl. Phys. Lett.* **27**: 155 (1975).
- 7 W.A. Little; *Physica* **109** B, C: 2001 (1982).
- 8 P.L. Richards; *Phil. Trans. Roy. Soc.* **307**: 77 (1982)
- 9 S.M. Faris; *Phys. Bulletin* **34**: 420 (1983).
- 10 W.F. Giaque, J.W. Stout; *J. Am. Chem. Soc.* **58**, 1144 (1936).
- 11 S.A. Friedberg *et al*; *Physica* **19**: 1072 (1953).
- 12 G.A. Baker, J.W. Essam; *J. Chem. Phys.* **55**: 861 (1971).
- 13 S. Hoshino; *J. Phys. Soc. Jap.* **12**: 315 (1957).
- 14 W.V. Johnston *et al*; *J. Chem. Phys.* **51**: 3739 (1969).
- 15 B.B. Owens, G.R. Argue; *J. Electrochem. Soc.* **117**: 898 (1970).
- 16 R.H. Busey, W.F. Giaque; *J. Am. Chem. Soc.* **74**: 4443 (1952).

- 17 W.K. Robinson, S.A. Friedberg; *Phys. Rev.* **117** 402 (1960).
- 18 J.O. Clayton, W.F. Giaque; *J. Am. Chem. Soc.* **54**: 2610 (1932).
- 19 M.W. Melhuish, R.L. Scott; *J. Phys. Chem.* **68**: 2301 (1964).
- 20 L.A.K. Staveley; NATO ASI Series (1984).
- 21 W. Gaede; *Physik Z.* **4**: 105 (1902).
- 22 W. Nernst, A. Eucker; *Physik Z.* **10**: 586 (1909).
- 23 W. Nernst; *Chem. Abs.* **4**: 2397 (1910).
- 24 J.P. McCullough; *Experimental Thermodynamics*, Vol 1, Chapter 8
(Butterworths, 1968).
- 25 *ibid*, Chapter 1.
- 26 *ibid*, Chapter 6.
- 27 T.M. Dauphinee, D. MacDonald; *Proc. Roy. Soc.* **A221**: 267 (1954).
- 28 J.C. Southard, D.H. Andrews; *J. Franklin Inst.* **209**: 349 (1930).
- 29 F.E. Hoare, L.C. Jackson, N. Kurti; *Experimental Cryophysics*,
p123. (Butterworths, 1961).
- 30 R.W. Hill, D.L. Martin, D.W. Osborne; *Experimental
Thermodynamics - Vol 1*, Chapter 7. (Butterworths, 1961).
- 31 A.K. Gupta, L.A.K. Staveley; *Trans Faraday Soc.* **45**: 50 (1949).
- 32 E.F. Westrum *et al*; *J. Chem. Phys.* **21**: 419 (1953).
- 33 C.F. Mate *et al*; *Rev. Sci. Instr.* **36**: 369 (1965).
- 34 R.S. Crisp, P. Turner; *Cryogenics* **25** (1): 45 (1985).

- 35 C.S. Barrett; *Brit. J. of Appl. Phys.* **7**: 427 (1956).
- 36 H.L. Johnston, E.C. Kerr; *J. Am. Chem. Soc.* **72**: 4733 (1950).
- 37 K.F.D. Sterrett; *J. Res. Natl. Bureau. St.* **69C**: 19 (1965).
- 38 K. Adachi, H. Suga, S. Seki; *Bull. Chem. Soc. Jap.* **41**: 1073 (1968).
- 39 F.J. Webb, J. Wilks; *Proc. Roy. Soc.* **A230**: 549 (1955).
- 40 M. Jewess; D. Phil. Thesis, Oxford (1978).
- 41 P.R. Clayton; D. Phil, Thesis, Oxford (1981).
- 42 R.M. Clay; D. Phil. Thesis, Oxford (1965).
- 43 G.K. White; *Experimental Techniques in Low Temperature Physics*
(Clarendon Press, 1979).
- 44 A.J. Croft; *Experimental Cryophysics*, Chapter 6.
(Butterworths, 1961).
- 45 J. Wilks; *An Introduction to Liquid Helium*.
(Clarendon Press, 1970).
- 46 D.W. Osborne; *Experimental Cryophysics*, Chapter 10 p284,
(Butterworths, 1961).
- 47 R.D. Worswick; *J. Chem. Soc. Farady Trans. I* **70**: 1590 (1974).
- 48 M. Jewess; *J. Chem. Soc. Farady Trans II* **77**: 1757 (1981).
- 49 J.S. Blakemore; *Rev. Sci. Instr.* **33**: 106 (1962).
- 50 G. Ahlers, J.F. Macre; *Rev. Sci. Instr.* **37**: 962 (1966).
- 51 N.F. Mott; *Endeavour* **26**: 155 (1967).

- 52 B.G. Cohen, A.R. Tretola, R. Whienthal; *Rev. Sci. Instr.* **37**: 962 (1966).
- 53 G.L. Pearson, H. Suhl; *Phys. Rev.* **83**: 768 (1951).
- 54 J.S. Blakemore, J. Winstel, R.V. Edwards; *Rev. Sci. Instr.* **41**: 835 (1970).
- 55 D.J. Blundell, B.W. Ricketson; *Cryogenics* **16**: 687 (1976).
- 56 P. Lindenfield; *Temperature - Its Measurement and Control in Science and Industry*, Vol III, Part 1, p399. (Reinhold Press, 1962).
- 57 C.A. Swenson, P.C. Wolfendale; *Rev. Sci. Instr.* **44**: 339 (1973).
- 58 E.F. Westrum, G.T. Furukawa; *Experimental Thermodynamics*, Vol 1, Chapter 5, p168. (Butterworths, 1968).
- 59 Automatic Systems Laboratories Ltd.
- 60 Cryogenic Calibrations Ltd.; Pitchcott, Aylesbury, Bucks. HP22 4HT.
- 61 G.T. Armstrong; *J. Res. Nat. Bur. Stand.* **53**: 263 (1954).
- 62 R.L. Powell; *Temperature - its Measurement and Control in Science and Industry*, Vol III, Part 2, p65. (Reinhold Press, 1962).
- 63 J. Kondo; *Prog. Theoret. Phys.* **32**: 37 (1964).
- 64 A.J. Hegger; *Solid State Physics* **23** (Academic Press, N.Y., 1969).
- 65 J.P. McCullough; *Experimental Thermodynamics*, Vol I, Chapter 3. (Butterworths, 1968).
- 66 *Handbook of Chemistry & Physics* (Chemical Rubber Co.) **D137**, 138

- 67 G.T. Furukawa, R.E. McCoskey, G.J. King; *J. Res. Nat. Bur. Stand.* **47**: 256 (1951).
- 68 A.A. Sklyankin, P.G. Strelkov; *Zhw. Priklad. Mech, i Tech. Fiz* **2**: 100 (1960).
- 69 R.M. Clay, L.A.K. Staveley; *Trans. Faraday Soc.* **62**: 3065 (1966).
- 70 C. Brot, B. Lassier-Govers; *Ber. Bunsen-Ges. Phys. Chem.* **80**: 31 (1976).
- 71 I. Darmon, C. Brot; *Mol. Cryst.* **2**: 301 (1967).
- 72 J.H. Colwell, E.K. Gill, J.A. Morrow; *J. Chem. Phys.* **39**: 635 (1963).
- 73 D.G. Thomas, L.A.K. Staveley; *J. Chem. Soc.* 4569 (1952).
- 74 R.D. Worswick, J.C. Cowell; *J. Chem. Soc. Faraday Trans. I* **70**: 1590 (1974).
- 75 H. van Kempen; *Physica* **30**: 1131 (1964).
- 76 J. Eckert, W. Press; *J. Chem. Phys.* **73**: 451 (1980).
- 77 A.R. Bates, I.L.A. Crick; *J. Phys. C: Solid State Phys.* **9**: 3013 (1976).
- 78 T.E. Jenkins, A.R. Bates; *J. Phys. C: Solid State Phys.* **14**: 817 (1981).
- 79 F.W. Klaaysen, H. Suga, Z. Dokoupil; *Physica* **51**: 630 (1971).
- 80 H. van Kempen, T. Garofano, W.J. Huiskamp; *Physica* **31**: 1096 (1965).
- 81 A.R. Bates, K.W.H. Stevens; *J. Phys. C: Solid State Phys.* **2**: 1573 (1969).

- 82 G.R. Murray, J.S. Waugh; *J. Chem. Phys.* **29**: 207 (1958).
- 83 T. Ito, T. Chiba; *Bull. Chem. Soc. Jap.* **42**: 108 (1969).
- 84 P.H. Kim; *J. Phys. Soc. Jap.* **18**: 445 (1960).
- 85 P.R. Clayton, R.D. Weir, L.A.K. Staveley; *J. Chem. Phys.* **75**: 5464 (1981).
- 86 J.W. Mellor; *Comprehensive Treatise on Inorganic & Theoretical Chemistry.* (N.Y. Press, 1935).
- 87 W.W. Wendlandt; *J. Inorg. Nucl. Chem.* **25**: 545 (1963).
- 88 W.W. Wendlandt; *J. Inorg. Nucl. Chem.* **25**: 843 (1963).
- 89 W.W. Wendlandt; *J. Inorg. Nucl. Chem.* **25**: 1267 (1963).
- 90 G.W. Watt, D.A. Butler; *Inorg. Chem.* **5**: 1106 (1966).
- 91 A.B. Lamb, J.P. Simmons; *J. Am. Chem. Soc.* **43**: 2189 (1921).
- 92 R. Tsuchiya, A. Uehara, T. Nakayama; *Bull. Chem. Soc. Jap.* **56**: 3248 (1983).
- 93 I. Nakagawa, T. Shimanouchi; *Spectrochim. Acta.* **22**: 1707 (1966).
- 94 L. Sacconi, A. Sabatini; *Inorg. Chem.* **3** (12): 1772 (1964).
- 95 T.W. Swaddle, P.J. Craig; *Spectrochim. Acta.* **26A**: 1559 (1970).
- 96 J. Fujita, K. Nakamoto, M. Kobayashi; *J. Am. Chem. Soc.* **78**: 3295 (1966).
- 97 K. Burger, E. Fluck; *J. Inorg. Nucl. Chem.* **37**: 55 (1975).
- 98 G.J. Kruger, E.C. Reynhardt; *Acta. Cryst.* **B34**: 915 (1978).

- 99 Y. Shigeta, Y. Komiyama, H. Kuroya; *Bull. Chem. Soc. Jap* **36** (9): 1159 (1963).
- 100 G.A. Krestov, K.B. Yatsimirskii; *Russian J. Inorg. Chem.* **6** (10): 1165 (1961).
- 101 Gmelin's *Handbuch*; **58**: 228.
- 102 R.F. Gloden; *Euratom Report EUR 4349f* (1970).
- 103 E.B. Wilson; *J. Chem. Phys.* **3**: 276 (1935).